

# Biologically Derived Metal Organic Frameworks

Samantha L. Anderson and Kyriakos C. Stylianou\*

Laboratory of Molecular Simulations (LSMO), Institut des Sciences et Ingénierie Chimiques (ISIC), École Polytechnique Fédérale de Lausanne (EPFL Valais Wallis), Rue de l'Industrie 17, CH-1951 Sion, Switzerland

Metal organic frameworks (MOFs) are extended structures composed of a network of organic ligands and metal ions or clusters connected to each other *via* coordination bonds. The numerous choices of organic ligands and metal coordination geometries have led to the construction of porous MOFs with various compositions, network topologies, pore sizes and shapes and they possess high surface areas and low densities. The structures of MOFs can be tailor-tuned in such a way that any desired ligand or/and metal ion can be incorporated; this has given to researchers the advantage of designing MOFs for a targeted application. Within this review, we overview recent examples of a sub-class of MOFs namely biologically derived MOFs (bio-MOFs), made of multifunctional and commercially available biologically derived ligands (bio-ligands) such as: amino acids, peptides, nucleobases and saccharides and focus on their coordination chemistry with a variety of metals. Central to this review are four tables detailing the coordination modes of bio-ligands to metals, along with a visual representation of the bio-MOF that is subsequently formed. Through the detail analysis of these structures, we highlight the structural impact of these ligands on the structure, and their contribution to the MOFs properties and applications. Finally, we showcase the potential of bio-MOFs in several research areas such as CO<sub>2</sub> capture, separation, catalysis, drug delivery and sensing.

## 1. Introduction

Metal organic frameworks (MOFs) are crystalline coordination based materials consisting of an infinite network of metal-ions, or metal-ion clusters, bridged by organic ligands through coordination bonds into porous two- or three- dimensional extended structures.[1, 2] The judicious selection of the metal ion and ligand has led to the discovery of a broad array of highly porous MOF materials with various topologies, compositions and properties such as record-breaking internal surface areas (up to 7000 m<sup>2</sup>/g),[3] high void volumes (up to 90%),[4] and low densities (as low as 0.126 g/cm<sup>3</sup>).[5] The ability to chemically modify the pore surface of MOFs through pre- and post- synthetic introduction of functional groups, combined with the potential for the formation of open metal coordination sites, can also provide the means to tailor internal surfaces for applications related to gas separation and storage, catalysis, and sensing.[6] Compared with other frequently used ligands for MOF synthesis, biologically related ligands (such as amino acids, peptides, nucleobases and saccharides) offer the potential to utilize multiple coordination sites, and contain a variety of functional groups that can be advantageous in areas such as CO<sub>2</sub> capture, separation and catalysis. They also, have added advantages such as controlling hydrogen-bonding interactions, resulting in structures that can be flexible or robust. Ultimately, bio-ligands allow researchers to buy any combination of chirality, aromaticity, cyclic or aliphatic features desired, or by buying the necessary backbone and synthetically altering it for further research investigations. This saves time, and can accelerate the rate of MOF discovery. With the vast amount of bio-ligands readily available, it is not surprising that these ligands have found their way into several applications, such as CO<sub>2</sub> capture/storage, enantioselective synthesis, etc. that other well-known MOFs (e.g HKUST-1, MOF-74) have been known for.[7] To control the size and shape of a cavity in a particular MOF for a given application can still prove challenging to researchers, however the ligand design strategy (and their incorporation within the MOF structure) plays a significant role in the construction of functional MOFs.

In this review, we highlight the importance of ligands in general and more specifically the impact of biologically related ligands (hereafter bio-ligands), in the design, structure and applications of biologically derived MOFs (hereafter bio-MOFs). More so, we will discuss the current work and challenges of incorporating bio-ligands

into MOFs, and offer insights into this exciting sub-discipline of research.

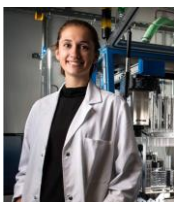
## 2. Ligand Design in MOFs

Typically, the self-assembly of metal ions or clusters with ligands to form MOFs can be achieved through classical coordination chemistry methods (<100 °C),[1, 8] diffusion methods, solvothermal synthesis (>100 °C),[9] electrochemical methods, microwave synthesis,[10, 11] or high-throughput techniques. [12-14] While a variety of metal ions throughout the periodic table can be used, rigid organic ligands are generally preferred (over flexible) since the resulting MOFs can be robust and/or porous. [15-17] Commonly used organic ligands within MOFs are divided into families such as: *i.* carboxylic acid containing ligands, *ii.* nitrogen containing ligands (pyridyl, pyrrol, imidazolyl, etc), *iii.* cyano ligands, *iv.* phosphonic acids ligands, *v.* ligands based on mixed functional groups, *vi.* sulfonyl ligands and *vii.* metal-bearing ligands. [18, 19] While cationic ligands are less common in the synthesis of MOFs (low affinity to coordinate to metal cations), both neutral and charged ligands can be used. [8] Functionalities pointing towards their internal pore surface are often utilized to introduce strong interactions with a target molecule and can influence the framework structure. [18] In addition, they may have interconnecting functions, which could extend the coordination motifs, creating secondary interactions such as hydrogen bonding and aromatic stacking. [18], [20-23]

With a wide variety of ligands available, many different strategies have been used to synthesize MOFs that target a specific application. Some of them can be summarized into six different categories:

*i.* Using ligands that are identical in size but contain different functional groups can afford multivariate MOFs (MTV-MOFs). [22, 23] This was demonstrated by Reimer *et al.*, who combined Zn<sub>4</sub>O and BDC to form a MTV-MOF-5 family, which showed four-fold selectivity for CO<sub>2</sub> over CO. [22]

*ii.* Replacing the organic ligands in a MOF with units that are topologically similar or identical, but instead increasing in length, can extend the pore size, resulting in the construction of new families of isorecticular MOFs (IRMOFs) with unique properties. [24-29] This method can be used to increase the BET, CO<sub>2</sub> capacity, and pore of the material. For example, in the IR-MOF-74-I to -IX series the pore apertures were increased for 14 to 98 Å, allowing for molecules such



**Samantha L. Anderson** is from Winnipeg, Manitoba, Canada. She received her B.Sc (Hon) degree from the University of Winnipeg, and her M.Sc in Chemistry at Queen's University in Kingston, Ontario, Canada. She is currently pursuing a Ph.D in the LSMO group under the supervision of Prof. Berend Smit and co-supervision of Dr. Kyriakos C. Stylianou at the Institute of Chemical Sciences and Engineering in Sion, ISIC-Valais at EPFL Valais Wallis. Her research interests include the rational design, synthesis and characterization of biologically derived MOFs for optical and energy related applications.

as vitamin B<sub>12</sub>, or green fluorescent protein (GFP) to reside in their pores. [27]

iii. Using ligands with specific functionalities to target applications such as CO<sub>2</sub> capture and storage, or ligands that have specific functionalities to enhance their interaction with target molecules. For example, amine functionalized MOFs can be used to achieve a higher total adsorption energy of CO<sub>2</sub> molecules. [28]

iv. Increasing the conjugation of organic ligand can aid in the formation of MOFs with hydrophilic pores, or that can be used for light absorbing or sensing applications. [30-39] Ligands such as H<sub>4</sub>TCPB have been incorporated into MOFs, allowing for selective uptake of *p*-xylene over other isomers such as *m*-xylene. [35] While porphyrin based MOFs (Al-PMOF) have been used to harvest light for water reduction. [36] For fluorescent MOFs, emission is dependent on the MOF structure, and effects such as metal-to-ligand charge transfer, ligand-to-ligand charge transfer and ligand-to-metal charge transfer have been reported.[40] Intra-ligand based luminescence is typically observed with organic ligands that are highly conjugated, susceptible to  $\pi$ -stacking in the solid state.[40], [41]

v. Fluorescent ligands can also be used in MOFs that are intended for biological applications, due to their ability to perform real-time measurements. [7], [42-49] For MOFs to be applicable for *in vivo* administration, the components of their framework should not intervene in the body's cycle, and ideally be excreted from the body. [43] Some examples of exogenous MOFs found in biomedical applications are magnesium-2,5-dihydroxoterephthalate [CPO-27 (Mg)], [50] Fe<sup>III</sup> polycarboxylates [MIL-100-Fe<sup>III</sup>], [51] and zinc adeninate-4,4'-biphenyldicarboxylate (bio-MOF-1). [52] Organic ligands such as muconic acid, fumaric acid, trimesic acid, amino terephthalic acid and terephthalic acid have been used in the construction of non-toxic Fe<sup>III</sup> MOFs (MIL-89, -88A, -100, -100\_NH<sub>2</sub>, and -53, respectively). [53]

vi. Chiral ligands can be used for the generation of homochiral porous MOFs, or chirality can be induced from the arrangement of achiral ligands within the structure. [54-57] Among the chiral ligands available, [58-64] bio-ligands, such as natural occurring peptides, are structurally rich and versatile with numerous metal binding sites. However, robust and highly porous MOFs based on these ligands are scarce in the literature. [56], [65-67]

**Dr. Kyriakos C. Stylianou** was born in Larnaca, Cyprus. He obtained his Ph.D degree in materials chemistry at the University of Liverpool, UK under the supervision of Prof. Matthew J. Rosseinsky and co-supervision of Prof. Darren Bradshaw. His thesis was based on the rational design, synthesis and characterization of open porous MOFs for advanced applications. Upon completion of his PhD, the award of the prestigious Marie Curie fellowship allowed him to move at the Catalan Institute of Nanoscience and Nanotechnology and collaborate with Prof. Daniel Maspoch. He chose to apply his synthetic background in surface chemistry and growth of porous materials on surfaces using nanolithography and inkjet printing methodologies. Currently, he holds a Scientist position within the LSMO group led by Prof. Berend Smit at the Institute of Chemical Sciences and Engineering in Sion, ISIC-Valais at EPFL Valais, where he leads the synthetic activity of the group. He was recently awarded with the Ambizione Energy Grant from the Swiss National Science Foundation, to investigate the potential of MOFs as photocatalysts. Additionally, his research activity focuses on the utilization of high-throughput methodologies to accelerate the discovery of novel nanoporous materials for energy- and optical-related applications.

### 3. Coordination Binding Modes of Bio-Ligands in MOFs

We consider biologically derived MOFs (bio-MOFs), the MOFs which are constructed from biologically based ligands (bio-ligands). In this review, we will overview the coordination capabilities of four families of bio-ligands such as amino acids, peptides, nucleobases and saccharides within the MOF structures and their impact on the structural robustness/flexibility and physical properties of these materials. [7] Recently, there has been increasing interest in using bio-ligands as they offer several advantages such as commercial availability, simple synthetic routes for the development of new ligands, structural diversity, multiple different metal binding sites, and preinstalled chirality. [7] While the use of bio-ligands can lead to biologically compatible MOFs, some of them have added features such as self-assembly properties, which could be used to direct the structure and function of the bio-MOFs. [7] Over the last 5 years, bio-MOFs have shown a great promise in several research fields such as CO<sub>2</sub> capture, catalysis, sensing, and separation. This review is structured as follow: *i.* review of the coordination capabilities of bio-ligands and their orientation around metal ions for the formation of extended frameworks and *ii.* research highlights on the potential applications of bio-MOFs.

#### 3.1. Amino Acids

Amino acids are organic ligands containing both a carboxyl (-COOH) and amino (-NH<sub>2</sub>) group that dominate their functional and physical properties. The organic side chain of amino acids can impart hydrophobic or hydrophilic character, with the presence of a polar

(e.g. alcohols) or non-polar (e.g. alkyl chains) side chain, which is important for the formation of protein structures. Their rich coordination chemistry (through the carboxylate, amino groups and side chains) makes them as an attractive class of organic ligands for the formation of extended MOF structures. This however, has been limited due to the ease of formation of low-dimensional and compact frameworks. [7] To circumvent this challenge and form porous amino acid based MOFs, additional polydentate organic ligands and bridging anions, or chemically modified amino acids have been used to increase dimensionality in bio-MOFs made from natural occurring amino acids.[7]

With both carboxylate and amino metal binding sites, amino acids tend to form discrete complexes through an O,N-chelating mode, forming a five-membered glycinate chelate ring. However, in some cases coordination of the  $\alpha$ -carboxylate group to the metal ions can occur either through bi- or tri-dentate bridging modes creating extended frameworks.[7] One-dimensional coordination networks are commonly formed when pure amino acids are used however, [68] 2- and 3-dimensional MOFs can also be constructed. In the case of 2-dimensional metal-ion amino acids frameworks, a typical  $\mu_2$ -O<sub>1</sub>:O<sub>2</sub> coordination mode can be obtained with glycine (Gly) and Ni<sup>II</sup> (Table 1, entry 1), [69] Mn<sup>II</sup>, [70] and Co<sup>II</sup>. [71] Two amino acid ligands can coordinate through an O,N-chelation mode with a metal ion that allows octahedral coordination. However, by using the second oxygen atom of the amino acids carboxylate, bridging to a neighboring metal ions can occur through a  $\mu_2$ -N<sub>1</sub>O<sub>1</sub>:O<sub>2</sub> coordination mode. [7] This is found in bio-MOFs combining L-phenylalanine (L-Phe) with Mn<sup>II</sup>, [72] and Cu<sup>II</sup> (Table 1, entry 2), [73] as well as L-glutamine (L-Gln) with Cu<sup>II</sup> (Table 1, entry 3). [74]

Three-dimensional bio-MOFs using pure amino acids are rare, however examples can be found when additional organic ligands or altered amino acids are used. Amino acids bearing side chains with metal binding groups can be used to bridge metal ions together. For example, Anokhina and Jacobson reported the first examples of a chiral 1-dimensional, optically pure product, with an extended helical subnetwork formulated as [Ni<sub>2</sub>O(L-Asp)(H<sub>2</sub>O)<sub>2</sub>]-4H<sub>2</sub>O (where Asp is aspartic acid). [75] However, the increase of the pH to 7.2, leads in the formation of a 3-dimensional [Ni<sub>2.5</sub>(OH)(L-Asp)<sub>2</sub>]-6.55H<sub>2</sub>O (Table 1, entry 4) material that is based on comparable helices that are connected by additional [NiAsp<sub>2</sub>]<sup>-2</sup> units to generate a porous chiral framework. [76] It was proposed that the formation of common helices in both complexes could be due to the strong tendency of the aspartate ligand to favor a tridentate chelation coordination mode, limiting the orientation and range of its bonds to additional metal centers. [76] Following this, Zhang *et al.* demonstrated the synthesis of two enantiomeric MOFs with a SOD zeotype topology using enantiopure D- or L-alanine (D- or L-Ala). [77] The coordination environment of Ni(D-Ala)<sub>2</sub> (Table 1, entry 5) demonstrated the presence of a 3-dimensional 4-connected SOD network in which the D-Ala anion chelates to the Ni<sup>II</sup> metal center, acting as a  $\mu_2$ -bridging ligand. [77]

Side chains that feature additional metal binding groups, such as methionine (Met) have also been used in the construction of 3-dimensional bio-MOFs. Specifically, in the preparation of a homochiral heterobimetallic [Ag<sub>3</sub>Cu<sub>3</sub>(L-Met)-6(NO<sub>3</sub>)<sub>3</sub>(H<sub>2</sub>O)]-7H<sub>2</sub>O (Table 1, entry 6), where the L-Met ligands were found to bind to Cu<sup>II</sup> ions (O,N-chelation mode) and Ag<sup>I</sup> ions through the monodentate thioether group. [78] Metal-glutamate (Glu) complexes have also been recently investigated due to their model system simplicities, metal-protein interactions, and have been created into a series of

nearly isostructural 3-dimensional bio-MOFs with metal ions such as Cd<sup>II</sup>, [79, 80] Zn<sup>II</sup>, [81] Cu<sup>II</sup>, [82, 83] and Co<sup>II</sup> (Table 1, entry 7).[84] Within [M(L- or D-Glu)(H<sub>2</sub>O)]·H<sub>2</sub>O, the Glu ligands are multidentate, coordinating to three different metal ion *via*  $\mu_2$ -N<sub>1</sub>O<sub>1</sub>:O<sub>2</sub>,  $\mu_1$ -O<sub>3</sub>:O<sub>4</sub> and  $\mu_2$ -O<sub>3</sub>:O<sub>4</sub> coordination modes. Other examples of amino acids bearing side chains with metal binding sites are the imidazole group of histidine (His) (Table 1, entry 8), [85] the thiol group of cysteine (Cys), as well as the phenol ring of tyrosine (Tyr).

Increasing dimensionality can be achieved by using both amino acids and additional organic ligands or inorganic anion/clusters that act as linkers. [7] Recently, a non-chiral 3-dimensional bio-MOF, comprised of Gly and azide, was reported with the formula [Cu<sub>2</sub>(Gly)<sub>2</sub>(N<sub>3</sub>)<sub>n</sub>], (Table 1, entry 9) that displayed an unusual 4-connected 3-dimensional net with a Lonsdaleite (hexagonal diamond) topology and was the first example of a coordination polymer with a flexible amino acid as the secondary bridging ligand in metal-azido complex. [86] Another 3-dimensional non-chiral bio-MOF was obtained using chiral L-Ala, Cu and Gd. It was the first heterometallic MOF containing both 3d Cu<sup>II</sup> and 4f Gd<sup>III</sup> metal ions, and contains both an amino acid and a bridging dicarboxylic ligand (1,3-benzene dicarboxylate) (Table 1, entry 10). [87]

Isostructural 3-dimensional homochiral porous bio-MOFs [Co<sub>2</sub>(L-Asp)<sub>2</sub>(4,4'-bipy)]·1.5H<sub>2</sub>O (ferromagnetic) and [Co<sub>2</sub>(D-Asp)<sub>2</sub>(4,4'-bipy)]<sub>n</sub> were constructed when the 2-dimensional Co<sup>II</sup> and L-Asp layers were interlinked with the linear bipy ligands.[88] In this case, each Asp dianion binds to three Co<sup>II</sup> ions through a tridentate coordination mode (amine and  $\alpha$  and  $\beta$ -carboxylate groups) as well as through a monodentate fashion, in which the oxygen from the  $\alpha$ - or  $\beta$ -carboxylate group links to a Co<sup>II</sup> ion.[88] Interestingly, bio-MOFs such as [Ni<sub>2</sub>(L-Asp)(bipy)] (Table 1, entry 11), can be extended through the substitution of the bipy pillars with ligands that have a similar connectivity, such as azpy, bpe, and 3rbp. [89] This includes ligands such as py<sub>3</sub>T and 35bpp which have a different topology and supplementary pyridyl group. [89] [Ni<sub>2</sub>(L-Asp)<sub>2</sub>(bipy)] displays a significant degree of enantioselectivity in the sorption of a family of small diols (*e.e.* up to 54%) due to the chirality of the pores, which is induced by the use of an enantiopure amino acid building block. The 35bpp system, with channel dimensions ranging from 6.7 x 4.9 Å to 10.3 x 5.4 Å, illustrates the possibility to introduce a basic active site within the pores. [89]

*In-situ* dimerization of Asp (referred to as IDS), with bipy and Zn carbonate basic, lead to the formation of a mixed-ligand 3 dimensional [Zn<sub>2</sub>(IDS)(bipy)] MOF (Table 1, entry 12). [90] The IDS ligand binds to 5 separate Zn<sup>II</sup> metal centers which are crystallographically present as two independent Zn<sup>II</sup> centers that are five (Zn<sub>2</sub>) and six (Zn<sub>1</sub>)-coordinated. Three coordination modes are present: *i.* an eight-membered ring through Zn<sub>1</sub> is formed through two oxygen atoms and a nitrogen atom in an O-N-O tridentate *mer* chelation (two carboxylate groups and the amino group from the IDS ligand), *ii.* from the previous mode, the remaining oxygens bind two Zn<sub>2</sub> metal centers, *iii.* finally, two crystallographically distinct Zn<sup>II</sup> metal centers are coordinated to the remaining carboxylate groups. [90] This work demonstrates the crucial role of the rigid organic ligands, and their ability to prevent filling of available spaces by flexible amino acid ligands, generating porosity in metal-amino acid extended frameworks. [90]

In a similar system, the solvothermal reaction of ZnCO<sub>3</sub>·2ZnO·3H<sub>2</sub>O with Asp and bipy yielded a homochiral 3-dimensional Zn-Asp-MOF with three distinct coordination geometries and coordination modes of Asp to Zn<sup>II</sup> (Table 1, entry 13).

[91] Three distinct coordination modes of Zn<sup>II</sup> ions are 4-, 5-, and 6-coordinated, with distortion away from their respective ideal geometries. [91] Within the motif, there are three crystallographically non-equivalent Asp ligands with three different coordination modes to Zn: *i.* one Asp ligand is bound to three different Zn metal centers with two types of coordination which are comprised of a commonly reported 5- and 6-membered N-O metallocycle, and where the remaining oxygens bridge to neighboring ions, *ii.* and *iii.* display three types of coordination modes and are bound to four Zn<sup>II</sup> ions. [91] These modes are: *iv.* through a five membered N-O metallocycle that is commonly found in metal-amino acid chemistry, *vi.* via a pendant carboxylate group bridging to other Zn<sup>II</sup> ions, *v.* where the remaining oxygens form the bridge to other neighboring ions, similar to conformation *i.* [91] This structure represents the first example of a chiral amino-acid derived compound with this structural framework. It should be noted that Asp has been reported in Cu<sup>II</sup> frameworks with imidazole to form [Cu(L-Asp)(Im)]·2H<sub>2</sub>O. [92] The structure (Table 1 entry 14), is a 2-dimensional framework with Cu<sup>II</sup> atoms coordinated in a distorted square-pyramidal geometry *via* one Im molecule and three Asp ions. [92]

Switching to the amino acid L-Tryptophan (L-Trp) with bpe and Zn<sup>II</sup> affords a MOF with formula of {[Zn<sub>2</sub>(L-Trp)<sub>2</sub>(bpe)<sub>2</sub>(H<sub>2</sub>O)<sub>2</sub>]·2H<sub>2</sub>O·2NO<sub>3</sub>]<sub>n</sub> in which the Trp ligand acts as a bridging ligand and adopts a *syn-anti* mode by displaying both monodentate and chelate coordination modes, thereby forming 1-dimensional chiral chains (Table 1 entry 15). [93] An extended neutral 2-dimensional coordination layer with homochiral rectangle-like (4,4) topology is formed through the linking of adjacent chiral chains *via* a μ<sub>2</sub>-bpe bridges. [93] AAA packing is achieved *via* the stacking of [Zn<sub>2</sub>(L-Trp)<sub>2</sub>(bpe)<sub>2</sub>] layers, with the presence of significant hydrogen bonding interactions between the coordinated guest and water molecules. [93] Emission spectra confirmed that this MOF exhibited a green emission at 546 nm, and *via* dielectric studies revealed a low dielectric constant (κ = 2.53 at 1 MHz), confirming it's candidacy for interlayer dielectrics. [93] After treatment with different solutions of anions, the results showed a change of κ value in experiments with the phosphate anion, it was also noted that secondary harmonic generation studies were double the intensity of SiO<sub>2</sub>. [93]

Due to the intrinsic homochirality, multidentate coordination sites, and commercial availability, serine (Ser) is an attractive and functional bio-ligand for the formation of 3-dimensional, homochiral and isostructural nanoporous frameworks. [94] Within this bio-MOF, [Zn<sub>4</sub>(bdc)<sub>2</sub>(L-Ser)<sub>2</sub>], there are homochiral chains which are built from the Ser ligand and Zn<sup>II</sup> centers linked together by achiral bdc ligands affording a rod-and-spacer motif that has large rhombic channels (Table 1, entry 16). [94] The structure has notable coordination features such as the NH<sub>2</sub> groups of L-Ser bridging two Zn<sup>II</sup> centers, with each five-coordinate Zn center having a trigonal bipyramid geometry, and an unusual μ<sub>4</sub>-Ser ligand (dianion) bound to four Zn<sup>II</sup> ions which is due to the deprotonation of the hydroxy group. [94] This bio-MOF exhibits high selectivity for CO<sub>2</sub> over N<sub>2</sub> and CO at ambient conditions (more in section 6). [94]

The alteration of natural amino acid side chains allows for the potential to increase dimensionality of bio-MOFs. For example, the modification of the phenyl ring in Phe with a tetrazole affords a 3-dimensional bio-MOF whereas 1- and 2-dimensional structures are common using a metal ion and non-modified Phe. [95] The two compounds, mono[(S)-5-(3-tetrazoyl)-phenylalaninato]zinc(II) and

mono[(S)-5-(3-tetrazoyl)-phenylalaninato]cadmium(II) monoqua reported by Li *et al.*, were isostructural with a non-interpenetrated SrAl<sub>2</sub> topology (Table 1, entry 17). [48] Rational design to adjust the "depth" and the "width" of the ligands showed that one could control the size and shape of the 2-dimensional Zn<sup>II</sup> and Cd<sup>II</sup> chiral bio-MOFs by introducing different functionalities into the phenyl ring. [48]

Moving out of the transition metals, isomorphous crystals with the composition of [Ln<sub>2</sub>(L-Glu)<sub>2</sub>(ClO<sub>4</sub>)<sub>4</sub>·9H<sub>2</sub>O] (Ln: Dy<sup>III</sup> or Ho<sup>III</sup>) have been reported by Huskowska *et al.* [96] In these structures, four carboxylate groups bridge two lanthanide ions in each complex, with two of the oxygens coordinated to both cations. [96] Bringing the coordination number to a total of nine, four water oxygens are found surrounding each cation; finally, the infinite layers are linked *via* L-Glu acid ligands and the perchlorate groups located in the voids. [96] Other lanthanide based bio-MOFs have been reported; such as Tb<sup>III</sup> and Eu<sup>III</sup> (DL-Cys and DL-Hval, L-Asp, and DL-Val, respectively), [97] as well as Sm<sup>III</sup>, Nd<sup>III</sup>, and Er<sup>III</sup> (Gly, Ala, and Val, respectively). [98]

### 3.2. Peptides

Polymeric biomolecules that are composed of short chains of naturally occurring amino acids, and linked by a NHCO bond are peptides, and constitute the rational second step of complexity to evaluate the role of bio-ligands as bridging ligands in MOF structures. Each peptide has a distinct sequence depending on the conformation, and stereochemical configuration of their constituted amino acids. [99] Because of this, each peptide has specific recognition properties and intrinsic chirality that may be useful for a wide range of applications, including asymmetric catalysis and enantioselective separation. [99] More so, the majority of peptides are aliphatic which can give rise to MOFs with flexibility, and give researchers insight into how more complex molecules (proteins) fold or 'move'. [100]

Similar to amino acids, peptides can coordinate through an O,N-chelating mode, where the amino group coordinates to the metal ions either through chelation or a monodentate form, while the carbonyl oxygen coordinates to the same metal ion. Coordination of the carboxylate occurs through any of the well-known modes such as chelation, monodentate, *syn-syn* bridging, etc. Such features can be seen in even the simplest peptide, GlyGly. More importantly, the infinite versatility to design peptides by adding suitable amino acids to their sequence, can allow for the incorporation of more metal binding groups. For example, the incorporation of more carboxylate groups can be achieved by simply synthesizing peptides made from combining Asp and Glu. [7] This versatility opens the door to an unlimited number of flexible polydentate bio-ligands that could be used and form 1-, 2- and 3-dimensional robust or flexible bio-MOFs, which we will describe throughout this section.

To date, most examples of bio-MOFs constructed from peptides only contain two amino acids. While some tripeptides are commercially available, they are more expensive and can be synthetically more demanding to make compared to dipeptides. The simplest and shortest peptide, GlyGly, has been used to construct 2-dimensional bio-MOFs with formula of [M(GlyGly)<sub>2</sub>]·2H<sub>2</sub>O (M: Zn<sup>II</sup> or Cd<sup>II</sup>) (For Zn, Table 2, entry 1). [101] At pH 6, each GlyGly ligand, bridges two metal ions in a monodentate mode through the terminal carboxylate group and the amino group coordinates through a five membered chelation ring. Increasing the pH to 9 (and where M: Cd<sup>II</sup>) the GlyGly ligands bind to two Cd<sup>II</sup> ions through their terminal carboxylates, and the amino group to another Cd<sup>II</sup> ion in a

monodentate mode. [101] Changing the peptide to GlyGlu affords a structure with two ligands coordinated through the carboxylates ( $O_{10}$ ,  $O_{11}$ , and  $O_{13}$ ,  $O_{14}$ ) with a coordination sphere that is described as a distorted square antiprism due to the coordination angles of the carboxylates ( $53.27^\circ$  and  $53.66^\circ$ , respectively) (Table 2, entry 2). [102] Changing the metal to  $Co^{II}$  affords a configuration where the  $Co^{II}$  ions are positioned at the vertices of the  $Co$ -L-GlyGlu ladders (Table 2, entry 3). [65] The ladders are strongly connected *via* hydrogen bonds involving the amino group and carboxylate of GlyGlu in the neighboring ladders. [65] Along the *c*-axis, the ladders are also hydrogen bonded through a coordinated  $H_2O$  molecules to the carboxylate group of an adjacent ladder. [65]

Peptide derived bio-MOFs constructed from networks made from dipeptides such as  $[Zn(GlyThr)_2] \cdot H_2O$ , [103]  $[Cd(AlaThr)_2] \cdot 4H_2O$ , [104] and  $[Zn(GlyAla)_2] \cdot \text{solvent}$  [105] have been reported (Table 2, entries 4-6), and in the case of  $Zn^{II}$  based bio-MOF  $[Zn(GlyThr)_2]$ , show good  $CO_2/CH_4$  sorption selectivity. [106] The aforementioned 2-dimensional metal-peptide layered structures are connected through strong hydrogen bonds and exhibit coordination modes to  $[M(GlyGly)_2] \cdot 2H_2O$  ( $M$ :  $Zn^{II}$  or  $Cd^{II}$ ). [101] The stack of the 2-dimensional layered structures of  $[Zn(GlyThr)_2]$  and  $[Zn(GlyAla)_2]$  results in the generation of 1-dimensional channels, however in the former bio-MOF, the presence of Thr leads in the formation of strong interactions with the adjacent layer, reinforcing the stability in the 3-dimensional crystal structure. [106] For the latter  $[Zn(GlyAla)_2]$ , the pores collapse upon desolvation but they can be recovered when polar molecules diffuse into its pores. [105]

GlyAsp based bio-MOFs can be prepared with either  $Co^{II}$  or  $Zn^{II}$  generating 3-dimensional frameworks with different topologies (Table 2, entry 7 and 8, respectively). [106] The structure of the  $Co^{II}$  framework consists of dipeptides connecting four metal ions, and a unique seven membered ring formed through the coordination of a metal ion with alpha and beta carboxylate groups of the Asp residue in the dipeptide. [106] In this structure, the dimensionality arises from the side chains of Asp bridging two  $Co^{II}$  ions. In the  $Zn^{II}$  framework, the metal center is penta-coordinated, with each dipeptide connecting four Zn metal ions through a five-membered glycinate chelate ring. [106] While the coordination mode of  $Co^{II}$  and orientation of GlyAsp results in the formation of a 3-dimensional framework, the  $Zn^{II}$  based bio-MOF gives a 2-dimensional structure with layer parallel to the *ab* plane, and a rigid conformation of GlyAsp dipeptide with water molecules trapped in the intersheet plane. [106]

Changing the bio-ligand to GlySer, the reposition of the OH-bearing Ser side chain allows for ordered cooperative, displacive, and conformational changes of the peptide (Table 2, entry 9). [107] This change from a methyl, to a primary alcohol, is a sufficient change in the framework to go from a solvated porous state (GlyAla) to a non-porous state. The  $Zn(XY)_2$  (with XY representing the dipeptide of choice) dipeptide based bio-MOFs demonstrate the ability to tune properties within a family due to the synergic interactions between the varying functional groups on the constituent peptides.

Natural dipeptides, such as carnosine (Car), ( $\beta$ -Ala-L-His) have been reported in the construction of MOFs (Table 2, entry 10). The carnosine chain contains an extra  $CH_2$  group due to the  $\beta$ -amino acid structure of the  $\beta$ -alanine, and an additional metal binding site can be found from the histidine residue which incorporates an imidazole moiety, therefore giving carnosine two more potential linking sites compared to GlyThr and GlyAla. [108] In the  $ZnCar$ -DMF 3-dimensional bio-MOF, each carnosine links four tetrahedral Zn

cations, and two of those cations are bridged by the deprotonated imidazolate ring, forming a microporous material (please see section 5 for more details).

The incorporation of different functional groups in peptides can be achieved in most cases through simple synthetic routes. This strategy was adopted in the formation of GlyHis, a peptide containing carboxylate, amine and imidazole functional groups, with two different coordination modes around two different metal centers. The structure of the  $Ni^{II}$  framework consists of 1-dimensional chains along the *a* and *b*-axes, with two imidazolate N atoms coordinated to the Ni affording an octahedral geometry around the metal center (Table 2, entry 11). [109] Interestingly, unlike a lot of peptides, the carboxylate group in this framework does not participate in metal binding, and is therefore protonated. This is also observed in the framework with  $Cu^{II}$ , which has square pyramidal geometry and is coordinated to three N atoms, thereby forming 1-dimensional chains along the *b*-axis (Table 2, entry 12).

Recently, work has focused on rigid and flexible metal-dipeptide frameworks (some previously discussed), that show permanent porosity, and demonstrate interesting adsorption properties with the ability to be synthesized with a variety of different functional groups. However, it is difficult to tailor dipeptide MOFs with all the desired attributes, such as water stability, which is a hot topic in metal-peptide polymer chemistry. [110] Earlier this year, Bronić *et al.* designed a new metal-dipeptide MOF with a relatively large side chain, that would impose stability on the synthesized product, affording a MOF with enhanced properties such as water and greater thermal stability, as well as structural flexibility. [110] The crystal structure of  $[Zn(Gly-L-Phe)_2]$  (Table 2, entry 13) consists of a tetrahedrally coordinated  $Zn^{II}$  metal center coordinated twice via the amino groups of the Gly component, and twice via the carboxylate functional groups of the Phe. [110] Here, both sets of functional groups are coordinated in a monodentate fashion. In comparison,  $[Cd(Gly-L-Phe)_2]$  (Table 2, entry 14) contains a hexacoordinated  $Cd^{II}$  comprised of four dipeptide ligands where the two ligands are coordinated through the Gly amino functional groups, and the carboxylate groups coordinate to the Phe moiety through a bidentate mode. [110]

It should be noted, that the use of a tripeptide, GlyGlyGly, published by Marsh *et al.* was the first example of a bio-MOF containing more than two amino acids (Table 2, entry 15). [104] Interestingly, from a structural point of view, it is similar to Takayama's  $[Cd(GlyGly)_2]$  at pH: 9. [101] Here,  $[Cd(Gly_3)_2]$  contains octahedrally coordinated Cd metal ions ligated by six peptides: the N-termini of two peptides provide two nitrogen ligands, with one oxygen from each of the four terminal carboxylates providing four ligands. [104] Each carboxylate group bridges two  $Cd^{II}$  metal ions forming 1-dimensional framework with chains eight-membered rings, the second-dimension is formed via the backbone of the peptide where the  $(Gly_3)$  moiety adopts an extended confirmation: two peptides run antiparallel to each other affording a closed ring through the coordination of two  $Cd^{II}$  ions. [104] They also explored how the introduction of chirality would modulate the structure of the metal-peptide framework, which was accomplished by examining  $[Cd(Ala)_3]$  (Table 2, entry 16). This bio-MOF formed a 1-dimensional extended molecular chain that was comprised of a series of rings linked by  $Cd^{II}$  ions. [104] Similar to the  $(Gly)_3$  structure, two  $(Ala)_3$  peptide linkers in an antiparallel fashion bridge between two Cd ions forming a ring. Interestingly, due to the folding of the peptide terminal nitrogen group of the Ala moiety, the methyl groups are

found pointing into the central cavity of the ring forming a hydrophobic pore. [104, 111] Meanwhile, the methyl groups of the second and third residues face outwards, these interact with the methyl groups of the adjacent methyl-peptide chains affording another hydrophobic contact which propagates through the structure in the second-dimension. [104] The work of the authors reinforces the idea of the possibility to engineer the properties of extended networks through the choice of amino acid side chains.

Protein folding has been reported in a 2014 paper by Fujita *et al.* who constructed a short peptide with 3-py groups with amide bonds in the short peptide Gly-Pro-Pro (Table 2, entry 17). [112] Single crystal X-ray analysis clearly reveals that the peptide ligand is fixed in a P<sub>II</sub> helix conformation with all ligands linked by a py-Ag<sup>I</sup>-py coordination similar to natural polypeptide chains (N→C direction terminal manner). [112] The linear helical strand of the MOF repeats, affording a unique hexagonal entanglement in the crystal giving a 3-dimensional honeycomb network. [112]

Recently, Rosseinsky *et al.* reported two isorecticular 3-dimensional peptide-based porous frameworks with Gly-L-His-Lys and Gly-L-His-L-Gly to Cu<sup>II</sup> (Table 2, entries 18 and 19, respectively) which displayed higher solvent accessible volumes (47 % and 60.2 %, respectively), than previously reported with shorter dipeptides. [113] Upon desolvation both undergo structural collapse, however, they exhibit sponge-like amorphous-to-crystalline transformation when exposed to water, recovering their open porous framework. During desolvation, the frameworks are not porous to CO<sub>2</sub>, and both frameworks exhibited very low uptakes at 195 and 298 K at 1 bar and 10 bar respectively. [113]

Yaghi *et al.* reported the synthesis of fibers based on Cd linked with the pentapeptide NH<sub>2</sub>-Glu-*p*CO<sub>2</sub>Phe-*p*CO<sub>2</sub>Phe-Ala-Gly-OH, (Table 2, entry 20), in which two infinite Cd<sup>II</sup> chains were linked by the peptide in a double-ladder fashion and proliferate along the longitudinal axis of the fibers. [114] The structure has the terminal Glu amino acid reacting in an intramolecular fashion to form a 2-pyrrolidone moiety in the assembly process. Here, the Cd binds the ligands through both the *p*CO<sub>2</sub>Phe and Gly moieties, [114] with the *p*CO<sub>2</sub>Phe moiety bridging between the two Cd<sup>II</sup> ions and a monodentate coordination mode through Gly. [114] The structure is further stabilized by a complex net of intra- and inter-molecular hydrogen bonding, where the amide bonds of the stacked ligands stabilize the double ladder (intramolecular). [114] While intermolecular hydrogen bonding occurs between water ligands and the 2-pyrrolidone carbonyl, the non-coordinating carboxylic component in the amino acid of *p*CO<sub>2</sub>Phe and terminal carboxylate of the entire structure, and finally between then 2-pyrrolidone amide and the non-coordinating carboxylic component of *p*CO<sub>2</sub>Phe which are donor-acceptor hydrogen pairs, further acting as a secondary interaction in the formation of the macroscopic structure. [114]

### 3.3. Nucleobases

Nucleobases are suitable bio-ligands for the design and synthesis of metal-organic supramolecular arrays due to their large number of oxygen and nitrogen donor sites of different basicity. This is a strong motivation to employ nucleobases for the formation of bio-MOFs as they have the potential to form numerous interactions, including coordination bonds, hydrogen-bonds and  $\pi$ - $\pi$  stacking interactions. The multifunctionality and variety of binding modes in nucleobases within a structure can give rise to structural flexibility as seen in biological molecules such as proteins and peptide based frameworks.

Transition metal complexes containing nucleobases have also been studied in order to explore the DNA-metal binding processes which are vital for the development of new biologically active metallodrugs. With the added benefits of being biologically and environmentally friendly, they are also naturally abundant and easy to produce, thereby keeping industrial costs low. To date, the most commonly reported bio-MOFs are based on Adenine (Ade). [52, 115-120]

Despite the advantages, bio-MOFs containing nucleobases are not exhaustive, which may be the result of no control over their binding modes to metal ions, and their inherent lack of symmetry which inhibit packing in the formation of crystalline materials. Most of the examples reported in the literature highlight the rich coordination modes of Ade leading in the formation of highly porous bio-MOFs. Ade has five N atoms with different basicity; two pyrimidinate N1 and N3, two imidazolate N7 and N9 and one amino group N6 and all are available for metal coordination. Ade can be then mono-, bi-, tri-, or tetradentate coordinating ligand within the bio-MOF structure through [N3], [N9], [N3, N9], [N7, N9], [N1, N9], [N1, N7], [N3, N7], [N3, N7, N9], [N1, N6, N9], [N2, N6, N9] or [N1, N3, N7, N9] (Table 3, entries 1-20). [121-129]

Rosi *et al.* demonstrated that the use of a symmetric zinc-adeninate secondary building unit can overcome problems such as undesired coordination modes between Ade and metal ions, while increasing symmetry. [52, 115] The first nucleobase bio-MOF with formula of [Zn<sub>8</sub>(Ade)<sub>4</sub>(bpdca)<sub>6</sub>O-2Me<sub>2</sub>NH<sub>2</sub>]<sub>8</sub>·8DMF·11H<sub>2</sub>O was composed with eight Zn<sup>II</sup> ions linked to four Ade ligands via [N1], [N3], [N7] and [N9] coordination modes, and infinite Zn<sup>II</sup>-Ade columns made of apex sharing Zn<sup>II</sup>-Ade octahedral cages. [52] This is compared to [Co<sub>2</sub>(Ade)<sub>2</sub>(COOCH<sub>3</sub>)<sub>2</sub>]<sub>2</sub>·2DMF·0.5H<sub>2</sub>O, which consists of Co<sup>II</sup>-Ade-acetate paddlewheel clusters made of two Co<sup>II</sup> ions bridged by Ade *via* N3 and N9 coordination, and two acetate ligands. [115, 130] [Co<sub>2</sub>(Ade)<sub>2</sub>(COOCH<sub>3</sub>)<sub>2</sub>]<sub>2</sub>·2DMF·0.5H<sub>2</sub>O is built by further linking the clusters to Ade *via* [N7] coordination, and has cavities that are periodically distributed.

The versatility of Ade as an organic ligand has continually proven itself to be a key in designing multidimensional frameworks. In combination with aliphatic monocarboxylic acids and Cu<sup>II</sup>, the 3-dimensional, robust open frameworks [Cu<sub>2</sub>( $\mu_3$ -ade)<sub>2</sub>( $\mu_2$ -OOC(CH<sub>2</sub>)<sub>n</sub>CH<sub>3</sub>)<sub>2</sub>]<sub>3</sub>·xH<sub>2</sub>O [*n* from 0 (acetate) to 5 (heptanoate)] can be constructed using inexpensive reagents. [131] The basic building unit of these bio-MOFs is a center symmetric dimer where two carboxylic ligands ( $\mu$ -O,O' coordination mode) and two Ade ligands ([N3] and [N9] atoms) are coordinated to two Cu<sup>II</sup> atoms forming a paddlewheel unit. [131] Ade displays a tridentate coordination mode  $\mu$ -[N3, N7, N9], due to the cross-linking of units through the coordination of the [N7] atom in the adeninate ligand to four adjacent entities with a 5.97 Å Cu...Cu separation across the imidazole N9/N7 bridge. Hydrogen bonding interactions between the [N6]-H6A group of the Hoogsteen face of the nucleobase and the coordinated O atom of the carboxylic ligand reinforces the linkage, as well as forms a R<sub>1</sub><sup>1</sup> (7) ring. [131]

Similar to amino acids, Ade was mixed with a carboxylic acid and Cd<sup>II</sup> (IN: isonicotinic acid) in order to isolate a porous bio-MOF. Kang and Wang reported a new 3-dimensional bio-MOF [Cd<sub>2</sub>(Ade)<sub>2</sub>(IN)<sub>2</sub>(DMF)(H<sub>2</sub>O)]·DMF with a cadmium-adeninate paddlewheel subunit (Table 3, entry 14). [132] Within [Cd<sub>2</sub>(Ade)<sub>2</sub>(IN)<sub>2</sub>(DMF)(H<sub>2</sub>O)]·DMF, there are two cadmium (Cd1 and Cd2) atoms; one is square-pyramidal (Cd1) with four different nitrogen atoms (Ade) and one oxygen atom (IN), while the other (Cd2) is octahedrally coordinated with three oxygen atoms (one

water, one DMF molecule and one carboxylate from IN), and three nitrogen atoms ([N7, N3, N9] from Ade, and N from IN). [132] Adenine acts independently as a  $\mu_3$ -linker to bridge three Cd atoms, and the structure consists of a cadmium-Ade paddle-wheel units, in which two Cd1 atoms are bridged by four Ade. [132] The  $\text{Cd}_2(\text{Ade})_4$  units are further bridged by Cd2 atoms to form a chain along the a axis. [132] The axial position is occupied by two pendent IN ligands, while one links two adjacent Cd2 atoms to form a chain, and the other coordinates a Cd1 atom by acting as a pendent ligand. [132]

To overcome the disadvantage of low symmetry, the introduction of a highly symmetric co-ligand has proven to be useful strategy for the introduction of nucleobases into MOFs. [133] Within  $\text{Zn}_3[\text{Zn}_2(\mu_2\text{-H}_2\text{O})_3(\text{Ade})_6(\text{TATB})_4(\text{DMF})_2]$ , two distinctive building units were identified in the structure due to the multiple binding modes of Ade. The first building unit contains two adenines which are linked by a four-coordinated  $\text{Zn}^{\text{II}}$  via the imidazolate [N7] atoms and two carboxylates. [133] In the second building unit, the binuclear  $\text{Zn}^{\text{II}}$  unit is bridged by two Ade ligands through [N3, N9], at the two equatorial positions, while two carboxylates coordinate at the two axial positions. [133] One-dimensional Zn-adeninate chains were formed with adeninate connected to both building units in a 1:1 ratio. [133] In each adeninate, it should be noted, that the [N7] donors coordinate to the first building unit, the [N3], and [N9] coordinate to the second building unit and the [N1] and [N6] atoms were uncoordinated. [133]

Using  $\text{Co}^{\text{II}}$ , Ade and aromatic tetracarboxylic acids  $\text{H}_4\text{TCPB}$  and  $\text{H}_4\text{BTcC}$ , 3-dimensional bio-MOFs were composed. [121]  $[\text{Co}_3(\mu_6\text{-TCPB})(\mu_4\text{-H}_2\text{TCPB})(\text{Ade})_2]\cdot\text{H}_2\text{O}$  is a compact network, in which three  $\text{Co}^{\text{II}}$  ions are bridged by two bidentate Ade ligands through [N3] and [N9]. [121, 134]  $[\text{Co}_2(\text{Ade})(\mu_6\text{-BTcC})(\mu\text{-H}_2\text{O})(\text{H}_2\text{O})_2]\cdot 4(\text{H}_2\text{O})$  is comprised of bidentate Ade ligands forming binuclear  $\text{Co}^{\text{II}}$  clusters through both the [N3] and [N7] sites, leading to 1-dimensional  $\text{Co}^{\text{II}}$ -Ade chains. [121, 134] The latter structure is shown to have reversible structural transformations upon removal and addition of  $\text{H}_2\text{O}$ , giving a color change from pink to purple, respectively. [134] The indication of a color change implies a change in the coordination geometry of  $\text{Co}^{\text{II}}$  from an octahedral to tetrahedral upon removal of coordinated  $\text{H}_2\text{O}$ . [134-137]

While the above examples highlight the rich coordination modes of Ade leading in the formation of highly porous bio-MOFs, nucleobases such as Gua and their derivatives, are known to form G-quartet, and G-quadruplexes structures which have emerged as powerful tools for developing nanoscale porous materials and devices. [138-145] Verma *et al.* reacted N9-allylguanine and N9-propargylguanine with cupric halides to form three structures ranging from discrete trinuclear motif to a mixed valence coordination polymer (Table 3, entry 16). [146]

The first existing example of a crystallographically characterized nucleobase-incorporated metal-organic polyhedron (TMOP-1, Thy-incorporated MOP) has also been reported by Zhou *et al.* (Table 3, entry 17). [133] Block crystals of TMOP-1,  $\text{Cu}_{24}(\text{MDPI})_{24}(\text{DMA})_4(\text{H}_2\text{O})_{20}$  were obtained, and following XRD analysis, they found two types of  $\text{Cu}_2$ -paddlewheel secondary building blocks in the structure due to different coordinating solvents at the axial position of the  $\text{Cu}_2$ -paddlewheels on the exterior surface of the cage. [133] Packing of TMOP-1 could have been facilitated by the coordination of a DMA molecule, forming a  $\pi$ - $\pi$  interaction pair with the synthetically attached Thy in the isophthalate moiety, from an adjacent MOP. [133] As well as through hydrogen bonding between two adjacent Thy molecules from two different MOPs. [133]

### 3.4. Saccharides

Cyclodextrins (CD) are  $\alpha$ -1,4-linked cyclic oligomers of glucopyranose, which commonly fall into  $\alpha$ -CD,  $\beta$ -CD and  $\gamma$ -CD, containing six, seven and eight glucopyranose units respectively. [147], [148] The structure of the cavity is toroidal, containing an apolar cavity with primary hydroxyl groups lying on the outside while the secondary groups are inside. Their ability to form inclusion complexes has been exploited in various areas of research (including MOFs) for drug carrier systems, the food industry, cosmetics and more. [149] The guest-host complex formation factors with organic molecules are Van der Waals, hydrophobic interactions, size effects and hydrogen bonding. [149]

Saccharides, such as CD, are appealing bio-ligands for the construction of bio-MOFs as they can be prepared entirely from edible ingredients. For example, the synthesis of  $\gamma$ -CD can be synthesized using a salt substitute (KCl) in bottled water and Everclear grain spirit. [150]  $\gamma$ -CD is mass produced enzymatically from starch, and comprised of eight asymmetric  $\alpha$ -1,4-linked  $\beta$ -glucopyranosyl residues. [150] These bio-ligands are linked by potassium ions to form a symmetrical cyclic oligosaccharide, which forms a body-centered cubic structure. The symmetrical arrangement in  $\gamma$ -CD of eight asymmetric  $\alpha$ -1,4-linked  $\beta$ -glucopyranosyl residues is thought to be a key parameter for the construction of CD-MOF-2 by Stoddart *et al.* who reported their exploitation of  $\gamma$ -CD as a multidentate organic ligand to form functional bio-MOFs with the empirical formula  $[(\gamma\text{-CD})(\text{MOH})_2]$  (where M:  $\text{K}^+$  or  $\text{Rb}^+$ ). [150] Overall, six  $\gamma$ -CD units of the  $(\gamma\text{-CD})_6$  cube are held together by four  $\text{K}^+$  ions that are associated with the C6 OH groups and the glycosidic ring oxygen atoms of four  $\alpha$ -1,4-linked  $\beta$ -glucopyranosyl residues on the primary face of the  $\gamma$ -CD tori. [150] The  $(\gamma\text{-CD})_6$  cubes are coordinated to four  $\text{K}^+$  ions to the C2 and C3 OH groups of the other residues on the secondary faces of the  $\gamma$ -CD tori. [150] Therefore, each  $\text{K}^+$  ion is eight-coordinated with two primary OH groups, two glycosidic ring oxygen atoms and four secondary OH groups. [150]

Stoddart *et al.* reported a six-membered cyclic variant,  $\alpha$ -cyclodextrin ( $\alpha$ -CD) with  $\text{RbOH}$  to form long needles with hollow interiors – CDMOF. [151] The hollow nature of the  $\alpha$ -CD based MOF is a rare example of a solid-state material containing sorting domains and porosity on both the nanoscopic and macroscopic scales. Structurally, the  $\text{Rb}^+$  cations are linked to the  $\alpha$ -1,4- $\beta$ -Glucp residues through the C2, C3, and C6 ring oxygen atoms on their primary and secondary faces, however not every residue in the  $\alpha$ -CD ring is coordinated to a  $\text{Rb}^+$  cation. [151] There are two different coordination modes present, one in which four  $\alpha$ -1,4- $\beta$ -Glucp residues interact with the  $\text{Rb}^+$  cation and the other where five interact. Furthermore, the bio-MOF consists of three different 4-, 8- and 10-coordinated SBUs. [151] Both the 8- and 10-coordinated SBUs have similar arrangements in their  $\alpha$ -1,4- $\beta$ -Glucp residues, however it is speculated that the two O atoms that are not part of any  $\alpha$ -ring in the 10-coordinate SBU correspond to  $\text{OH}^-$  counterions associated with  $\text{Rb}^+$  counterions or lingering  $\text{H}_2\text{O}$  molecules remaining from the synthesis of the material. [151]

Recently, MasPOCH *et al.* have described the first coordination polymer made of octakis-[6-deoxy-6-(3-mercaptopropanoic sodium)]- $\gamma$ -cyclodextrin and  $\text{Cu}^{\text{II}}$ , here after referred to as Cu-SD, that shows selective water-induced reversible structural transformations (Table 4, entry 2). [152] Here, SD is an octacarboxylate  $\gamma$ -CD in which one of the eight C6 hydroxy groups has been exchanged with sulfonyl

propionic acid, which was initially proposed to strengthen the bonds between the CD ligand and metal ions. [152] The  $[\text{Cu}_4(\text{SD})(\text{H}_2\text{O})_4]\cdot 46\text{H}_2\text{O}$  material crystallizes into a 2-dimensional structure comprised of dinuclear  $\text{Cu}_2(\text{OOC})_4(\text{H}_2\text{O})_2$  paddle-wheel clusters, with all  $\text{Cu}^{\text{II}}$  adopting a square base pyramid geometry coordinated to four oxygen atoms from four carboxylic groups, and one water molecule occupying the apical position. Crystals dried at room temperature rapidly lost guest molecules undergoing a structural transformation observable through the development of cracks in the solvated crystals. Powder X-ray diffraction revealed a shift and a widening of most of the peaks indicating a loss in crystallinity. However, upon immersion in water, the resulting crystals recovered their initial phase. Remarkably, crystals soaked in other solvents (acetonitrile, ethanol, and DMF) did not result in a reversible transformation, indicating that this bio-MOF is selective only to water. [152]

#### 4. Porous bio-MOFs

While MOFs have emerged as an extensive class of crystalline materials, their attractive properties such as crystallinity, variability of both the organic and inorganic components within their structure and high porosity make them appealing for a plethora of applications. [153] Many of their applications hinge on important properties of MOFs: porosity, stability, tailored pore surface and crystallinity. [154] Porous MOFs are the bread and butter of applications such as adsorption/desorption of gases (gas storage), gas separation, ion exchange, enantiomer separation and selective catalysis. Permanently porous material is generally required for enantioselective separation and/or catalysis. Generally, challenges associated with porosity are linked to the host or framework stability upon removal of coordinated to the metal center solvent molecules or in the removal of guest molecules, with both still remaining synthetically challenging to “design” and construct robust and porous MOFs for reversible adsorption and desorption of guest molecules (e.g. gas storage and catalysis) while they retain their crystallinity. [155]

Zhang *et al.* reported two homochiral  $\text{Zn}^{\text{II}}$  based bio-MOFs constructed from  $\text{D}$ - or  $\text{L}$ -Ser, an amino acid that contains -OH, -COOH, and  $-\text{NH}_2$  polar functional groups and  $\text{H}_2\text{BDC}$ . [94] For  $[\text{Zn}_4(\text{L-Ser})_2(\text{BDC})]\cdot 6\text{DMF}$  (referred to as 1-L), the homochiral structure chains built from enantiopure  $\text{L-Ser}$  and Zn are linked by achiral BDC ligands forming a rod-and-spacer motif with large rhombic channels, and the  $-\text{NH}_2$  group of  $\text{L-Ser}$  bridging two Zn centers with a  $\text{Zn}\cdots\text{Zn}$  distance of 3.52 Å. [94] Each of the five-coordinate Zn centers ( $\text{ZnO}_4\text{N}$ ) has a distorted trigonal bipyramidal geometry, connected by the  $\text{L-Ser}$  ligands into homochiral chains running along the  $c$ -axis. [94] The O atoms in the achiral BDC ligand occupy the equatorial positions of the homochiral chains, bridging these parallel chains to form a neutral 3-dimensional framework which has large channels running along the  $c$ -axis. [94]  $[\text{Zn}_4(\text{D-Ser})_2(\text{BDC})]\cdot 6\text{DMF}$  (1-D) is isostructural with 1-L but with  $\text{D-Ser}$  incorporated in the structure instead of  $\text{L-Ser}$ . Both 1-L and 1-D showed high storage capacity of  $\text{CO}_2$  at ambient temperature and is selective to  $\text{CO}_2$  over  $\text{N}_2$  and  $\text{CO}$ , which is associated to the presence of  $\pi$ -electrons of the ligands and the polar  $-\text{NH}_2$  groups, forming an electric field thereby inducing a dipole in  $\text{CO}_2$ , leading to efficient interactions occurred between  $\text{CO}_2$  and  $\text{NH}_2$ . [94]

Most of the open bio-MOFs fall into the microporous category with pore sizes  $< 2$  nm. Enlarging their channel sizes to the

mesoporous range (2-50 nm) remains challenging, with only a few of these frameworks containing mesoporous channels. [27, 115, 154, 156-160] However, bio-MOF-100 with a formula of  $\text{Zn}_8(\text{Ade})_4(\text{BPDC})_6\text{O}_2\cdot 4\text{Me}_2\text{NH}_2\cdot 49\text{DMF}\cdot 31\text{H}_2\text{O}$  was found to be porous with BET surface area of  $4300\text{ m}^2/\text{g}$ , and low crystal density ( $0.302\text{ g}/\text{cm}^3$ ). The shape of the  $\text{N}_2$  isotherm collected at 77K (type IV) suggests that bio-MOF-100 has interconnected mesoporous channels running throughout the structure with a pore volume exceeding  $4\text{ cm}^3/\text{g}$ . [3, 115] The structure consist of zinc-adeninate octahedral building units (ZABUs) with eight zinc cations, four Ade ligands, and two apical oxo groups bridging two Zn cations together.

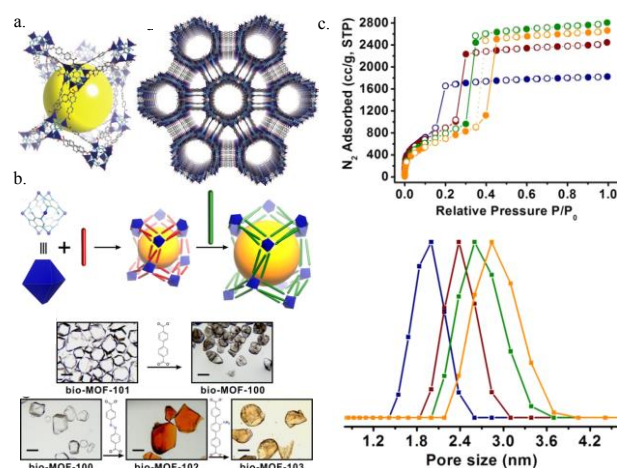


Figure 1: Isoreticular series bio-MOF-100 to -103, with increasing pore size based on systematically changing and increasing ligand size. a) and b) SBU of bio-MOF-100 and illustration of ligand exchange, c)  $\text{N}_2$  isotherms with surface areas ranging from 2704-4410  $\text{m}^2/\text{g}$ , color coding: Bio-MOF-1 (navy), Bio-MOF-100 (red), Bio-MOF-102 (green) and Bio-MOF-103 (orange). (© 2013 American Chemical Society, reprinted with permission) [161]

[115] Twelve BPDC linkers connect each cage to four neighboring cages, which is repeated in the framework generating large cavities in the structure and solvent channels measuring about 28 Å in diameter. [115] The ZABU units further adopt a distorted truncated tetrahedron topology with two angles of  $100.01^\circ$  and two angles of  $130.73^\circ$ , therefore, these ligands do not pack into an ideal diamond lattice, but they adopt an augmented LCS topology, and an open structure. [115] These characteristics distinguish bio-MOF-100 from bio-MOF-1, which has a framework comprised of infinite columnar stacks of apex-sharing  $\text{Zn}^{\text{II}}$ -Ade octahedral units, with a BET surface area that is smaller ( $1680\text{ m}^2/\text{g}$ ). Rosi *et al.* reported new isoreticular analogues of bio-MOF-100: bio-MOF-101, -102 and -103 (Figure 1). [161] This was the first demonstration of systematically increasing the pore dimensions using ligand exchange in bio-MOFs which represents a universal method for increasing the porosity in MOFs while avoiding interpenetration (provided the original MOF is also non-interpenetrated), and allowing access to bio-MOF materials that may be thermodynamically unfavorable. [161] The ligands NDC (bio-MOF-101), ABDC (bio-MOF-102) and  $\text{NH}_2\text{-TPDC}$  (bio-MOF-103), all with type IV adsorption isotherms) were used to methodically increase the pore size, and while this is an isoreticular series of MOFs, the exchange of ligands is possible due to the fact that ZABUs are very stable. [161] As expected, bio-MOF-102 and 103 have the largest pore volumes that exceed  $4\text{ cm}^3/\text{g}$  ( $4.36$  and  $4.13\text{ cm}^3/\text{g}$  respectively) and bio-MOF-101 has the smallest pore volume of  $2.83\text{ cm}^3/\text{g}$ . [161] This strategy demonstrates that ligand exchange can be used to increase pore size, creating a more porous isoreticular



analogue without sacrificing crystallinity. [161] Nucleobases have the ability to bind to metals through a variety of different donor atoms, leaving the non-coordinated atoms open, which can in turn be used to enhance the interactions within the pores of MOFs. For the spatial host-guest binding within a MOF, there are two prerequisites: 1) guest accessible nanoscale sized pores, 2) nucleobase residues are required to be immobilized on the internal surface, leaving the base-pairing sites with open Watson-Crick faces. [162] Purine ligands are well-known for their ability to build binuclear complexes *via* their [N3] and [N9] bridging modes, and previous literature has demonstrated that Adeninate ligands can form paddle-wheel complexes, with the entities self-assembling via Watson-Crick ([N6]-H, [N1]) and Hoogsteen faces ([N6]-H, [N7]) *via*  $\pi$ - $\pi$  stacking. [163]

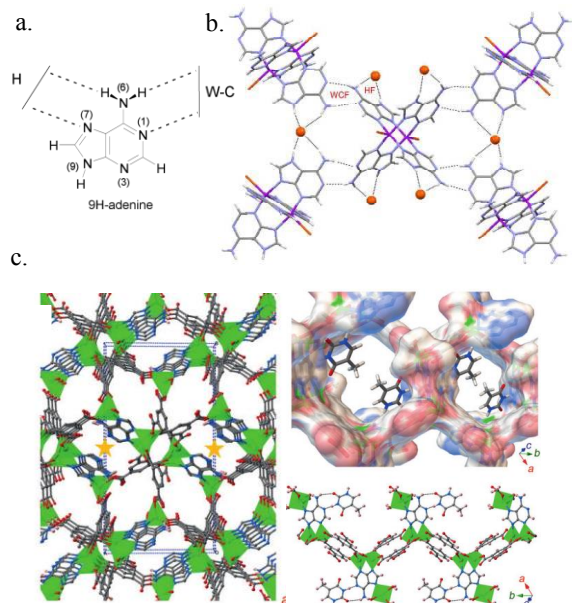


Figure 2: a) Watson Crick (W-C) and Hoogsteen (H) face of Ade, b) Hydrogen bonding of Ade through both faces in the framework (© 2014 American Chemical Society, reprinted with permission), [163] c) the W-C face of Ade in ZnBTCA are pointing towards the pores and are readily available for hydrogen-bonding with Ade's pair nucleobase, Thy. (©2015 Wiley-VCH VerlagGmbH & Co. KGaA, Weinheim, reprinted with permission) [162]

Thomas-Gipson *et al.* reported  $[\text{Cu}_2(\mu\text{-Ade})_4(\text{X})_2]^{2+}$  and  $[\text{Cu}_2(\mu\text{-Ade})_4(\mu\text{-X})_2(\text{X})_2]^{2+}$  (where X is either  $\text{Cl}^-$  or  $\text{Br}^-$ ) metal-nucleobase binuclear entities to develop supramolecular bio-MOFs based on Watson-Crick and Hoogsteen hydrogen bonding interactions of adjacent Ade molecules. [163] The non-coplanar propensity of  $[\text{Cu}_2(\mu\text{-Ade})_4(\text{X})_2]^{2+}$  building blocks, afforded an open framework with 1-dimensional channels of 6 Å, in both  $\text{Cl}^-$  and  $\text{Br}^-$  frameworks, that are sustained through the hydrogen bonding base pairing interactions of the Watson-Crick faces, while the  $[\text{Cu}_2(\mu\text{-Ade})_4(\mu\text{-X})_2(\text{X})_2]^{2+}$  synthons did not allow a 3-dimensional architecture based on such interactions between the nucleobases. [163] Instead, in  $[\text{Cu}_2(\mu\text{-Ade})_4(\mu\text{-Cl})_2(\text{Cl})_2]^{2+} \cdot 2\text{MeOH}$ , base pairing interactions produced an 1-dimensional supramolecular ribbon of binuclear entities, establishing additional hydrogen bonds between the Hoogsteen faces and the  $\text{Cl}^-$  of the adjacent ribbons, reinforced by the  $\pi$ - $\pi$  stacking amidst the Ade, affording a robust microporous 3-dimensional structure (Figure 2). [111, 163]

Highly porous Ade-based bio-MOFs have been prepared using co-ligands of different mono-, di- and tri-carboxylic acids. [52, 111,

115, 130, 161, 164, 165] This has also very recently been demonstrated by Li *et al.*, reporting an Ade-based bio-MOF with formula of  $\text{Zn}_3(\text{Ade})(\text{BTC})_2(\text{H}_2\text{O}) \cdot (\text{CH}_3)_2\text{NH}_2 \cdot x\text{DMF} \cdot y\text{H}_2\text{O}$  (denoted as ZnBTCA). The Watson-Crick faces (Ade-amino sites and neighboring pyrimidine N sites are vacant) of Ade within ZnBTCA are pointing towards the pores of the framework (Table 3, entry 15). [162] ZnBTCA contains 1-dimensional channels, and 68.5% void volume defined by the Connolly surface (used to visualize solvent-accessible surfaces), with a surface area of 3057.5  $\text{m}^2/\text{g}$ . [162] The Connolly surface highlights the guest-contacting regions of the open Watson-Crick sites and the pendant carboxyl oxygen donors. [162] The channels are further interconnected giving an overall three-periodic pore connectivity, and the open Watson-Crick sites are aligned almost parallel to the contacting surface affording channel-connecting windows. [162] Twelve organic dyes that are commonly used as DNA-staining agents (nucleic-acid research) are used, to explore the host-guest chemistry of ZnBTCA, which differed in dimensions, contacting sites, and ionic charges. [162] The authors reported that two guests,  $\text{PfH}^+$  and  $\text{MB}^+$  had special properties in terms of sorption kinetics. [162] Uptake experiments were performed and found that because of the size of  $\text{MB}^+$ , which exceeds the minimum channel diameter of ZnBTCA, it is limited to surface sorption, whereas  $\text{PfH}^+$  takes priority with a moderate uptake amount. Since the channels are large enough to host both  $\text{MB}^+$  and  $\text{PfH}^+$ ,  $\text{MB}^+$  has uptake priority, indicating that the framework and  $\text{PfH}^+$  interact weakly, minimizing the uptake of  $\text{PfH}^+$ . [162] In comparison to bio-MOF-1, ZnBTCA has smaller, less uniform channels and the uptake of guests is found to be much faster. [162] Furthermore, the hysteretic behavior of  $\text{PfH}^+$  is absent in bio-MOF-1 due to open Watson-Crick sites contributing to chemisorption host-guest interactions in ZnBTCA. [162] They further exploited this behavior for Ade-Thy (A-T as in RNA) binding within the constrained pores and found the host framework responded to the Thy binding, as supported indirectly by several pieces of consistent evidence. [162] The implications of their work may enable the boundaries of biology and material science to be extended.

As described, the coordination chemistry of amino acids, peptides, nucleobases and saccharides is rich and MOFs with various structural topologies, different thermal/chemical stabilities and porosities have been constructed. However, bio-MOFs can be structural flexible or robust and they have been assessed for their potential in many areas including: a.  $\text{CO}_2$  capture, b. catalysis and separation, c. sensing and d. biological applications.

## 5. Structural Flexibility and Robustness in bio-MOFs

The adaptability of the porosity of MOFs is limited by the metal coordination geometry and degrees of freedom by the ligands. [105] If the metal coordination geometry does not change, ligands are limited to configurations that are only accessible by uniaxial rotations. [105, 166] Differing from the classical rigid aromatic-based MOFs, ligands such as aliphatic peptides can access to extensive conformational space through low-energy torsions. [107] In response to environmental changes, protein folding can take place between well-defined structures that are associated with large atomic displacements. [167] Overall, peptides have many advantages such as the formation of flexible MOFs (comparable with protein folding), but depending on the interactions between the

layers/chains (via hydrogen-bonding), robust peptide based MOFs can be also generated.

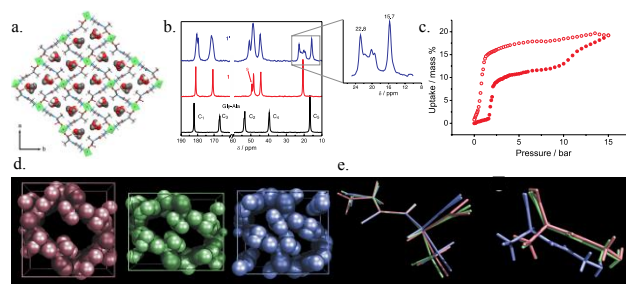


Figure 3: a) The packing of the 2-dimensional layered  $[Zn(GlyAla)_2] \cdot (\text{solvent})$  leads in the generation of pores running along  $c$ -axis, b)  $^{13}C$  (CP/MAS) NMR of the desolvated  $[Zn(GlyAla)_2]$  showing a change in the peptide torsion angle c)  $CO_2$  isotherms collected at 273K and 15 bars show a sigmoidal shape – up to 2 bar there is no uptake revealing that the pores are collapsed but after 2 bar there is a gate-opening, d) representation of the deformation of the  $zn(\text{glyala})$  upon desolvation which is resulted from the torsion of the flexible glyala peptide (e) (© 2010 American Association for the advancement of Science, reprinted with permission) [105]

A bio-MOF constructed with  $Zn^{II}$  and the dipeptide ligand GlyAla, possesses conformational degrees of freedom as observed in protein folding. [105] The framework of  $[Zn(GlyAla)_2] \cdot (\text{solvent})$  is based on tetrahedrally coordinated Zn ions in which each Zn is coordinated to four dipeptide ligands; two dipeptide ligands are coordinated via the N-terminal Gly amine groups, while two are coordinated by the C-terminal Ala carboxylate groups (Figure 3). [105] A grid like structure with layers is formed through the coordination of two zinc ions to each ligand. [105] The porosity has a complex topology defined by the side chains of the methyl groups in the  $L$ -Ala component of the dipeptide within the channels. [105] The polar methanol solvent that has been used as a solvent to construct this bio-MOF, occupies the pores interacting with the pore wall –carboxylate and amine groups *via* hydrogen bonding. [105] The  $^{13}C$  (CP/MAS NMR) of the desolvated  $[Zn(GlyAla)_2]$  showed the expected five resonances, slightly shifted from the single crystallographically distinct peptide itself. However, the resonance corresponding to the methyl group splits into several resonances suggesting that the methyl group is surrounded by different chemical environments. In combination with the sigmoidal  $CO_2$  isotherms (gate opening) and simulations, it was concluded that the pores collapse upon desolvation. However small molecules with polar bonds such as  $CO_2$  and methanol trigger the pores to open gradually. [105] The adaptability of the pores is a direct effect of the peptide ligand, in which the four synergistic torsional degrees of the GlyAla permit the accessible void volume to be controlled by the methyl group. [105]

Deformation of the host framework, and the low energy states that are accessed, are characterized by cooperative torsions that are thermally accessible in the arrangement of the ligands in  $[Zn(GlyAla)_2]$  by interactions of the coordinated metal center, and the hydrogen bonding in the rigidly planar amide unit hanging the ligand from GlyAla to GlyThr affords  $[Zn(GlyThr)_2] \cdot MeOH$ , an also 2-dimensional bio-MOF which displays 1-dimensional pores.[168] Here,  $Zn^{II}$  has a distorted octahedral geometry and each  $Zn^{II}$  metal center is coordinated six-fold by four dipeptide molecules. [168] Two peptides interact through the monodentate C-terminus of the Thr carboxylate group, and two other forming a five-membered N,O-chelate with the amine and oxo groups of the N-terminus Gly

residue. [168] Each GlyThr acts as a  $\mu_2$ -ligand, connecting two metal ions thereby forming 2-dimensional grid-like layers along the  $b$ -axis, whereas the 1-dimensional channels are packed along the  $a$ -axis, occupied by methanol guest molecules. [168]

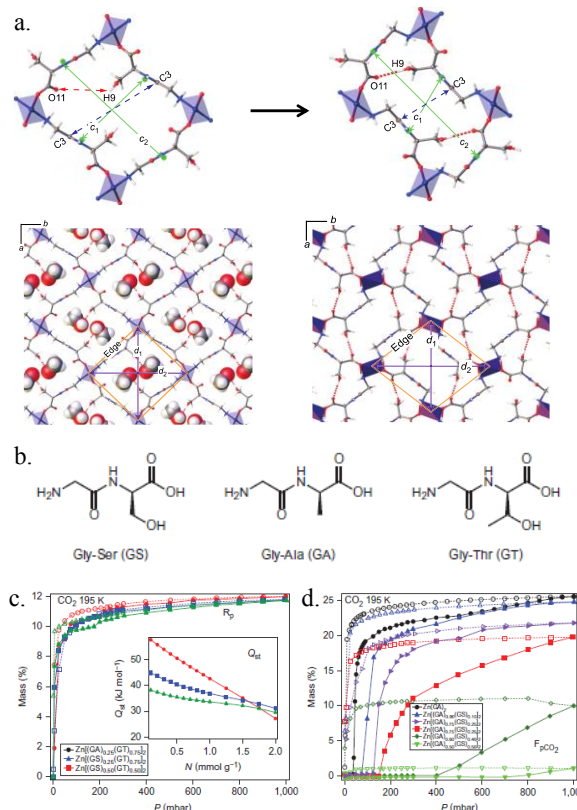


Figure 4: a) top: open-to-closed SCSC transformation highlighting changes in peptide-to-peptide separation, bottom: square and rhomboidal (left and right, respectively) packing of both structures (before and after desolvation) viewed along the  $c$ -axis showing that the distances between metal centers  $d_1$  and  $d_2$  decrease upon desolvation, b) structure of peptides used for the construction of mixed-peptide bio-MOFs c)  $CO_2$  isotherm at 195 K of mixed ligand systems with isosteric heats of adsorption (inset) for  $Zn[(GA)_{0.25}(GT)_{0.75}]_2$  (black),  $Zn[(GS)_{0.25}(GT)_{0.75}]_2$  (blue), and  $Zn[(GS)_{0.50}(GT)_{0.75}]_2$  (red) d)  $CO_2$  isotherms at 195 K of  $Zn(GA)_2$  (black),  $Zn[(GA)_{0.90}(GS)_{0.10}]_2$  (blue),  $Zn[(GA)_{0.75}(GS)_{0.25}]_2$  (purple),  $Zn[(GA)_{0.75}(GS)_{0.25}]_2$  (red),  $Zn[(GA)_{0.60}(GS)_{0.40}]_2$  (dark green),  $Zn[(GA)_{0.50}(GS)_{0.50}]_2$  (light green). (©2014 Macmillan Publishers Limited, reprinted with permission). [107]

$[Zn(GlyThr)_2]$  behaves as a "classically" rigid microporous framework due to the rigidity of the GlyThr ligand which is due to its conformation *via* intralayer hydrogen bonding, as well as the structure remaining unchanged upon activation. [168] Reinforcement of structural stability can be attributed to the -OH groups found in the side chains of the Thr amino acid, which enable inter- and intra-layer hydrogen bonding, overall favoring chelation between the metal ion and the peptide. [168] This reinforcement and interaction is specific to the Thr in the framework, and operates between adjacent layers providing the strengthened structural stability in three-dimensions, resulting in higher cooperativity. [168] Through these features the potential torsional flexibility of the peptide is locked.[168] It should be noted, that the additional hydrogen bonding between the adjacent layers is not present in  $[Zn(GlyAla)_2]$ , further confirming the enhanced rigidity of  $[Zn(GlyThr)_2] \cdot MeOH$ . [168]

Another bio-MOF  $[\text{Zn}(\text{GlySer})_2]$  has also been examined, and has been noted as isostructural to  $[\text{Zn}(\text{GlyAla})_2](\text{solvent})$ . [107] The incorporation of hydroxyl groups in the  $\alpha$ -carbon position of the C-terminus in the oligopeptide, thus imposes a different structure compared to the secondary hydroxyl group of the Thr in  $[\text{Zn}(\text{GlyThr})_2]$ . [107] The structure of  $[\text{Zn}(\text{GlySer})_2]$  is 2-dimensional, with layers built from stacking square like neutral  $[\text{Zn}(\text{GlySer})_2]$  sheets, which are formed by tetrahedral  $\text{Zn}^{\text{II}}$  ions linked to four peptides which act as  $\mu_2$ -bridges. [107] Reposition of the OH-bearing side chain is associated with the torsional degrees of freedom of the Ser residue, which facilitates a significant translation displacement of the peptide. [107] Rosseinsky *et al.* went on to further mix ligands (in a multivariate (MTV)-concept) such as GlySer and GlyAla, this method of combining ligands with similar topology or metals to form MOF solid solutions and modulate their responsiveness and flexibility (Figure 4). [23] [169-173] The mixed-peptide based bio-MOFs were isostructural with those when pure dipeptides were used, with peptide ratios determining the topology of the framework, whereas GlyAla/GlySer/GlyThr: 33/33/33 and GlyAla/GlySer: 50/50 ratios gave  $[\text{Zn}(\text{GlySer})_2]$ -like topologies. [107] At levels of doping  $\geq 75\%$  of GlyThr, GlyThr drives the formation of bio-MOFs with a  $[\text{Zn}(\text{GlyThr})_2]$  structure in GlyAla/GlyThr families, and at  $\geq 50\%$  in the GlySer/GlyThr series, while lower substitution levels adopt the  $[\text{Zn}(\text{GlySer})_2]$  structure. [107] Upon solvent removal, the effects of the hydrogen bonding in the Ser side chain are

demonstrated by the structural change in isostructural  $[\text{Zn}(\text{GlySer})_{0.75}(\text{GlyThr})_{0.25}]_2$  affording a well-ordered material on the local level, whereas guest removal from  $[\text{Zn}(\text{GlyAla})_2]$  produced local torsional disorder of the GlyAla peptide. [107] Removal of guest molecules in  $[\text{Zn}(\text{GlySer})_{0.75}(\text{GlyThr})_{0.25}]_2$  brought about a cooperative single-crystal-to-single-crystal rearrangement of the framework from an open/solvated to closed/desolvated state. [107] Upon MeOH removal, the hydrogen bonds in the -OH side-chain are lost, with the resulting porosity not accessible, and lost hydrogen bonding restored *via* torsional changes in the GlySer ligand, enabling translational ordered displacements of the peptides. [107] The crystallinity transformation enabled by the flexibility of the GlySer ligand, which folds to occupy the empty space, reduces the void space to 2.9% in the closed state, compared to 22.0% in the open one. [107] The conformational change upon guest removal (collapse of the structure) is attributed to the energetically favorable formation of intra-layer hydrogen bonds between the terminal -COO- and the -OH side chain on opposite faces of the channel wall. [107] These three examples highlight that charge on the side chains of peptides can lead in the construction of robust or flexible MOFs, therefore increasing the possibility to design flexible MOFs. They also have similar properties to previously discussed MTV-MOF series.

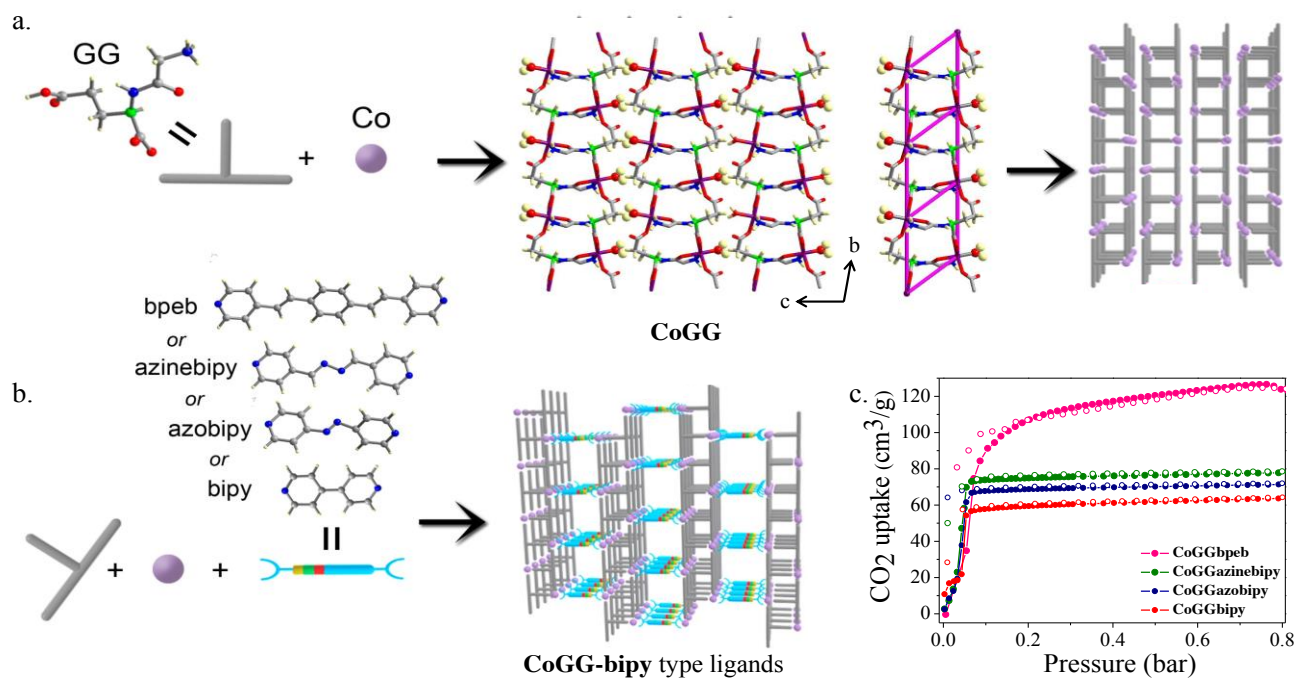


Figure 5: a) Construction of  $(\text{Co-L-GlyGlu})$  chiral rigid ladder, b) Replacement of the terminal coordinated  $\text{H}_2\text{O}$  of  $\text{Co-L-GlyGly}$  with pillared ligands that vary in length, led in the generation of porous, homochiral MOFs  $\text{Co-L-GlyGlu}$ -pillar ligand, c) the  $\text{CO}_2$  uptake at 195 K and 0.8 bar of the isorecticular series increases upon using large ligands to link the  $\text{Co-L-GlyGlu}$  chains. Color scheme (only linker listed for clarity): bpeb (pink), azinebipy (green), azobipy (blue), bipy (red). (© 2015 Wiley-VCH Verlag GmbH & Co. KGaA, Weinheim, reprinted with permission). [65]

Carnosine (Car), with a molecular structure  $\beta$ -Ala-L-His is a natural dipeptide that it has been recently used for the construction of a new 3-dimensional flexible peptide based bio-MOF, ZnCar-DMF. ZnCar is permanent porous upon removal of the guest DMF (see section 3.2 for structural details) with a BET surface area of 448 m<sup>2</sup>/g, and it has an affinity to bind small molecules such as CO<sub>2</sub> and CH<sub>4</sub>. [108] The flexibility is attributed to the hydrogen bonds formed between the dipeptide and guests, which lead to different torsional conformations of Car. [108] The structural stability in the presence of guest molecules proved to be adaptable, as the peptide conformation of ZnCar-H<sub>2</sub>O and ZnCar-MeOH changed without breaking the connectivity motif of 4:4 between Zn and Car. [108] Both MeOH and DMF were found to distort the framework locally by hydrogen bonding, but without generating a phase transition in the framework itself. [108] The loading and removal of MeOH into the ZnCar bio-MOF demonstrates that it can be reused. [108]

In 2006, Rosseinsky *et al.* reported the synthesis of a porous bio-MOF by connecting metal-amino acids (Ni<sup>II</sup>-aspartate) layers with pillar ligands. However, the use of pillar ligands larger than bipy resulted in their crystallization within the pores of NiAspbipy, thus blocking the accessible volume for gas uptake. [174] The open-framework [Ni<sub>2</sub>(L-Asp)<sub>2</sub>(bipy)]·1.28MeOH·0.72H<sub>2</sub>O, contains neutral chiral Ni(L-Asp) layers which are connected by bipy ligands affording a pillared 3-dimensional structure with 1-dimensional channels defined by the separation between the Ni centers in the Ni(L-Asp) layers, and the length of the pillar ligand. [174] The synthesis of [Ni<sub>2</sub>(L-Asp)<sub>2</sub>(azpy)]·(guests) showed a similar layered structure to that observed in [Ni<sub>2</sub>(L-Asp)<sub>2</sub>(bipy)] with a weight loss of 2.9% between 30-200°C (solvent loss), and 70.9% between 350-800°C (decomposition of guest molecules and framework), as determined by thermogravimetric analysis. [89] The thermal stability of [Ni<sub>2</sub>(L-Asp)<sub>2</sub>(azpy)]·(guests) is demonstrated by the high decomposition temperature. Replacing the bipy ligand with its respective derivatives (azpy, bpe, 3rbp, py<sub>3</sub>T and 35bpp), but longer bridging linkers, affords analogous materials with larger channels. [174] CO<sub>2</sub> sorption isotherms were recorded on samples with the ligands azpy, bpe, 35bpp and py<sub>3</sub>T, with the expectation that the materials would be permanently porous due to their robust backbones and solvent-accessible volumes. [89] Unfortunately, even though the ligand size increased, the BET surface areas were very low and CO<sub>2</sub> uptake was less than 0.5 % wt. [89] For the bio-MOFs based on azpy and bpe, the presence of large amount of ligands within the channels prevents access to guest species such as CO<sub>2</sub>. [89] The bio-MOF containing py<sub>3</sub>T was found to be intrinsically non-porous due to the bulky pendant pyridyl group projecting inside the channels, effectively eliminating porosity. [89] To eliminate the presence of excess ligands in the channels, restoration of porosity was achieved by sublimating the excess pillar ligands under high vacuum, which may be attributed to the high stability of the layered structures in these frameworks. [89] Interlayer spacing modification in the ligand (depending on pressure, temperature and guest molecules), suggests that the dimension of the channels could respond selectively and specifically to guest molecules. [89]

While most of the examples previously described have provided researchers with insight on how to design robust or flexible MOFs, there is still a huge challenge to synthesize highly porous and robust peptide MOFs with control over pore size, and that can be used for separations such as gas capture. This was addressed by Maspoeh *et*

*al.* by following the pillar ligand strategy. The use of a peptide with two carboxylate and one amino functions, glycyl-L(S)-glutamate (L-GlyGlu) with Co<sup>II</sup>, leads in the construction of a chiral and rigid ladder (Co-L-GlyGlu) that was used in reticular synthesis to link the ladders and induce porosity (please see section 3.2 for structural description) (Figure 5). [65] Replacing the coordinated terminal H<sub>2</sub>O molecules with pillar ligands with different length such as bipy (Co-L-GlyGlu**bipy**), azobipy (Co-L-GlyGlu**azobipy**), azinebipy (Co-L-GlyGlu**azinebipy**) or bpeb (Co-L-GlyGlu**bpeb**) afforded BET surface areas of 261 m<sup>2</sup>/g, 299 m<sup>2</sup>/g, 315 m<sup>2</sup>/g, and 601 m<sup>2</sup>/g, respectively, allowing for the assembly of porous homochiral MOFs from an originally non-porous structure. [65] The Co-L-GlyGlu units and their stacking are not affected by this process and subsequently the size of the pores is defined by the length of the pillar ligand used. [65] While these MOFs are stable in air or in common organic solvent, they are not stable in H<sub>2</sub>O (as they are hydrolyzed).

## 6. CO<sub>2</sub> Capture

With environmental issues becoming one of the most pressing issues of our age, developing new materials for the selective capture of CO<sub>2</sub> is alarmingly important. MOFs have emerged as promising materials for the selective capture and utilization of CO<sub>2</sub>. To date, research efforts have focused on generating open metal sites or incorporating ligands functionalized with Lewis basic groups; both strategies have shown to be promising for the selective capture of CO<sub>2</sub> over other gasses such as N<sub>2</sub> (flue gas) or CH<sub>4</sub> (natural gas). [1, 20, 28, 175-183] Bio-ligands can be decorated with multiple groups which can be incorporated into bio-MOFs which can be promising candidates for the selective capture of CO<sub>2</sub>.

Adenine based bio-MOFs have shown to be good candidates for the selective capture of CO<sub>2</sub>, and this is attributed to the presence of Lewis basic sites that decorate their pore surface of bio-MOFs. [130, 184] Post-synthetic exchange of extra-framework cations within bio-MOF-1 was used by Rosi *et al.* to modify the pore dimensions, optimize its adsorption properties for CO<sub>2</sub>, and highlights the importance of cations present in the channels of Ade based bio-MOFs. [185] The introduction of cations with different sizes: tetramethylammonium (TMA), tetraethylammonium (TEA) and tetrabutylammonium (TBA), into the pores led in the decrease of the pore volume and BET surface areas from 1680 m<sup>2</sup>/g for bio-MOF-1 to 830 m<sup>2</sup>/g for the TBA loaded bio-MOF-1. [185] It is found however, that the CO<sub>2</sub> adsorbed capacity did not scale with the pore volume or BET surface area, as the TMA loaded bio-MOF-1 adsorbed the most CO<sub>2</sub> (4.5 mmol/g at 1 bar) followed by the TEA loaded bio-MOF-1 (4.2 mmol/g at 1 bar) and the TBA loaded bio-MOF-1 adsorbed 3.41 mmol/g at 1 bar. [185] At elevated temperatures (1 bar) bio-MOF-1 had the lowest CO<sub>2</sub> capacity compared to those MOFs with TEA which had the largest capacity while both TMA and TBA loaded bio-MOFs were equally as effective. [185] It should be noted that the TBA loaded bio-MOF-1 was more effective as a CO<sub>2</sub> sorbent compared to bio-MOF-1, even with half the pore volume and surface area. [185] At lower pressures (up to 0.2 bar) small pore volume positively influenced the uptake of CO<sub>2</sub>. Through further investigation of the isosteric heats of adsorption, it is concluded that small pores lead to stronger interactions occurred between the loaded bio-MOF-1 with CO<sub>2</sub>. [185]

While amine functionalization of a MOF has been proven useful for separating CO<sub>2</sub> and N<sub>2</sub>, the Lewis acid-base interaction between NH<sub>2</sub> and CO<sub>2</sub> has also been shown to improve the selectivity of CO<sub>2</sub>/CH<sub>4</sub> gas separations. [186] Rosseinsky *et al.* constructed [Ni<sub>3</sub>(pzdc)<sub>2</sub>(7Hade)<sub>2</sub>(H<sub>2</sub>O)<sub>4</sub>](H<sub>2</sub>O)<sub>1.5</sub> (where Hade: adenine and pzdc: 3,5-pyrazoledicarboxylic acid) which is stable in standing in liquid water and air for at least 4 weeks. [187] The pH was modified to 5-7 *via* metal ion concentration, allowing for the selective deprotonation of 9Hade [N9] compulsory to form the [N3, N9] bidentate bridging mode, and migration of a hydrogen to the neighboring imidazolate [N7], affording 7Hade coordination as a neutral terminal ligand. [187] In [Ni<sub>3</sub>(pzdc)<sub>2</sub>(7Hade)<sub>2</sub>(H<sub>2</sub>O)<sub>4</sub>](H<sub>2</sub>O)<sub>1.5</sub>, the Ni<sup>II</sup>/7Hade/pzdc chains run parallel to the *c*-axis, and are linked in a 3-dimensional noncovalent network *via* hydrogen bonding and  $\pi$ -stacking. [187] The chains, based on a [Ni(7Hade)<sub>2</sub>]<sup>4+</sup> blade dimer, are formed through the bridging coordination of the imidazolate [N9] and pyrimidinate [N3] atoms to two of the Ni<sup>II</sup>. [187] The pzdc anion links the blade units and also bridges the two Ni cations in the 7Hade-defined blade through a  $\mu$ -O bridge from oxygen. [187] Furthermore, the pzdc completes the Ni<sup>II</sup> coordination via an N16 chelate, forming the chain by the second pyrazole nitrogen N17 binding to a mononuclear Ni<sup>II</sup> center which is also coordinated by the oxygen from the second carboxylate of the anion. [187] Therefore pzdc links Ni<sup>II</sup> dimers via mononuclear Ni<sup>II</sup> centers with each chain linked by two hydrogen bonds (one strong, the other weak) from the 7Hade amino group [N10], to two pzdc carboxylate oxygens and an N(10)  $\rho$ - $\pi$ / $\pi$ - $\pi$  interaction between the 7Hade pyrimidinate rings. [187] Removal of the coordinated H<sub>2</sub>O ligands allows for the mononuclear Ni<sup>II</sup> to become accessible from the principle channel space upon full desolvation. Exposure of the desolvated crystals to air for several minutes regenerates the original diffraction patterns, associated with the reversible atmospheric H<sub>2</sub>O coordination to the Ni<sup>II</sup>. [187]

Following desolvation, a BET surface area of 165.0  $\pm$  4.2 m<sup>2</sup>/g was reported, and the isosteric heats of adsorption measure at 273 K and 298 K for CO<sub>2</sub> increased from 22.4 kJ/mol at 0.8% loading to 34.6  $\pm$  1.7 kJ/mol with an increase in CO<sub>2</sub> loading (5.6% CO<sub>2</sub> uptake). [187] These results are promising since a majority of porous materials show a decrease in isosteric heat of adsorption with an increase in CO<sub>2</sub> loading, this is attributed to the occupation of the favorable sites within a relatively rigid structure. [187] Breakthrough experiments were conducted using a column packed with the material, where an equimolar mixture of CO<sub>2</sub> and CH<sub>4</sub> was passed over it. [187] The authors reported that CH<sub>4</sub> was released at 129 s and after a delay of 28 s CO<sub>2</sub> was detected indicating a clear separation between the gases. [187]

For CO<sub>2</sub> and N<sub>2</sub> separation, bio-MOF MPM-1-TIFSIX [Cu<sub>2</sub>(Ade)<sub>4</sub>(TIF<sub>6</sub>)<sub>2</sub>], has been reported to have a high CO<sub>2</sub> uptake and selectivity under ambient conditions and up to 1 atm, and can be synthesized from commercially available materials in a single step. [188] MPM-1-TIFSIX exhibited higher CO<sub>2</sub> uptake compared to MPM-1-Cl [Cu<sub>2</sub>(Ade)<sub>4</sub>Cl<sub>2</sub>]Cl<sub>2</sub>. Single-gas uptake of CO<sub>2</sub>, CH<sub>4</sub> and N<sub>2</sub> were reported for MPM-1-Cl as 44.2, 13.8 and 4.7 cm<sup>3</sup>/g, respectively, whereas MPM-1-TIFSIX uptake values are 89.6 cm<sup>3</sup>/g, 18.5 cm<sup>3</sup>/g and 8 cm<sup>3</sup>/g. [188] The selectivity was analyzed using 10/90 CO<sub>2</sub>/N<sub>2</sub> and 50/50 CO<sub>2</sub>/CH<sub>4</sub> binary mixtures, which mimic those found in post-combustion and biogas purification, respectively. Separations increased six-fold and five-fold in CO<sub>2</sub> selectivity when TIFSIX replaced Cl<sup>-</sup> (CO<sub>2</sub>/N<sub>2</sub>: 74.1 vs 12.5; CO<sub>2</sub>/CH<sub>4</sub> 20.3 vs 4.0) at 1 atm. [188] Materials that possess thermal and water stability are inherently more practical for CO<sub>2</sub> separations, therefore MPM-1-TIFSIX was tested for those criteria. It was reported that the crystal structure was retained at 568 K and after immersion in water at room temperature for 24 hrs with minimal effects on CO<sub>2</sub> uptake. [188]

Table 5: BET, CO<sub>2</sub> uptake capacities and Q<sub>st</sub> of selected bio-MOFs.

Entry	MOF	BET (m <sup>2</sup> /g)	CO <sub>2</sub> (cm <sup>3</sup> /g) 273K 1 bar	CO <sub>2</sub> (cm <sup>3</sup> /g) 298K 1 bar	Q <sub>st</sub> (1 bar, kJ/mol) (zero coverage)	Ref.
1	bio-MOF-1	1680	77/88	46/50	21.9/24.2	185
2	bio-MOF-1 @ TMA	1460	101	60	23.9	185
3	bio-MOF-1 @ TEA	1220	94	61	26.5	185
4	bio-MOF-1 @ TBA	830	78	51	31.2	185
5	GND <sup>+</sup> @ bio-MOF-1	1640	108	57	28.8	191
6	AmGND <sup>+</sup> @ bio-MOF-1	1600	109	62	28.3	191
7	DiAmGND <sup>+</sup> @ bio-MOF-1	1500	115	68	29.4	191
8	bio-MOF-11	1148	147	105	33.1	164
9	bio-MOF-12	1008	100	71	38.4	164
10	bio-MOF-13	412	60	45	40.5	164
11	bio-MOF-14	17	45	31	---	164
12	II @ bio-MOF-14	N/A	92	N/A	---	190
13	MPM-1-TIFSIX	809	---	90	44.4	188
14	MPM-1-Cl	30*	---	44	---	188
15	[Ni <sub>3</sub> (pzdc) <sub>2</sub> (7Hade) <sub>2</sub> (H <sub>2</sub> O) <sub>4</sub> ](H <sub>2</sub> O) <sub>1.5</sub>	165	---	---	22.4	187
16	TIF-A1	718	82	62	---	124
17	[Zn <sub>4</sub> (bdc) <sub>2</sub> (L-ser) <sub>2</sub> ] <sub>3</sub> ·6DMF	136.9	55.5	37.1	8.2	94
18	[Zn <sub>4</sub> (bdc) <sub>2</sub> (L-ser) <sub>2</sub> ] <sub>3</sub> ·6DMF (1'-L-ht)	224.7	43.7	30.3	7.5	94
19	[Zn(GlyThr) <sub>2</sub> ](CH <sub>3</sub> OH)	192	---	---	15.8	168

\* Langmuir Surface area

--- Not listed

Rosi *et al.* further examined bio-MOF-11 and its isoreticular series bio-MOF-12, 13 and 14 which consists of an Ade linker with two free Lewis-basic sites (pyrimidinate N1 and the amino group N6). [165] It should be noted, that compared to other bio-MOFs, bio-MOF-11 is still the best adsorbent for CO<sub>2</sub> (capacity and selectivity). [189] The authors decorated the pores of bio-MOF-11-12-13-14 with acetate, propionate, butyrate, and valerate, respectively, and the N<sub>2</sub> and CO<sub>2</sub> adsorption properties were then studied. As the length of the aliphatic chains increase, the BET surface areas decrease from 1148 m<sup>2</sup>/g to 17 m<sup>2</sup>/g and the CO<sub>2</sub>:N<sub>2</sub> mixtures range from 73:1 (bio-MOF-11), 123:1 (bio-MOF-12) and 107:1 (bio-MOF-13) at 273 K and 1 bar (determined by ideal adsorbed solution theory calculations, IAST). [165] When the temperature was increased, the selectivities for bio-MOF-11-13 decreased to 43:1, 52:1 and 40:1, respectively. [165] The authors reported that bio-MOF-14 exhibits a molecular sieving property, allowing it to adsorb only CO<sub>2</sub> at 273 and 298 K, and that there is no loss of crystallinity or porosity when the material is soaked in water for one month. [165] An 'ideal' material for CO<sub>2</sub> capture would combine the properties of bio-MOF-11 (high capacity for CO<sub>2</sub> uptake) with that of bio-MOF-14 (high CO<sub>2</sub>:N<sub>2</sub> selectivity and water stability). Implementing a design strategy, Rosi *et al.* targeted the core material of bio-MOF-11 for CO<sub>2</sub> storage and the shell of bio-MOF-14 to act as a gas sieve and shield the material against water. [190] A cobalt-adeninate core-shell structure with a porous mixed ligand core and a water stable bio-MOF-14 shell was successfully prepared by doping valerate into the bio-MOF-11 lattice. This further allowed for growth of the bio-MOF-14 shell and, after repeating the procedure three times, afforded II@bio-MOF-14, where II denotes the core C<sub>2</sub><sub>0.60</sub>C<sub>5</sub><sub>0.57</sub> (with C<sub>2</sub>: acetate and C<sub>5</sub>: valerate). [190] The hybrid material adsorbed 30% more CO<sub>2</sub> than bio-MOF-14 (44.8 cm<sup>3</sup>/g) with a much lower N<sub>2</sub> uptake at 77 K, suggesting that the shell efficiently prevents any significant N<sub>2</sub> uptake by the core. [190] To confirm this, the material was ground, and found that a significantly higher amount of N<sub>2</sub> was adsorbed at 77 K (108 cm<sup>3</sup>/g compared to 54 cm<sup>3</sup>/g), thus it is likely that the N<sub>2</sub> molecules have to pass through the bio-MOF-14 shell to enter the porous core. [190]

In addition, the encapsulation of guanidium (GND<sup>+</sup>), aminoguanidinium (AmGND<sup>+</sup>) and diaminoguanidinium (DiAmGND<sup>+</sup>) within bio-MOF-1 was also studied and determined how this can impact on the CO<sub>2</sub> adsorption properties, as well as their capacities and isosteric heat of adsorption. [191] These cations were selected because of their multiple Lewis basic sites, size comparability to DMA<sup>+</sup> (pore volume does not significantly decrease after cation exchange in bio-MOF-1) and these guanidine derivatives have previously been studied as catalysts for CO<sub>2</sub> chemical fixation. [192, 193] Bio-MOF-1 and GND<sup>+</sup>@bio-MOF-1 had comparable BET surface areas and pore volumes (1630 m<sup>2</sup>/g, 0.70 cm<sup>3</sup>/g and 1640 m<sup>2</sup>/g, 0.70 cm<sup>3</sup>/g respectively). [191] The encapsulation of larger cations: AmGND<sup>+</sup>@bio-MOF-1 and DiAmGND<sup>+</sup>@bio-MOF-1 have observed that the surface areas and pore volumes decreased slightly (1600 m<sup>2</sup>/g, 0.68 cm<sup>3</sup>/g and 1500 m<sup>2</sup>/g, 0.66 cm<sup>3</sup>/g, respectively). [191] At 273 K (1 bar) bio-MOF-1 adsorbed 88 cc/g, GND<sup>+</sup>@ bio-MOF-1 increased to 108 cc/g, along with AmGND<sup>+</sup>@ bio-MOF-1 to 109 cc/g, and DiAmGND<sup>+</sup>@bio-MOF-1 adsorbed 115 cc/g (30% higher than bio-MOF-1). [191] Increasing the temperature to 298 K, 303 K, 308 K

and 313 K, resulted in CO<sub>2</sub> isotherms that followed the same trend as with those collected at 273 K, therefore concluding that for bio-MOF-1, the CO<sub>2</sub> adsorption can be enhanced with the introduction of Lewis basic molecules, and that these sites are beneficial for CO<sub>2</sub> capture. [191]

Recently, it has become of particular interest to create tetrahedral MOFs that would share structural topologies and coordination factors similar to zeolite chemistry. [194-197] Tetrahedral imidazolate frameworks (TIF) tetrahedrally coordinated with divalent cations (Zn<sup>II</sup> or Co<sup>II</sup>) by the uni-negative (when an atom only accepts one electron) imidazolate ligands. [198-202] A new approach was taken by Zhang *et al.* by adding an auxiliary uni-negative ligand into a zinc-imidazolate tetrahedral assembly to generate tetrahedral frameworks with the formula Zn(Im)<sub>x</sub>(L<sub>2</sub>)<sub>2-x</sub>, where L<sub>2</sub> is (Ade)(Int) in TIF-A1, (Im)<sub>3</sub>(Int) in TIF-A2 and (Im)(Int)<sub>2</sub>(OH) in TIF-A3. [124] The authors reported the construction of three new materials (TIF-A1, -A2, and -A3. [Table 3, entry 6](#) and [Table 5, entry 16](#)) with distinct topologies and mixed ligands. Interestingly, TIF-A1 uptakes 82 cm<sup>3</sup>/g and 61.7 cm<sup>3</sup>/g CO<sub>2</sub> at 273K and 298K respectively which is much higher than the current best performing zeolitic imidazolate framework (ZIF-69) (70 cm<sup>3</sup>/g). [124] This is attributed to the amine-functionalized imidazolate ligand, adeninate, incorporated within the structure. [124] In addition, the adsorption selectivity of TIF-A1 for CO<sub>2</sub>/N<sub>2</sub> was measured as 17.5 at 273K and 40.1 at 298K, they further measured adsorption isotherms of N<sub>2</sub> and found hardly any adsorbed at all (4.7 cm<sup>3</sup>/g at 273K and 1.4 cm<sup>3</sup>/g at 298K). [124] The selectivity for CO<sub>2</sub> is thought to be attributed to the specific pore geometry in the structure, with possible interactions between CO<sub>2</sub> and -NH<sub>2</sub> in the pores. [124]

Multidentate ligands, such as Ser, containing -OH, -COOH and -NH<sub>2</sub> have opened up a new approach towards CO<sub>2</sub> capture and selective separation due to its special coordination mode. [94] It is demonstrated that bio-MOF [Zn<sub>4</sub>(BDC)<sub>2</sub>(L-Ser)<sub>2</sub>]<sub>3</sub>·6DMF (1-L-ht) has a lower uptake of N<sub>2</sub> (42 cm<sup>3</sup>/g) and a higher uptake of CO<sub>2</sub> (127 cm<sup>3</sup>/g) which could be a result of the strong polar environment in the pores (see previous structure description of 1-L and 1-D). [94] The BET surface area was shown to be 136.9 m<sup>2</sup>/g, with a pore volume of 0.063 cm<sup>3</sup>/g. [94] This bio-MOF however undergoes through a structural change upon removal of the DMF guest molecules. A similar material was prepared, where DMF was exchanged with MeOH by soaking the 1-L-ht crystals in MeOH for a week. The second DMF free MOF (1'-L-ht) had a maximum N<sub>2</sub> uptake of 92.3 cm<sup>3</sup>/g, a BET surface area of 224.7 m<sup>2</sup>/g and pore volume of 0.081 cm<sup>3</sup>/g. The authors further explored the properties of both materials for CO<sub>2</sub>/N<sub>2</sub> separation under ambient conditions and found that the selectivity is 185:1 for 1-L-ht and 17.5:1 for 1'-L-ht. [94] From a structural standpoint, the gas adsorption selectivity could correlate with the existence of π-electrons in the ligands and the polar -NH<sub>2</sub> groups. [94] Groups such as -NH<sub>2</sub> and C=O in neighboring ligands provides the opportunity for interactions between both CO<sub>2</sub> and N<sub>2</sub>, leading to an increased in lone pair polarization of the electron density in CO<sub>2</sub>. [94] This work highlights the importance of activation on porous materials as well as the impact of the pore geometry in the structure of [Zn<sub>4</sub>(BDC)<sub>2</sub>(L-Ser)<sub>2</sub>]<sub>3</sub>·6DMF. [94]

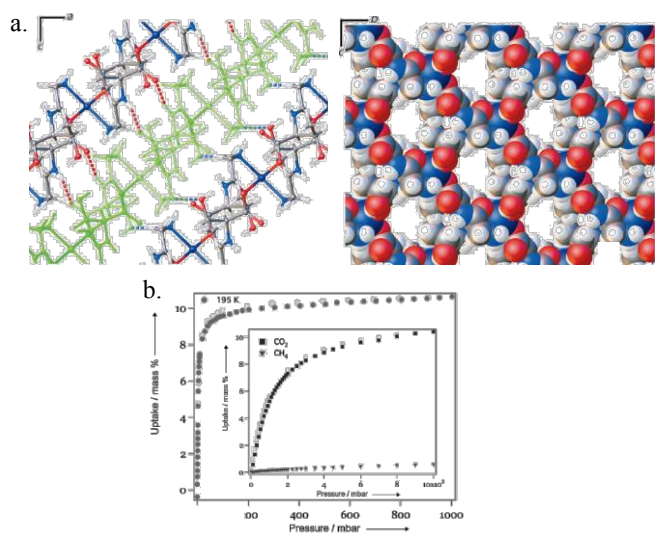


Figure 6: a) Interlayer hydrogen-bonding interactions (dashed lines) (right), and grid-like space filling representation of [Zn(GlyThr)<sub>2</sub>] (left), b) CO<sub>2</sub> isotherm at 195 K – inset shows that [Zn(GlyThr)<sub>2</sub>] is selective to CO<sub>2</sub> over CH<sub>4</sub> at 273 K and 10 bar. (©2012 Wiley-VCH Verlag GmbH & Co. KGaA, Weinheim, reprinted with permission).[168]

Bio-MOFs based on dipeptides, such as [Zn(GlyAla)<sub>2</sub>], have led to adaptable porosity, in which the pore conformation adapts to the loaded guest. [105] However, ‘rigid’ dipeptide ligands could play an important role in the next generation of biomimetic porous materials. [168] Rosseinsky *et al.* reported that the bio-MOF [Zn(GlyThr)<sub>2</sub>]-CH<sub>3</sub>OH (Figure 6), behaves as a classic rigid porous open framework due to the conformational rigidity of the GlyThr ligand, which is driven by the hydrogen bonding intra-layer. [168] Adsorption isotherms revealed that CO<sub>2</sub> was preferentially sorbed over CH<sub>4</sub> with a single-component separation ratio of 14:1 (wt% : wt% at 1 bar). [168] Given the pore sizes of [Zn(GlyThr)<sub>2</sub>] (2.7-5.3 Å), it is shown that selectivity is not size-exclusive in origin, suggesting that a higher quadrupole moment of CO<sub>2</sub> increased quadrupole-dipole interactions with the amino/hydroxy groups found within the framework. [168]

Reversible CO<sub>2</sub> capture in MOFs can occur in two ways: 1) CO<sub>2</sub> binding to open metal sites, leading to materials with high selectivity for CO<sub>2</sub>, and 2) using weakly polar functional groups that bind CO<sub>2</sub> by means of dipole interaction. [203] While both of these methods have their advantages and disadvantages, recycling CO<sub>2</sub> has to be practical and not require more energy than necessary to regenerate the starting material. Inspired by weak nucleophilic functional groups, Stoddart *et al.* found that CDMOF-2 had an atypically strong affinity between CO<sub>2</sub> and the MOF indicative of a chemisorption process (see section 3.4 for structural details). [203] At low pressures, the selectivity for CO<sub>2</sub> over CH<sub>4</sub> was nearly 3000-fold. [203] The steep slopes in the isotherms suggest covalent bonding, which was confirmed by the abrupt transition in high pressure regimes (>1 Torr) which becomes more dependent on temperature (30% greater uptake at 273K vs 298K). Therefore, at low pressures covalent bonding is preferential, giving way to physisorption at high pressures, with the change in mechanism occurring when the CO<sub>2</sub> adsorbed by the MOF is approximately 23 cm<sup>3</sup>/g. [203] It is shown that the diffusion of CO<sub>2</sub> into the extended framework of CD-MOF-2 resulted in the formation of alkyl carbonic acid functions on the γ-CD, by covalent bonding to non-coordinated free primary hydroxyl groups, affording CA-CDMOF-2. [204] While there has been a lot of data on CO<sub>2</sub> sequestration, there has been only one report using colorimetric

sensing, and no reports of electrochemical sensing of CO<sub>2</sub> by bio-MOFs and also in MOFs. [204] The authors employed electrochemical impedance spectroscopy to measure the changes in proton conductivity, and after observing a large drop in conductivity (approximately 550 fold) following infusion of CO<sub>2</sub> in CDMOF-2, associated this with the impediment in motility of free protons. [204] Decrease in the conductivity of CA-CDMOF-2 can be attributed to the loss of coordinated hydroxide that catalyzes the deprotonation of the methanolic medium, blocking of hydrophilic triangular shaped β-windows, therefore decreasing the mass transfer of the intermedium molecules. [204] Carboxylation occurs primarily in these windows as they are the only location of uncomplexed, primary alcohol functions. [204] CDMOF-2 was reported as having a high degree of reversibility, which occurs rapidly under mild conditions, liberating sequestered CO<sub>2</sub>. [204] Features like this one, are extremely attractive and important in the continuous reusability of bio-MOFs.

## 7. Catalysis and Separations

Bio-MOFs can be also considered as potential candidates for catalysis and separations. [75, 76, 174, 205-212] However, despite their rich chemistry, catalysis with bio-MOFs is scarce. [213] This is often associated with stability and cost in MOF catalysis which is suitable for fine chemical synthesis rather than bulk chemistry. [214] While this area of research still has room for growth, the ligands themselves offer conveniences such as pre-installed chiral centers for enantioselective separations and can give functional pores that can be used for many applications. In this section we will review heterogeneous asymmetric catalysis, enantioselective separations with the use of chiral peptide based bio-MOFs, and the separation of hydrocarbons.

Rosseinsky *et al.* protonated [Ni<sub>2</sub>(L-Asp)<sub>2</sub>(bipy)]-guest and [Cu<sub>2</sub>(L-Asp)<sub>2</sub>(bpe)]-guest (bpe: 1,2-bis(4-pyridyl)ethane) with HCl in Et<sub>2</sub>O to form the frameworks [Ni<sub>2</sub>(L-Asp)<sub>2</sub>(bipy)·(HCl)<sub>1.8</sub>(MeOH)] and [Cu<sub>2</sub>(L-Asp)<sub>2</sub>(bpe)·(HCl)<sub>2</sub>(H<sub>2</sub>O)<sub>2</sub>]. [213] The selective pore size of [Ni<sub>2</sub>(L-Asp)<sub>2</sub>(bipy)·(HCl)<sub>1.8</sub>(MeOH)] is due to the exceptional hydrogen bonding properties of MeOH, allowing it to overcome the framework-anion interactions allowing it to access the interior pores. [213] The HCl introduced into the framework denotes a full proton transfer to an aspartate carboxylate group forming a COOH moiety that is tethered to the metal center due to its confinement within the pore wall. [213] The structure of [Cu<sub>2</sub>(L-Asp)<sub>2</sub>(bpe)·(HCl)<sub>2</sub>(H<sub>2</sub>O)<sub>2</sub>] is porous to both MeOH and propylene oxide, however is non porous to CO<sub>2</sub> (-78 °C). The post-synthetic modification introduced Brønsted acidic -COOH sites forming bio-MOFs that were active as heterogeneous asymmetric catalysis in the methanolysis of *cis*-2,3-epoxybutane. [213] However, the materials displayed a modest chiral induction ability with the best results being 17% *e.e.* for the methanolysis of *cis*-2,3-epoxybutane to 3-methoxybutan-2-ol. [213]

[Ni<sub>2</sub>(L-Asp)<sub>2</sub>(bipy)]-guest molecules, was tested in the extent of its enantioselectivity in guest sorption using a library of small chiral molecules with closely related functionalities. [174] It is reported that the opposite enantiomer was increased by sorption when a host derived from *D*-Asp rather than *L*-Asp was used, confirming that geometry-dependent interactions between the bio-MOF and chiral diols were present. [174] The highest report sorption *e.e.* value observed was 53.7 % for 2-methyl-2,4-pentane-diol, a mono-substituted derivative of 2,4-pentanediol which had the second highest *e.e.* of 24.5 %, and a single chiral center. [174] Interestingly,

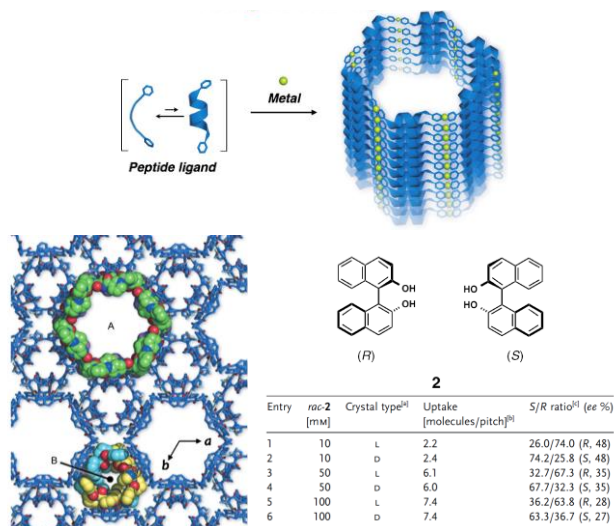


Figure 7: Coiled Gly-Pro-Pro peptide folded *via* a metal directing network (top). Space filling of the view within the whole framework, with the large nanopore A above smaller pore B (bottom, left). Table 2 shows the chiral recognition by channel A. *R* and *S* enantiomers are selectively encapsulated in enantiomeric crystals of the [(AgBF<sub>4</sub>)-Gly-D-Pro-D-Pro] material (entries 1-2). Increasing the concentration of the racemate showed a decrease in enantiomeric selectivity (entries 3-4 and 5-6, for 50 mM and 100 mM, respectively). (© 2014 Wiley-VCH Verlag GmbH & Co. KGaA, Weinheim, reprinted with permission). [112]

the derivatives with similar chain length, but different positions of the -OH group gave significantly different enantioselective sorption values. [174] Increasing the size of the ligand allows for the ability to introduce active sites into the pores. [65]

As described earlier, Maspoeh *et al.* reported a homochiral family of Co<sub>L</sub>-GlyGlubipy bio-MOFs with varying pore volumes (0.188 cm<sup>3</sup>/g to 0.256 cm<sup>3</sup>/g) when pillar ligands of different sizes were used. [65] Activated samples were immersed in a solution containing racemic mixtures of either glycidol or hydrobenzoin at room temperature, and after 48 hrs the crystals were washed and dried, then immersed in anhydrous methanol to extract the adsorbed glycidol and hydrobenzoin. [65] The authors reported *e.e.* values of (*S*-glycidol over *R*-glycidol) 54.1 ± 1.0% for Co<sub>L</sub>-GlyGlubipy, 38.2 ± 2.0% for Co<sub>L</sub>-GlyGluazobipy, 34.0 ± 1.5% for Co<sub>L</sub>-GlyGluazinebipy and 38.7 ± 1.0% for Co<sub>L</sub>-GlyGlubepb, which are inversely correlated to the total amount of adsorbed glycidol and the enantioselective adsorption of the *S*-form, with Co<sub>L</sub>-GlyGlubipy exhibiting the highest *e.e.* but adsorbing the least amount of glycidol. [65] It was postulated that the smaller pore size promoted stronger interactions between the chiral pore-wall and glycidol. [65] To demonstrate that these bio-MOFs could adsorb *S*-enantiomer-enriched glycidol or hydrobenzoin, the authors repeated the same glycidol adsorption process twice using Co<sub>L</sub>-GlyGlubipy, that had been previously loaded once with glycidol, and evacuated via immersion in methanol at 40°C. [65] In the second and third processes, the *e.e.* values (*S*-glycidol over *R*-glycidol) were 54.4 ± 1.0 % and 55.0 ± 1.5 %. The same process was repeated with Co<sub>L</sub>-GlyGlubepb and hydrobenzoin, with reported *e.e.* values (*S*-glycidol over *R*-glycidol) of 28.8 ± 4.0 % and 25.6 ± 0.5 %. [65] These results confirm that this isoreticular family of bio-MOFs is stable to be re-used for enantioselective adsorption, and that the adsorbed enriched molecules can be fully released. [65]

The peptide Gly-Pro-Pro reported by Fujita *et al.* was modified by introduction of 3-pyridyl groups with amides bonds at both termini

to produce a coordinative tripeptide ligand (structure previously described in section 3.2). [112] Through its slow diffusion into an aqueous solution of AgBF<sub>4</sub>, bio-MOF [(AgBF<sub>4</sub>)-GlyProPro] formed with two types of 1-dimensional chiral channels running along the crystallographic *c* axis (Figure 7). [112] The largest channel is surrounded by the peptide backbone forming a left handed duplex-like framework stabilized by π-stacking of the pyridyl groups, while the smaller second channel is closely packed with solvents and anions. [112] This includes independent BF<sub>4</sub><sup>-</sup> anions, with one securely trapped at the terminal amide of the GlyProPro bio-ligand, and the other at the other at the terminal pyridyl group via C-H...F hydrogen bond. [112] In the largest channel, a large degree of chiral recognition was reported when racemic compounds 1,1'-bi-2-naphthol was soaked in the single crystals of [(AgBF<sub>4</sub>)-GlyProPro] and encapsulated. [112] Analysis by chiral-phase HPLC indicated the *R*-form was favorably encapsulated with 48% *e.e.* while the *S*-form was also selectively encapsulated after repeating the same process with the Gly-D-Pro-D-Pro ligand. [112] The observation of relatively high *e.e.* values is interesting considering that 1,1'-bi-2-naphthol is smaller than the nano-sized channel, therefore, the guest molecule differentiation is assumed to be occurring in the nano-sized peptidic helical channel on the interior surface.

Flexible MOFs exhibit favorable characteristics for the selective adsorption of light hydrocarbons with similar size. [215] One of the most challenging separations in the chemical industry is that of BTEX-benzene, toluene, ethylbenzene, and the regioisomers of xylene, and while they act as antiknocking additives in gasoline, they are also critical chemical feedstocks, thus the need to separate and process them is essential. [216-221] Terephthalate-based MOFs with 1-dimensional channels have been the most widely investigated in the separation of aromatic hydrocarbons, [222-226] in particular, both MIL-47 and MIL-53 have demonstrated high *o*-xylene selectivity based on entropic differences and molecular packing. [223-225, 227] Due to pore morphology, and commensurate stacking, both MIL-125 and MAF-X8 have shown high *p*-xylene selectivity. [228] A flexible cerium tetradentate carboxylate MOF with restructuring driven by guest molecules, displaying molecular-level recognition for *p*- and *m*-xylenes giving high selectivities, thereby adding to the increasing number of flexible MOFs that can be used for separations. [35, 223, 229]

Stoddart *et al.* recently reported a high selectivity of CD-MOFs ( $\gamma$ -CD) (see section 3.4), which exhibited high shape selectivity, for separation of aromatic hydrocarbons using alkali metal cations. [215] The retention order of *o*- > *m*- > *p*-xylene separation was determined through adsorption isotherms and liquid-phase chromatographic measurements, with impressive regioselectivity of ethyltoluene and cymene regioisomers during the liquid-phase chromatography. [215] Furthermore, this work highlights the specificity of shape selectivity exhibited by CD-MOFs through the isolations of regioisomers of *i.* ethyl toluene, *ii.* cymene together with the purification of cumene from major impurities such as benzene, *n*-propylbenzene, and diisopropylbenzene and *iii.* the separation of the industrial relevant BTEX. [215] Monte Carlo molecular simulations suggest the  $\gamma$ -CD rings enable selectivity for *o*-xylene through a favorable host-guest interaction, and efficient packing of the isomer in the framework, which is confirmed by the host-guest interactions from virial equation analysis of vapor isotherms. [215] For isomers such as cymene, their larger size and steric bulk can decrease their ability to form favorable orientations thereby culminating in weaker interactions with the framework, the



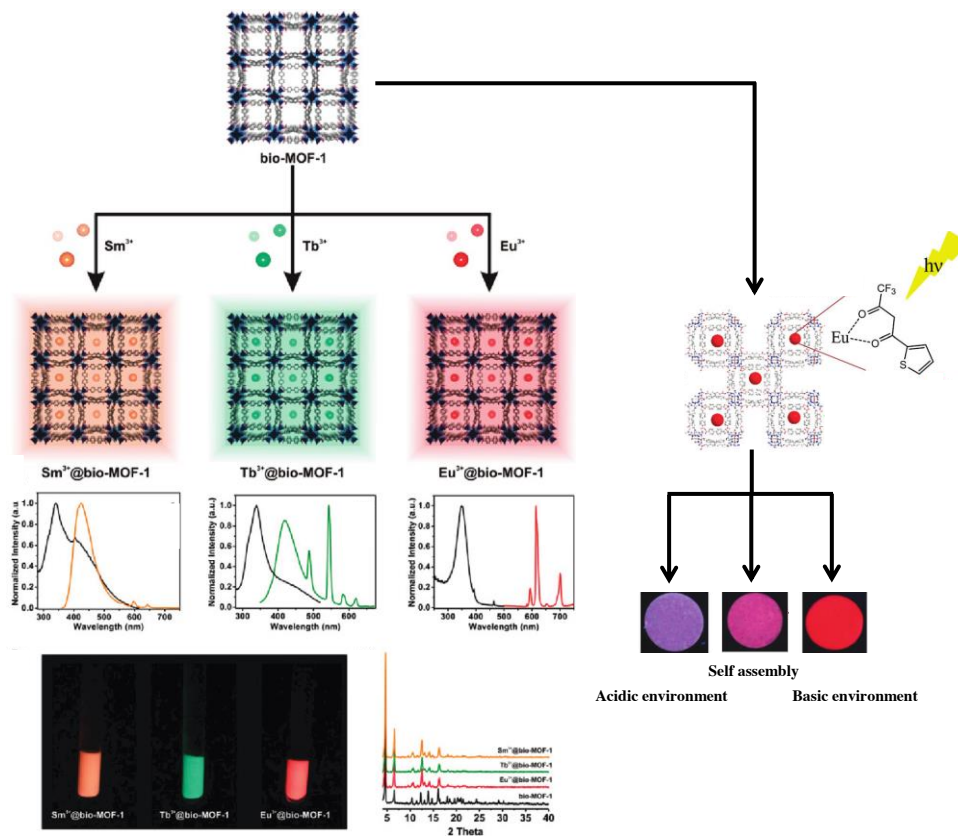


Figure 8: Illustration of lanthanide incorporation into bio-MOF-1, including the encapsulation and sensitization of cations Sm<sup>III</sup>, Tb<sup>III</sup>, and Eu<sup>III</sup> (top). Lanthanide samples illuminated with a 365 nm laboratory UB lamp (left) and PXRD patterns Ln<sup>III</sup>@Bio-MOF-1 (bottom, center). Eu<sup>III</sup>0.005-TTA@bio-MOF-1 can further be used as a fluorescence sensor to detect volatile organic amines based on pH (right, bottom) (© 2015 Royal Chemical Society,[236] © 2011 American Chemical society,[240] both reprinted with permission).

inability to discriminate between *m*- and *p*-cymene, as well as shorter retention times.[215]

In 2016, Stoddart *et al.* further reported the ability to separate a wide variety of mixtures, including ethylbenzene from styrene, haloaromatics, terpenes, pinenes, alkyl-, vinyl- and others, including chiral compounds, with CD-MOF-1. [230] The retention was influenced by *i.* the saturation of a compound, with those having a greater retention being saturated, *ii.* the placement of a double bond within the molecule, for example in the case of pinene and terpinene, isomers with an exocyclic double bond were more highly retained than their endocyclic counterparts. [230] Separations between mono- and di-substituted haloaromatic compounds were influenced by the size of the halogen substituent, and the strength between the analyte and framework through noncovalent bonding interactions. [230] Enantiomers of chiral analytes, including limonene and 1-phenylethanol, could be resolved due to the homochiral framework. [230] With a wide variety of separation abilities, CD-MOF-1 is not only versatile, environmentally benign, and biocompatible, but it can be additionally used as a stationary-phase material for separations.

Recently, Zhang and Fu constructed a microporous bio-MOF, [NH<sub>2</sub>(CH<sub>3</sub>)<sub>2</sub>][Zn<sub>3</sub>(4-Pca)<sub>3</sub>(Ade)]·10DMF·8H<sub>2</sub>O (Table 3, entry 20) which showed dynamic deformation with light hydrocarbons with large hysteresis and high capacity. [231] Adsorption of C<sub>1</sub> to C<sub>3</sub> paraffin's at 273K showed that the material adsorbed up to 117.5 cm<sup>3</sup>/g of C<sub>2</sub>H<sub>2</sub>, 76.6 cm<sup>3</sup>/g of C<sub>2</sub>H<sub>4</sub>, 70.0 cm<sup>3</sup>/g of C<sub>2</sub>H<sub>6</sub> and 70.7 cm<sup>3</sup>/g of C<sub>3</sub>H<sub>8</sub> at 294K and 1 bar; and 146.2 cm<sup>3</sup>/g of C<sub>2</sub>H<sub>2</sub>, 96.6 cm<sup>3</sup>/g of C<sub>2</sub>H<sub>4</sub>, 92.8 cm<sup>3</sup>/g of C<sub>2</sub>H<sub>6</sub>, and 88.1 C<sub>3</sub>H<sub>8</sub> at 273K at 1 bar. [231] Adsorption

behaviors in response to the light hydrocarbons were taken into consideration, and the authors reported that gate-opening pressure point follows the order of C<sub>3</sub><C<sub>2</sub>, while the lower gate opening pressure (as well as higher uptake capacity) of C<sub>2</sub>H<sub>2</sub> over C<sub>2</sub>H<sub>4</sub> and C<sub>2</sub>H<sub>6</sub> is attributed to the smaller kinetic diameter and stronger interactions of C<sub>2</sub>H<sub>2</sub> and the framework. [231]

Martí-Gastaldo *et al.* reported a chiral Cu<sup>II</sup> 3-dimensional bio-MOF based on Gly<sub>L</sub>-His-Gly (GHG) for the enantioselective separation of methamphetamine and ephedrine. [232] While both compounds are well known as recreational drugs, they are also components used in the preparation of therapeutics such as bronchodilators and respiratory stimulants. [232] Cu(GHG) is constructed through an interconnecting four-fold helicoidal Cu-peptide-Cu chains via a μ<sub>2</sub>-carboxylate bridging C-terminal Gly, with porosity forming via interconnected 1-dimensional empty channels. [232] Post-synthetic modification of the peptide allows a variety of functional groups (carboxylate, amide, amino and imidazole) to be added to the surface of the pore with the groups pointing into the channel. The Cu(GHG) crystals display a sponge-like behaviour with a reversible crystalline-to-amorphous transformation after activation. Initial studies to recognize the selectivity were performed by soaking the bio-MOF in racemic mixtures of methamphetamine and ephedrine, resulting in a 30 ± 3 % and 37 ± 3 % adsorption of (+)-methamphetamine and (+)-ephedrine, respectively. [232] These results are attributed to the preferential interaction of the (+)-enantiomers in the chiral pocket of the bio-MOF that aid in hydrogen bond formation with the His side chain. [232] The authors further demonstrated the applicability of their work by packing 50 mg of

Cu(GHG) into a polypropylene SPE cartridge and eluted a racemic mixture of ( $\pm$ )-ephedrine in 75:25 ratio of hexane:ethanol at 0.25 mL/min followed by HPLC. Quantitatively,  $54 \pm 2\%$  of (+)-ephedrine was separated from equimolar enantiomer mixtures, and the Cu(GHG) bio-MOF cartridges can be used for at least two runs without a significant loss of enantioselectivity. [232]

## 8. Sensing Applications

Fluorescence can be derived from highly fluorescent ligands or lanthanides, however to our knowledge there are currently no bio-MOFs based on lanthanides. The luminescence property of lanthanide-functionalized MOFs, makes them attractive candidates for the use in luminescent sensors or fluorescent probes. [233, 234] Trivalent lanthanide ions have attractive features such as sharp characteristic emissions and long excited state lifetimes, allowing for lower costs but still maintaining high signal output and a simple detection mechanism. [235-240]

Thus far, the use of bio-MOFs as sensors has been rarely reported. Rosi *et al.* reported that the porous anionic  $[\text{Zn}_8(\text{Ade})_4(\text{bpdc})_6\text{O}]\cdot 2\text{Me}_2\text{NH}_2$  in which the cations residing within the pores could be exchanged with lanthanide cations such as  $\text{Tb}^{\text{III}}$ ,  $\text{Sm}^{\text{III}}$  and  $\text{Eu}^{\text{III}}$  (Figure 8). [241] They further demonstrated that  $[\text{Zn}_8(\text{Ade})_4(\text{bpdc})_6\text{O}]\cdot 2\text{Me}_2\text{NH}_2$  sensitizes near-infrared (NIR) emitting lanthanide cations in water. [241] Luminescence even in water is necessary for the use of NIR-emitting lanthanides in biological environments, eventually leading to the possibility of their potential applicability as intracellular  $\text{O}_2$  sensors. [241] For example, a sample of  $\text{Yb}^{\text{III}}$  loaded bio-MOF-1 was dried, and observed a 40% decrease in  $\text{Yb}^{\text{III}}$  luminescence within the first 5 minutes of introducing the sample to  $\text{O}_2$ . [241] Upon purging the sample with  $\text{N}_2$ , the signal intensity was restored, even after several cycles of exposure to  $\text{O}_2$  and  $\text{N}_2$ . [241]

In addition, Yan and Shen reported that the encapsulation of  $\text{Eu}^{\text{III}}$ - $\beta$ -diketonate complexes within the same anionic Ade based bio-MOF-1, it can be applied in environmental and industrial sectors monitoring through sensing of volatile organic molecules, especially volatile amines. [237] The authors reported color switching due to the quenching of luminescence emission and lifetimes following exposure to acidic vapors (host luminescence still exists). [237] For environments with alkaline volatile organic molecules (e.g.  $\text{HNEt}_2$  - diethanolamine) the loaded bio-MOF-1 ( $\text{Eu}^{\text{III}}_{0.005}\text{-TTA@bio-MOF-1}$ ) showed an enhanced red fluorescence emission whereas the material displayed a light purple fluorescence emission in the presence of acidic vapor (e.g. formic acid). [237]

## 9. Biological Applications

Several methodologies have been reported to miniaturize MOFs into the nanoscale regime which is vital for their use in biology. Porous nanoscale MOFs have excellent properties such as drug storage-release capabilities, and the possibility of biocompatibility, making them appealing candidates for biomedical utility. [7, 120, 242, 244] Thus far, the biomedical applications of bio-MOFs have not been fully explored due to a lack of reported materials that are stable in both aqueous and buffer conditions. For example, Rosi *et*

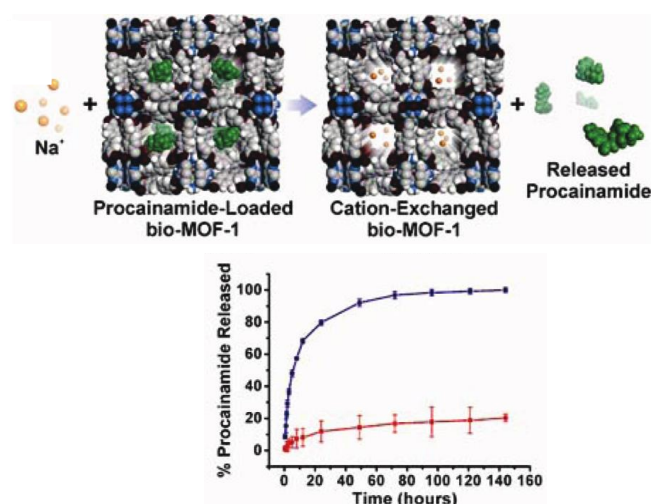


Figure 9: Loaded Procainamide via cation exchange, followed by release. The release profile was determined through HPLC by placing a sample of the procainamide-exchanged material in 0.1 M, pH 7.4, PBS buffer (blue). Steady release of procainamide was observed over 72 hrs. To verify that the procainamide release was mediated by the buffer, a control experiment in nanopure water was performed, and verified that the release is indeed mediated by the buffer. (© 2009 American Chemical Society, reprinted with permission). [52]

*al.* reported the construction of anionic  $[\text{Zn}_8(\text{Ade})_4(\text{bpdc})_6\text{O}]\cdot 2\text{Me}_2\text{NH}_2\cdot 8\text{DMF}\cdot 11\text{H}_2\text{O}$ , which is stable for up to several weeks in both water and biological buffers. [52] The cationic drug molecule, Procainamide, was loaded *via* cation exchange into the pores of the material along with DMA cations that were originally found within the pores (Figure 9). [52] The drug release was monitored in a PBS buffer, and found that the cations in the buffer exchanged with those in the drug, likely aiding in the drug release process. [52]

## 10. Conclusion and Future Outlook

Bio-ligands are an attractive family of ligands that can be incorporated into MOF structures, with beneficial features such as multiple coordination sites, preinstalled chirality, hydrophobic/hydrophilic tendencies, specific recognition/self-assembly capabilities, and they provide ideal characteristics for applications such as  $\text{CO}_2$  storage, catalysis and separation, sensing as well as drug-delivery. Bio-ligands are commercially available in high purities, or can be easily constructed through known literature procedures providing a nearly infinite variety of ligands, and allow researchers the ability to use different ligands than those typically explored.

While they can have many different functionalities, their ability to bind through multiple coordination sites can afford the formation of bio-MOFs that span over several applications. Additional features of bio-MOFs constructed from bio-ligands is the ability to form flexible or robust frameworks, where both families are important and allow researchers to better understand the folding or movement of proteins or create robust materials for gas and storage applications. Concepts such as MTV-bio-MOFs, Ade-Thy replication, and the construction of isorecticular series have been proven and

show impressive results. Furthermore, promising candidates such as  $[\text{Ni}_2(\text{-Asp})_2(\text{bipy})]$ -guest, the Co- $_{\text{-GlyGlu}}$  bio-MOF family, CD-MOF-1 and -2, as well as  $[\text{NH}_2(\text{CH}_3)_2][\text{Zn}_3(4\text{-Pca})_3(\text{Ade})]\cdot 10\text{DMF}\cdot 8\text{H}_2\text{O}$  have been demonstrated for applications such as heterogeneous asymmetric catalysis, enantioselective adsorption/desorption, separation of xylene isomers and other light hydrocarbons. The  $[\text{Zn}_8(\text{Ade})_4(\text{bpdc})_6\text{O}]\cdot 2\text{Me}_2\text{NH}_2\cdot 8\text{DMF}\cdot 11\text{H}_2\text{O}$  MOF was shown to take up and release the drug Procainamide, for drug delivery applications.

Through future research and construction of bio-MOFs, the properties, practical applications, structure and scope of this field will certainly grow. While there are very few bio-MOFs reported for applications such as catalysis, the discovery of new and novel bio-MOFs could further expand the scope in all areas and answer questions such as improving hydrolytic stability of bio-MOFs for their use in biology. Exploring individual biological ligands, such as peptides, can give us more insight into the flexibility and collapse of pores, and if this can be beneficial for other applications such as gas storage and catalysis.[243] Furthermore, is it possible to stabilize these flexible bio-MOFs upon loading with specific molecules? By altering the structure, either through pre- or post-synthetic modification can we change the structure as a whole? For example, if CD is functionalized with functional groups to form an extended structure, do we still form CD cubes and are these going to be selective to  $\text{CO}_2$ ? While the formation of bio-MOFs, and exploration of their applications, is an ever growing field, many questions still need to be addressed that broach both the interests of bio-MOFs and MOFs, allowing us to further our understanding on the field as a whole.

## Acknowledgements

SLA and KCS thank Prof. Berend Smit for useful discussions over the preparation of this review. KCS acknowledges Swiss National Science Foundation for funding under the Ambizione Energy Grant n.PZENP2\_166888.

## Abbreviations (order as they presented in the review)

MOFs: metal organic frameworks  
 Bio-MOF: biologically derived MOFs  
 Bio-ligands: biologically derived ligands  
 MTV-MOF: Multivariate MOF  
 IRMOF: Isoreticular MOF  
 GFP: Green fluorescent protein  
 HTCPB: tetradentate carboxylic acid  
 BET: Brunauer–Emmett–Teller  
 SCSC: single crystal to single crystal  
 I: intensity  
 CPO: coordination polymer  
 LEDs: light-emitting diodes  
 DMF: *N,N'*-dimethyl formamide  
 DEF: *N,N'*-diethyl formamide  
 FITC: Fluorescein isothiocyanate  
 NMOFs: Nanoscale MOFs  
 BTAsp: Benzene-1,3,5-tris aspartic acid  
 Gly: Glycine  
 Phe: Phenylalanine  
 Gln: glutamine

Asp: Aspartic acid  
 SOD: Sodalite  
 Met: methionine  
 Glu: Glutamic acid  
 His: Histidine  
 Cys: Cysteine  
 Tyr: Tyrosine  
 Bipy: 4,4'-bipyridyl  
 Py3T: tris(4-pyridyl)-35bpp: 3,5-bis(4-pyridyl)pyridine  
 IDS: meso-iminodisuccinic acid  
 Im: imidazole  
 Trp: Tryptophan  
 bpe: bis(4-pyridyl)ethylene  
 ser: serine  
 val: valine  
 BDC: benzene dicarboxylic acid  
 GlyGly: Glycyl-Glycine  
 GlyGlu: Glycyl-Glutamic acid  
 GlyThr: Glycyl-Threonine  
 AlaThr: Alanyl-Threonine  
 GlyAla: Glycyl-Alanine  
 GlyAsp: Glycyl-Aspartate  
 GlySer: Glycyl-Serine  
 MTV: multivariate  
 Car or AlaHis: Carnosine or Alanyl-Histidine  
 GlyHis: Glycyl-Histidine  
 GlyPhe: Glycyl-Phenalanine  
 GlyGlyGly: Glycyl-Glycyl-Glycine  
 GlyProPro: Glycyl-Prolinyl-Proline  
 BPDC: 4,4'-biphenyldicarboxylic acid  
 GlyHisLys: Glycyl-Histidyl-Lysine  
 GlyHisGly: Glycyl-Histidyl-Glycine  
 $\text{NH}_2\text{-Glu-pCO}_2\text{Phe-pCO}_2\text{Phe-Ala}$ ; Gly-OH: penta-peptide composed of the sequence of glutamic acid-phenylamine-phenylamine-alanine-glycine  
 Ade: adenine  
 Thy: thymine  
 TATB: 4,4',4''-s-Triazine-2,4,6-triyl-tribenzoic acid  
 BTeC: 1,2,4,5-benzene tetracarboxylic acid  
 Gua: guanine  
 MOP: metal organic polyhedron  
 TMOP: thymine based MOP  
 MDPI: 5-((5-methyl-2,4-dioxo-3,4-dihydropyrimidin-1(2H)-yl)methyl)isophthalate  
 DMA: dimethyl acetamide  
 XRD: X-ray diffraction  
 $\alpha$ -CD: alpha-Cyclodextrin  
 $\beta$ -CD: beta-Cyclodextrin  
 $\gamma$ -CD: gamma-Cyclodextrin  
 TCPB: 1,2,4,5-Tetrakis(4-carboxyphenyl)benzene  
 CDMOF: Cyclodextrin based MOF  
 $\alpha$ -1,4-D-Glup:  $\alpha$ -1,4-linked D-glucopyranosyl  
 SBUs: secondary building units  
 ZABUs: zinc-adeninate octahedral building units  
 NDC: 2,6-naphthalene dicarboxylic acid  
 ABDC: azo-benzene-4,4'-dicarboxylic acid  
 TPDC: terphenyldicarboxylic acid  
 $\text{NH}_2\text{-TPDC}$ : 2'-amino-1,1':4,1''-terphenyl-4,4''-dicarboxylate  
 BTC: 1,3,5-benzene tricarboxylic acid  
 Pfl<sup>+</sup>: proflavine hemisulfate ion  
 MB<sup>+</sup>: methylene blue ion

Azobipy: 4,4'-azobipyridine  
 Azinebipy: 4,4'-azinebipyridine  
 Bpeb: 1,4-bis(4-pyridylethynyl)-benzene  
 Azpy: 4,4'-azopyridine  
 3rbp: 1,4-bis(4-pyridyl)benzene  
 TMA<sup>+</sup>: tetramethyl-ammonium cations  
 TEA<sup>+</sup>: tetraethyl-ammonium cations  
 TBA<sup>+</sup>: tetrabutyl-ammonium cations  
 pzdc: pyrazole dicarboxylic acid  
 9Hade: adenine with protonated N9  
 7Hade: adenine with protonated N7  
 TiF6: titanium hexafluoride  
 IAST: ideal adsorbed solution theory calculations  
 GND<sup>+</sup>: guanidium cations  
 AmGND<sup>+</sup>: aminoguanidinium cations  
 DiAmGND<sup>+</sup>: diaminoguanidinium cations  
 DMA<sup>+</sup>: dimethyl ammonium cations  
 TIF: Tetrahedral imidazolate frameworks  
 int: isonicotinic acid  
 CA-CDMOF-2: Carbonic acid cyclodextrin based MOF  
 e.e.: enantioselectivity  
 HPLC: high performance liquid chromatography  
 BTEX: acronym that stands for benzene, toluene, ethylbenzene, and xylenes  
 4-Pca: 4-pyrazolecarboxylic acid  
 HNEt<sub>2</sub>: diethynaloamine  
 TTA: 2-thenoyltrifluoroacetate

## Notes and references

- [1] G. Férey, *Chem. Soc. Rev.*, 37 (2008) 191-214.
- [2] O.M. Yaghi, M. O'Keeffe, N.W. Ockwig, H.K. Chae, M. Eddaoudi, J. Kim, *Nature*, 423 (2003) 705-714.
- [3] O.K. Farha, I. Eryazici, N.C. Jeong, B.G. Hauser, C.E. Wilmer, A.A. Sarjeant, R.Q. Snurr, S.T. Nguyen, A.Ö. Yazaydin, J.T. Hupp, *J. Am. Chem. Soc.*, 134 (2012) 15016-15021.
- [4] H. Furukawa, N. Ko, Y.B. Go, N. Aratani, S.B. Choi, E. Choi, A.Ö. Yazaydin, R.Q. Snurr, M. O'Keeffe, J. Kim, O.M. Yaghi, *Science*, 329 (2010) 424-428.
- [5] H. Furukawa, Y.B. Go, N. Ko, Y.K. Park, F.J. Uribe-Romo, J. Kim, M. O'Keeffe, O.M. Yaghi, *Inorg. Chem.*, 50 (2011) 9147-9152.
- [6] M. Zhang, M. Bosch, T. Gentle Iii, H.-C. Zhou, *CrystEngComm.*, 16 (2014) 4069-4083.
- [7] I. Imaz, M. Rubio-Martinez, J. An, I. Sole-Font, N.L. Rosi, D. Maspocho, *Chem. Commun.*, 47 (2011) 7287-7302.
- [8] A. Corma, H. García, F.X. Llabrés i Xamena, *Chem. Rev.*, 110 (2010) 4606-4655.
- [9] P.M. Forster, P.M. Thomas, A.K. Cheetham, *Chem. Mater.*, 14 (2002) 17-20.
- [10] S.S.-Y. Chui, S.M.-F. Lo, J.P.H. Charmant, A.G. Orpen, I.D. Williams, *Science*, 283 (1999) 1148-1150.
- [11] S.H. Jhung, J.-H. Lee, P.M. Forster, G. Férey, A.K. Cheetham, J.-S. Chang, *Chem. Eur. J.*, 12 (2006) 7899-7905.
- [12] E. Biemmi, S. Christian, N. Stock, T. Bein, *Micropor. Mesopor. Mat.*, 117 (2009) 111-117.
- [13] N. Stock, T. Bein, *Angew. Chem. Int. Ed.*, 43 (2004) 749-752.
- [14] S. Bauer, T. Bein, N. Stock, *Inorg. Chem.*, 44 (2005) 5882-5889.
- [15] S.M. Hawxwell, G.M. Espallargas, D. Bradshaw, M.J. Rosseinsky, T.J. Prior, A.J. Florence, J. van de Streek, L. Brammer, *Chem. Commun.*, (2007) 1532-1534.
- [16] C.A. Black, L.R. Hanton, M.D. Spicer, *Chem. Commun.*, (2007) 3171-3173.
- [17] P. Ren, M.-L. Liu, J. Zhang, W. Shi, P. Cheng, D.-Z. Liao, S.-P. Yan, *Dalton Trans.*, (2008) 4711-4713.
- [18] K. Shen, M. Zhang, H. Zheng, *CrystEngComm.*, 17 (2015) 981-991.
- [19] F.A. Almeida Paz, J. Klinowski, S.M.F. Vilela, J.P.C. Tome, J.A.S. Cavaleiro, J. Rocha, *Chem. Soc. Rev.*, 41 (2012) 1088-1110.
- [20] A. Demessence, D.M. D'Alessandro, M.L. Foo, J.R. Long, *J. Am. Chem. Soc.*, 131 (2009) 8784-8786.
- [21] R. Poloni, B. Smit, J.B. Neaton, *J. Am. Chem. Soc.*, 134 (2012) 6714-6719.
- [22] X. Kong, H. Deng, F. Yan, J. Kim, J.A. Swisher, B. Smit, O.M. Yaghi, J.A. Reimer, *Science*, 341 (2013) 882-885.
- [23] H. Deng, C.J. Doonan, H. Furukawa, R.B. Ferreira, J. Towne, C.B. Knobler, B. Wang, O.M. Yaghi, *Science*, 327 (2010) 846-850.
- [24] M. Eddaoudi, J. Kim, N. Rosi, D. Vodak, J. Wachter, M. O'Keeffe, O.M. Yaghi, *Science*, 295 (2002) 469-472.
- [25] H. Li, M. Eddaoudi, M. O'Keeffe, O.M. Yaghi, *Nature*, 402 (1999) 276-279.
- [26] B. Chen, M. Eddaoudi, S.T. Hyde, M. O'Keeffe, O.M. Yaghi, *Science*, 291 (2001) 1021-1023.
- [27] H. Deng, S. Grunder, K.E. Cordova, C. Valente, H. Furukawa, M. Hmadeh, F. Gándara, A.C. Whalley, Z. Liu, S. Asahina, H. Kazumori, M. O'Keeffe, O. Terasaki, J.F. Stoddart, O.M. Yaghi, *Science*, 336 (2012) 1018-1023.
- [28] B. Arstad, H. Fjellvåg, K. Kongshaug, O. Swang, R. Blom, *Adsorption*, 14 (2008) 755-762.
- [29] J. Zheng, M. Wu, F. Jiang, W. Su, M. Hong, *Chem. Sci.*, 6 (2015) 3466-3470.
- [30] J.-P. Zhang, X.-M. Chen, *J. Am. Chem. Soc.*, 130 (2008) 6010-6017.
- [31] S.A. Moggach, T.D. Bennett, A.K. Cheetham, *Angew. Chem.*, 121 (2009) 7221-7223.
- [32] K.C. Stylianou, J. Rabone, S.Y. Chong, R. Heck, J. Armstrong, P.V. Wiper, K.E. Jelfs, S. Zlatogorsky, J. Bacsá, A.G. McLennan, C.P. Ireland, Y.Z. Khimyak, K.M. Thomas, D. Bradshaw, M.J. Rosseinsky, *J. Am. Chem. Soc.*, 134 (2012) 20466-20478.
- [33] S. Horike, R. Matsuda, D. Tanaka, S. Matsubara, M. Mizuno, K. Endo, S. Kitagawa, *Angew. Chem. Int. Ed.*, 45 (2006) 7226-7230.
- [34] C.-C. Wang, C.-C. Yang, C.-T. Yeh, K.-Y. Cheng, P.-C. Chang, M.-L. Ho, G.-H. Lee, W.-J. Shih, H.-S. Sheu, *Inorg. Chem.*, 50 (2011) 597-603.
- [35] J.E. Warren, C.G. Perkins, K.E. Jelfs, P. Boldrin, P.A. Chater, G.J. Miller, T.D. Manning, M.E. Briggs, K.C. Stylianou, J.B. Claridge, M.J. Rosseinsky, *Angew. Chem.*, 126 (2014) 4680-4684.
- [36] A. Fateeva, P.A. Chater, C.P. Ireland, A.A. Tahir, Y.Z. Khimyak, P.V. Wiper, J.R. Darwent, M.J. Rosseinsky, *Angew. Chem. Int. Ed.*, 51 (2012) 7440-7444.
- [37] I.J. Kang, N.A. Khan, E. Haque, S.H. Jhung, *Chem. Eur. J.*, 17 (2011) 6437-6442.
- [38] J.J. Low, A.I. Benin, P. Jakubczak, J.F. Abrahamian, S.A. Faheem, R.R. Willis, *J. Am. Chem. Soc.*, 131 (2009) 15834-15842.
- [39] K.C. Stylianou, R. Heck, S.Y. Chong, J. Bacsá, J.T.A. Jones, Y.Z. Khimyak, D. Bradshaw, M.J. Rosseinsky, *J. Am. Chem. Soc.*, 132 (2010) 4119-4130.
- [40] M.D. Allendorf, C.A. Bauer, R.K. Bhakta, R.J.T. Houk, *Chem. Soc. Rev.*, 38 (2009) 1330-1352.
- [41] C.A. Bauer, T.V. Timofeeva, T.B. Settersten, B.D. Patterson, V.H. Liu, B.A. Simmons, M.D. Allendorf, *J. Am. Chem. Soc.*, 129 (2007) 7136-7144.
- [42] C. He, K. Lu, W. Lin, *J. Am. Chem. Soc.*, 136 (2014) 12253-12256.

- [43] P. Horcajada, R. Gref, T. Baati, P.K. Allan, G. Maurin, P. Couvreur, G. Férey, R.E. Morris, C. Serre, *Chem. Rev.*, 112 (2012) 1232-1268.
- [44] C. Serre, S. Surble, C. Mellot-Draznieks, Y. Filinchuk, G. Férey, *Dalton Trans.*, (2008) 5462-5464.
- [45] C. Serre, F. Millange, S. Surblé, G. Férey, *Angew. Chem. Int. Ed.*, 43 (2004) 6285-6289.
- [46] R. Weber, G. Bergerhoff, *Kristallogr.*, 195 (1991) 878.
- [47] S.R. Miller, D. Heurtaux, T. Baati, P. Horcajada, J.-M. Greneche, C. Serre, *Chem. Commun.*, 46 (2010) 4526-4528.
- [48] Y. Xie, Z. Yu, X. Huang, Z. Wang, L. Niu, M. Teng, J. Li, *Chem. Eur. J.*, 13 (2007) 9399-9405.
- [49] S. Keskin, S. Kizilel, *Ind. Eng. Chem. Res.*, 50 (2011) 1799-1812.
- [50] P.D.C. Dietzel, R. Blom, H. Fjellvåg, *Eur. J. Inorg. Chem.*, 2008 (2008) 3624-3632.
- [51] P. Horcajada, S. Surble, C. Serre, D.-Y. Hong, Y.-K. Seo, J.-S. Chang, J.-M. Greneche, I. Margiolaki, G. Férey, *Chem. Commun.*, (2007) 2820-2822.
- [52] J. An, S.J. Geib, N.L. Rosi, *J. Am. Chem. Soc.*, 131 (2009) 8376-8377.
- [53] P. Horcajada, T. Chalati, C. Serre, B. Gillet, C. Sebrie, T. Baati, J.F. Eubank, D. Heurtaux, P. Clayette, C. Kreuz, J.-S. Chang, Y.K. Hwang, V. Marsaud, P.-N. Bories, L. Cynober, S. Gil, G. Férey, P. Couvreur, R. Gref, *Nat. Mater.*, 9 (2010) 172-178.
- [54] C.-D. Wu, A. Hu, L. Zhang, W. Lin, *J. Am. Chem. Soc.*, 127 (2005) 8940-8941.
- [55] M.C. Das, Q. Guo, Y. He, J. Kim, C.-G. Zhao, K. Hong, S. Xiang, Z. Zhang, K.M. Thomas, R. Krishna, B. Chen, *J. Am. Chem. Soc.*, 134 (2012) 8703-8710.
- [56] I. Burneo, K.C. Stylianou, I. Imaz, D. Maspoch, *Chem. Commun.*, 50 (2014) 13829-13832.
- [57] R.E. Morris, X. Bu, *Nat. Chem.*, 2 (2010) 353-361.
- [58] G. Nickerl, A. Henschel, R. Grünker, K. Gedrich, S. Kaskel, *CIT*, 83 (2011) 90-103.
- [59] T. Ezuhara, K. Endo, Y. Aoyama, *J. Am. Chem. Soc.*, 121 (1999) 3279-3283.
- [60] S.-T. Wu, Y.-R. Wu, Q.-Q. Kang, H. Zhang, L.-S. Long, Z. Zheng, R.-B. Huang, L.-S. Zheng, *Angew. Chem. Int. Ed.*, 46 (2007) 8475-8479.
- [61] C.J. Kepert, T.J. Prior, M.J. Rosseinsky, *J. Am. Chem. Soc.*, 122 (2000) 5158-5168.
- [62] Z. Lin, A.M.Z. Slawin, R.E. Morris, *J. Am. Chem. Soc.*, 129 (2007) 4880-4881.
- [63] J. Zhang, S. Chen, T. Wu, P. Feng, X. Bu, *J. Am. Chem. Soc.*, 130 (2008) 12882-12883.
- [64] J. Zhang, S. Chen, R.A. Nieto, T. Wu, P. Feng, X. Bu, *Angew. Chem. Int. Ed.*, 49 (2010) 1267-1270.
- [65] K.C. Stylianou, L. Gómez, I. Imaz, C. Verdugo-Escamilla, X. Ribas, D. Maspoch, *Chem. Eur. J.*, 21 (2015) 9964-9969.
- [66] J.S. Seo, D. Whang, H. Lee, S.I. Jun, J. Oh, Y.J. Jeon, K. Kim, *Nature*, 404 (2000) 982-986.
- [67] A. Schoedel, M. Li, D. Li, M. O'Keeffe, O.M. Yaghi, *Chem. Rev.*, 116 (2016) 12466-12535.
- [68] C.D.L. Saunders, N. Burford, U. Werner-Zwanziger, R. McDonald, *Inorg. Chem.*, 47 (2008) 3693-3699.
- [69] M. Fleck, L. Bohaty, *Acta Crystallogr. C*, 61 (2005) m412-m416.
- [70] T. Glowiak, Z. Ciunik, *Acta Crystallogr. B*, 34 (1978) 1980-1983.
- [71] K. Stenzel, M. Fleck, *Acta Crystallogr., Sect. E: Struct. Rep. Online*, 60 (2004) M1470-M1472.
- [72] J.B. Weng, M.C. Hong, R. Cao, Q. Shi, A.S.C. Chan, *Chin. J. Struct. Chem.*, 22 (2003) 195-199.
- [73] D. Van der Helm, M.B. Lawson, E.L. Enwall, *Acta Crystallogr. B*, 27 (1971) 2411-2418.
- [74] José M. Schweigkardt, Alberto C. Rizzi, Oscar E. Piro, Eduardo E. Castellano, Ricardo Costa d. Santana, R. Calvo, Carlos D. Brondino, *Eur. J. Inorg. Chem.*, 2002 (2002) 2913-2919.
- [75] E.V. Anokhina, A.J. Jacobson, *J. Am. Chem. Soc.*, 126 (2004) 3044-3045.
- [76] E.V. Anokhina, Y.B. Go, Y. Lee, T. Vogt, A.J. Jacobson, *J. Am. Chem. Soc.*, 128 (2006) 9957-9962.
- [77] E. Yang, L. Wang, F. Wang, Q. Lin, Y. Kang, J. Zhang, *Inorg. Chem.*, 53 (2014) 10027-10029.
- [78] T.-T. Luo, L.-Y. Hsu, C.-C. Su, C.-H. Ueng, T.-C. Tsai, K.-L. Lu, *Inorg. Chem.*, 46 (2007) 1532-1534.
- [79] R.J. Flook, H.C. Freeman, M.L. Scudder, *Acta Crystallogr. B*, 33 (1977) 801-809.
- [80] M.-X. Li, H.-J. Zhao, M. Shao, Z.-X. Miao, S.-W. Liang, *J. Coord. Chem.*, 60 (2007) 2549-2557.
- [81] C. Gramaccioni, *Acta Crystallogr.*, 21 (1966) 600-605.
- [82] M. Mizutani, N. Maejima, K. Jitsukawa, H. Masuda, H. Einaga, *Inorg. Chim. Acta* 283 (1998) 105-110.
- [83] C.M. Gramaccioni, R.E. Marsh, *Acta Crystallogr.*, 21 (1966) 594-600.
- [84] Y. Zhang, M.K. Saha, I. Bernal, *CrystEngComm.*, 5 (2003) 34-37.
- [85] L. Chen, X. Bu, *Chem. Mater.*, 18 (2006) 1857-1860.
- [86] Z.-L. Chen, C.-F. Jiang, W.-H. Yan, F.-P. Liang, S.R. Batten, *Inorg. Chem.*, 48 (2009) 4674-4684.
- [87] F. Luo, Y.-t. Yang, Y.-x. Che, J.-m. Zheng, *CrystEngComm.*, 10 (2008) 1613-1616.
- [88] P. Zhu, W. Gu, F.-Y. Cheng, X. Liu, J. Chen, S.-P. Yan, D.-Z. Liao, *CrystEngComm.*, 10 (2008) 963-967.
- [89] J. Perez Barrio, J.-N. Rebilly, B. Carter, D. Bradshaw, J. Bacsá, A.Y. Ganin, H. Park, A. Trewin, R. Vaidhyanathan, A.I. Cooper, J.E. Warren, M.J. Rosseinsky, *Chem. Eur. J.*, 14 (2008) 4521-4532.
- [90] J.A. Gould, J. Bacsá, H. Park, J.B. Claridge, A.M. Fogg, V. Ramanathan, J.E. Warren, M.J. Rosseinsky, *Cryst. Growth Des.*, 10 (2010) 2977-2982.
- [91] J.A. Gould, J.T.A. Jones, J. Bacsá, Y.Z. Khimiyak, M.J. Rosseinsky, *Chem. Commun.*, 46 (2010) 2793-2795.
- [92] L. Antolini, G. Marcotrigiano, L. Menabue, G.C. Pellacani, M. Saladini, *Inorg. Chem.*, 21 (1982) 2263-2267.
- [93] S. Mendiratta, M. Usman, T.-T. Luo, B.-C. Chang, S.-F. Lee, Y.-C. Lin, K.-L. Lu, *Cryst. Growth Des.*, 14 (2014) 1572-1579.
- [94] Y.-X. Tan, Y.-P. He, J. Zhang, *Inorg. Chem.*, 50 (2011) 11527-11531.
- [95] Z.-R. Qu, H. Zhao, X.-S. Wang, Y.-H. Li, Y.-M. Song, Y.-j. Liu, Q. Ye, R.-G. Xiong, B.F. Abrahams, Z.-L. Xue, X.-Z. You, *Inorg. Chem.*, 42 (2003) 7710-7712.
- [96] I. Csoregh, M. Czugler, P. Kierkegaard, J. Legendziewicz, E. Huskowska, *Acta Chem. Scand.*, 43 (1989) 735-747.
- [97] H.-y. Zhang, H.-j. Yu, H.-x. Xu, J.-s. Ren, X.-g. Qu, *Polyhedron*, 26 (2007) 5250-5256.
- [98] R. Wang, H. Liu, M.D. Carducci, T. Jin, C. Zheng, Z. Zheng, *Inorg. Chem.*, 40 (2001) 2743-2750.
- [99] a) Y. Liu, W. Xuan, Y. Cui, *Adv. Mater.*, 22 (2010) 4112-4135. b) V. Lillo, J. R. Galan-Mascaros, *Dalton Trans.* 2014, 43, 9821.
- [100] P.A. Wright, *Science*, 329 (2010) 1025-1026.
- [101] T. Takayama, S. Ohuchida, Y. Koike, M. Watanabe, D. Hashizume, Y. Ohashi, *Bull. Chem. Soc. Jpn.*, 69 (1996) 1579-1586.
- [102] R. Ferrari, S. Bernés, C.R. de Barbañin, G. Mendoza-Díaz, L. Gasque, *Inorg. Chim. Acta* 339 (2002) 193-201.

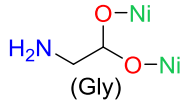
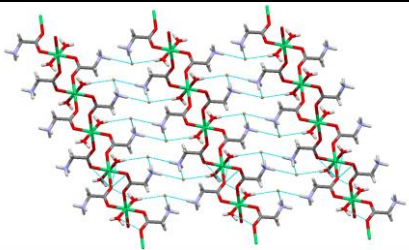
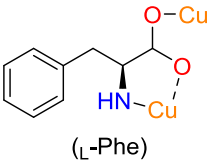
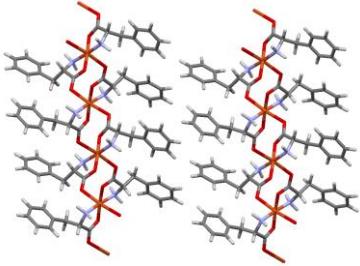
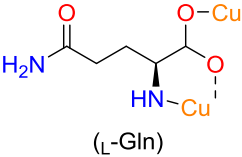
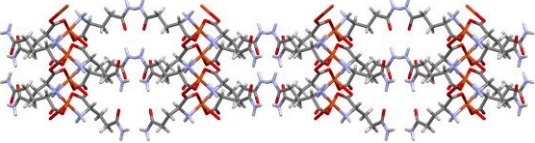
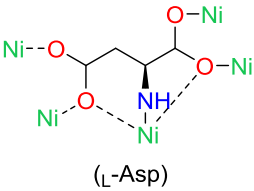
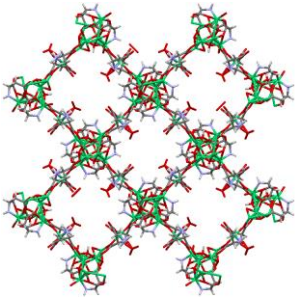
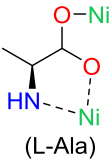
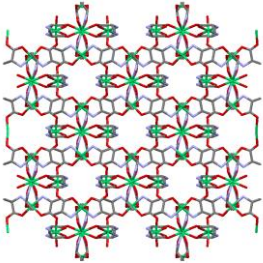
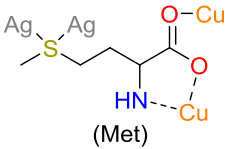
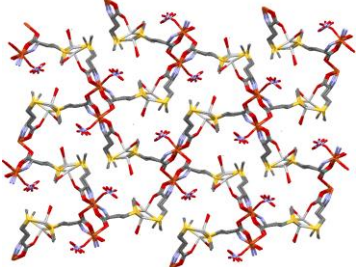
- [103] E. Ueda, Y. Yoshikawa, N. Kishimoto, M. Tadokoro, H. Sakurai, N. Kajiwara, Y. Kojima, *Bull. Chem. Soc. Jpn.*, 77 (2004) 981-986.
- [104] H.-Y. Lee, J.W. Kampf, K.S. Park, E.N.G. Marsh, *Cryst. Growth Des.*, 8 (2008) 296-303.
- [105] J. Rabone, Y.-F. Yue, S.Y. Chong, K.C. Stylianou, J. Bacsá, D. Bradshaw, G.R. Darling, N.G. Berry, Y.Z. Khimyak, A.Y. Ganin, P. Wiper, J.B. Claridge, M.J. Rosseinsky, *Science*, 329 (2010) 1053-1057.
- [106] S. Emami, F.A.A. Paz, A. Mendes, L. Gales, *Cryst. Growth Des.*, 14 (2014) 4777-4780.
- [107] C. Martí Gastaldo, AntypovD, J.E. Warren, M.E. Briggs, P.A. Chater, P.V. Wiper, G.J. Miller, Y.Z. Khimyak, G.R. Darling, N.G. Berry, M.J. Rosseinsky, *Nat. Chem.*, 6 (2014) 343-351.
- [108] A.P. Katsoulidis, K.S. Park, D. Antypov, C. Martí-Gastaldo, G.J. Miller, J.E. Warren, C.M. Robertson, F. Blanc, G.R. Darling, N.G. Berry, J.A. Purton, D.J. Adams, M.J. Rosseinsky, *Angew. Chem. Int. Ed.*, 53 (2014) 193-198.
- [109] C. Carbonell, K.C. Stylianou, J. Hernando, E. Evangelio, S.A. Barnett, S. Nettikadan, I. Imaz, D. MasPOCH, *Nat. Commun.*, 4 (2013).
- [110] A. Puskarić, I. Halasz, M. Gredicak, A. Palčić, J. Bronić, *New J. Chem.*, (2016).
- [111] P. Amo-Ochoa, F. Zamora, *Coord. Chem. Rev.*, 276 (2014) 34-58.
- [112] T. Sawada, A. Matsumoto, M. Fujita, *Angew. Chem. Int. Ed.*, 53 (2014) 7228-7232.
- [113] C. Martí-Gastaldo, J.E. Warren, M.E. Briggs, J.A. Armstrong, K.M. Thomas, M.J. Rosseinsky, *Chem. Eur. J.*, 21 (2015) 16027-16034.
- [114] D. Peri, J. Ciston, F. Gándara, Y. Zhao, O.M. Yaghi, *Inorg. Chem.*, 52 (2013) 13818-13820.
- [115] J. An, O.K. Farha, J.T. Hupp, E. Pohl, J.I. Yeh, N.L. Rosi, *Nat. Commun.*, 3 (2012) 604.
- [116] E. Sletten, *Acta Crystallogr. B*, 25 (1969) 1480-1491.
- [117] P.X. Rojas-González, A. Castiñeiras, J.M. González-Pérez, D. Choquesillo-Lazarte, J. Niclós-Gutiérrez, *Inorg. Chem.*, 41 (2002) 6190-6192.
- [118] J.P. García-Terán, O. Castillo, A. Luque, U. García-Couceiro, P. Román, L. Lezama, *Inorg. Chem.*, 43 (2004) 4549-4551.
- [119] E.-C. Yang, H.-K. Zhao, B. Ding, X.-G. Wang, X.-J. Zhao, *New J. Chem.*, 31 (2007) 1887-1890.
- [120] M. Zhang, Z.-Y. Gu, M. Bosch, Z. Perry, H.-C. Zhou, *Coord. Chem. Rev.*, 293-294 (2015) 327-356.
- [121] I. Burneo, K.C. Stylianou, S. Rodríguez-Hermida, J. Juanhuix, X. Fontrodona, I. Imaz, D. MasPOCH, *Cryst. Growth Des.*, 15 (2015) 3182-3189.
- [122] J.P. García-Terán, O. Castillo, A. Luque, U. García-Couceiro, P. Román, F. Lloret, *Inorg. Chem.*, 43 (2004) 5761-5770.
- [123] J.P. Garcia-Teran, O. Castillo, A. Luque, U. Garcia-Couceiro, G. Beobide, P. Roman, *Dalton Trans.*, (2006) 902-911.
- [124] F. Wang, Y.-X. Tan, H. Yang, H.-X. Zhang, Y. Kang, J. Zhang, *Chem. Commun.*, 47 (2011) 5828-5830.
- [125] S. Das, C. Madhavaiah, S. Verma, P.K. Bharadwaj, *Inorg. Chim. Acta* 358 (2005) 3236-3240.
- [126] H.-X. Huang, X.-Z. Tian, Y.-M. Song, Z.-W. Liao, G.-M. Sun, M.-B. Luo, S.-J. Liu, W.-Y. Xu, F. Luo, *Aust. J. Chem.*, 65 (2012) 320-325.
- [127] H. Bux, A. Feldhoff, J. Cravillon, M. Wiebcke, Y.-S. Li, J. Caro, *Chem. Mater.*, 23 (2011) 2262-2269.
- [128] J.-P. Charland, *Inorg. Chim. Acta.*, 135 (1987) 191-196.
- [129] J.P. Charland, A.L. Beauchamp, *Inorg. Chem.*, 25 (1986) 4870-4876.
- [130] J. An, S.J. Geib, N.L. Rosi, *J. Am. Chem. Soc.*, 132 (2010) 38-39.
- [131] S. Pérez-Yáñez, G. Beobide, O. Castillo, J. Cepeda, A. Luque, A.T. Aguayo, P. Román, *Inorg. Chem.*, 50 (2011) 5330-5332.
- [132] F. Wang, Y. Kang, *Inorg. Chem. Commun.*, 20 (2012) 266-268.
- [133] M. Zhang, W. Lu, J.-R. Li, M. Bosch, Y.-P. Chen, T.-F. Liu, Y. Liu, H.-C. Zhou, *Inorg. Chem. Front.*, 1 (2014) 159-162.
- [134] R. Murugavel, D. Krishnamurthy, M. Sathiyendiran, *Dalton Trans.*, (2002) 34-39.
- [135] L.G. Beauvais, M.P. Shores, J.R. Long, *J. Am. Chem. Soc.*, 122 (2000) 2763-2772.
- [136] M. Yamada, T. Sato, M. Miyake, Y. Kobayashi, *J. Colloid Interface Sci.*, 315 (2007) 369-375.
- [137] K. Uemura, S. Kitagawa, M. Kondo, K. Fukui, R. Kitaura, H.-C. Chang, T. Mizutani, *Chem. Eur. J.*, 8 (2002) 3586-3600.
- [138] G. Biffi, D. Tannahill, J. McCafferty, S. Balasubramanian, *Nat. Chem.*, 5 (2013) 182-186.
- [139] J. Zhu, L. Zhang, T. Li, S. Dong, E. Wang, *Adv. Mater.*, 25 (2013) 2440-2444.
- [140] I. Gadwal, S. De, M.C. Stuparu, R.J. Amir, S.G. Jang, A. Khan, *J. Polym. Sci. A Polym. Chem.*, 50 (2012) 1844-1850.
- [141] S. Lena, S. Masiero, S. Pieraccini, G.P. Spada, *Chem. Eur. J.*, 15 (2009) 7792-7806.
- [142] C. Arnal-Hérault, A. Pasc, M. Michau, D. Cot, E. Petit, M. Barboiu, *Angew. Chem. Int. Ed.*, 46 (2007) 8409-8413.
- [143] J.E. Betancourt, J.M. Rivera, *Org. Lett.*, 10 (2008) 2287-2290.
- [144] L. Ma, M. Melegari, M. Colombini, J.T. Davis, *J. Am. Chem. Soc.*, 130 (2008) 2938-2939.
- [145] Y.-L. Wu, N.E. Horwitz, K.-S. Chen, D.A. Gomez-Gualdrón, N.S. Luu, L. Ma, T.C. Wang, M.C. Hersam, J.T. Hupp, O.K. Farha, R.Q. Snurr, M.R. Wasielewski, *Nat Chem*, 9 (2017) 466-472.
- [146] N. Nagapradeep, V. Venkatesh, S.K. Tripathi, S. Verma, *Dalton Trans.*, 43 (2014) 1744-1752.
- [147] L. Li, X. Guo, L. Fu, R.K. Prud'homme, S.F. Lincoln, *Langmuir*, 24 (2008) 8290-8296.
- [148] E.M.M. Del Valle, *Process Biochem.*, 39 (2004) 1033-1046.
- [149] E. Norkus, *J. Incl. Phenom. Macrocycl. Chem.*, 65 (2009) 237-248.
- [150] R.A. Smaldone, R.S. Forgan, H. Furukawa, J.J. Gassensmith, A.M.Z. Slawin, O.M. Yaghi, J.F. Stoddart, *Angew. Chem. Int. Ed.*, 49 (2010) 8630-8634.
- [151] J.J. Gassensmith, R.A. Smaldone, R.S. Forgan, C.E. Wilmer, D.B. Cordes, Y.Y. Botros, A.M.Z. Slawin, R.Q. Snurr, J.F. Stoddart, *Org. Lett.*, 14 (2012) 1460-1463.
- [152] H. Xu, S. Rodríguez-Hermida, J. Pérez-Carvajal, J. Juanhuix, I. Imaz, D. MasPOCH, *Cryst. Growth Des.*, 16 (2016) 5598-5602.
- [153] H.-C. Zhou, J.R. Long, O.M. Yaghi, *Chem. Rev.*, 112 (2012) 673-674.
- [154] X.-S. Wang, S. Ma, D. Sun, S. Parkin, H.-C. Zhou, *J. Am. Chem. Soc.*, 128 (2006) 16474-16475.
- [155] S.K. Ghosh, S. Kitagawa, *CrystEngComm.*, 10 (2008) 1739-1742.
- [156] W. Xuan, C. Zhu, Y. Liu, Y. Cui, *Chem. Soc. Rev.*, 41 (2012) 1677-1695.
- [157] Q.-R. Fang, T.A. Makal, M.D. Young, H.-C. Zhou, *Comment Inorg. Chem.*, 31 (2010) 165-195.
- [158] W. Morris, B. Voloskiy, S. Demir, F. Gándara, P.L. McGrier, H. Furukawa, D. Cascio, J.F. Stoddart, O.M. Yaghi, *Inorg. Chem.*, 51 (2012) 6443-6445.
- [159] D. Feng, Z.-Y. Gu, J.-R. Li, H.-L. Jiang, Z. Wei, H.-C. Zhou, *Angew. Chem.*, 124 (2012) 10453-10456.
- [160] Y. Chen, T. Hoang, S. Ma, *Inorg. Chem.*, 51 (2012) 12600-12602.
- [161] T. Li, M.T. Kozlowski, E.A. Doud, M.N. Blakely, N.L. Rosi, *J. Am. Chem. Soc.*, 135 (2013) 11688-11691.

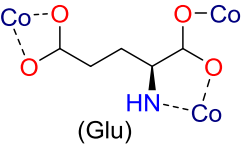
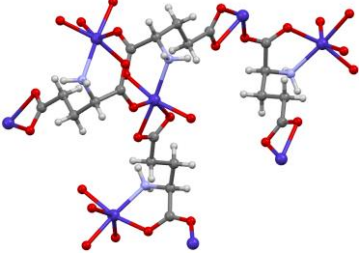
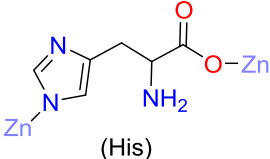
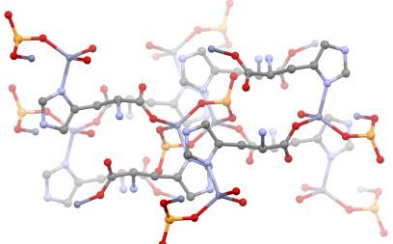
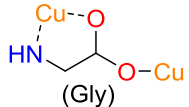
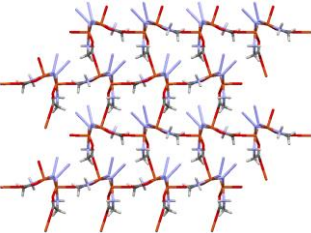
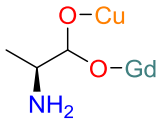
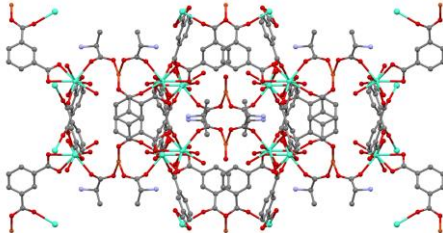
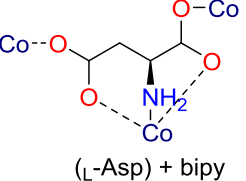
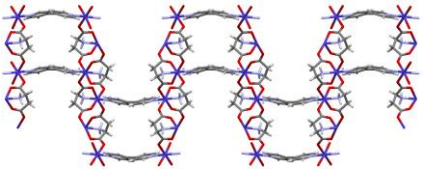
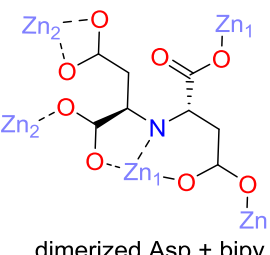
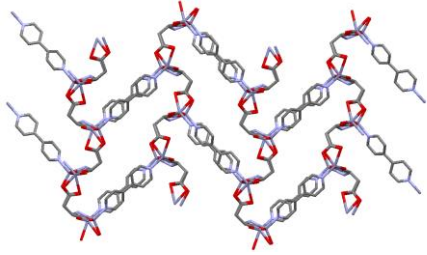
- [162] H. Cai, M. Li, X.-R. Lin, W. Chen, G.-H. Chen, X.-C. Huang, D. Li, *Angew. Chem. Int. Ed.*, 127 (2015) 10600–10605.
- [163] J. Thomas-Gipson, G. Beobide, O. Castillo, M. Fröba, F. Hoffmann, A. Luque, S. Pérez-Yáñez, P. Román, *Cryst. Growth Des.*, 14 (2014) 4019-4029.
- [164] G. Beobide, O. Castillo, J. Cepeda, A. Luque, S. Pérez-Yáñez, P. Román, J. Thomas-Gipson, *Coord. Chem. Rev.*, 257 (2013) 2716-2736.
- [165] T. Li, D.-L. Chen, J.E. Sullivan, M.T. Kozlowski, J.K. Johnson, N.L. Rosi, *Chem. Sci.*, 4 (2013) 1746-1755.
- [166] E.B. Winston, P.J. Lowell, J. Vacek, J. Chocholousova, J. Michl, J.C. Price, *Phys. Chem. Chem. Phys.*, 10 (2008) 5188-5191.
- [167] D.D. Boehr, R. Nussinov, P.E. Wright, *Nat. Chem. Biol.*, 5 (2009) 789-796.
- [168] C. Martí-Gastaldo, J.E. Warren, K.C. Stylianou, N.L.O. Flack, M.J. Rosseinsky, *Angew. Chem. Int. Ed.*, 51 (2012) 11044-11048.
- [169] T. Fukushima, S. Horike, Y. Inubushi, K. Nakagawa, Y. Kubota, M. Takata, S. Kitagawa, *Angew. Chem. Int. Ed.*, 49 (2010) 4820-4824.
- [170] A.D. Burrows, *CrystEngComm.*, 13 (2011) 3623-3642.
- [171] S. Henke, A. Schneemann, A. Wütscher, R.A. Fischer, *J. Am. Chem. Soc.*, 134 (2012) 9464-9474.
- [172] T. Lescouet, E. Kockrick, G. Bergeret, M. Pera-Titus, S. Aguado, D. Farrusseng, *J. Mater. Chem.*, 22 (2012) 10287-10293.
- [173] P. Serra-Crespo, E. Gobechiya, E.V. Ramos-Fernandez, J. Juan-Alcañiz, A. Martinez-Joaristi, E. Stavitski, C.E.A. Kirschhock, J.A. Martens, F. Kapteijn, J. Gascon, *Langmuir*, 28 (2012) 12916-12922.
- [174] R. Vaidhyanathan, D. Bradshaw, J.-N. Rebilly, J.P. Barrio, J.A. Gould, N.G. Berry, M.J. Rosseinsky, *Angew. Chem. Int. Ed.*, 45 (2006) 6495-6499.
- [175] J.L.C. Rowsell, O.M. Yaghi, *Micropor. Mesopor. Mat.*, 73 (2004) 3-14.
- [176] S. Kitagawa, R. Kitaura, S.-i. Noro, *Angew. Chem. Int. Ed.*, 43 (2004) 2334-2375.
- [177] J.-R. Li, R.J. Kuppler, H.-C. Zhou, *Chem. Soc. Rev.*, 38 (2009) 1477-1504.
- [178] A.R. Millward, O.M. Yaghi, *J. Am. Chem. Soc.*, 127 (2005) 17998-17999.
- [179] P.L. Llewellyn, S. Bourrelly, C. Serre, A. Vimont, M. Daturi, L. Hamon, G. De Weireld, J.-S. Chang, D.-Y. Hong, Y. Kyu Hwang, S. Hwa Jung, G. Férey, *Langmuir*, 24 (2008) 7245-7250.
- [180] S. Chen, J. Zhang, T. Wu, P. Feng, X. Bu, *J. Am. Chem. Soc.*, 131 (2009) 16027-16029.
- [181] R. Vaidhyanathan, S.S. Iremonger, K.W. Dawson, G.K.H. Shimizu, *Chem. Commun.*, (2009) 5230-5232.
- [182] Y.-S. Bae, O.K. Farha, J.T. Hupp, R.Q. Snurr, *J. Mater. Chem.*, 19 (2009) 2131-2134.
- [183] R. Banerjee, H. Furukawa, D. Britt, C. Knobler, M. O’Keeffe, O.M. Yaghi, *J. Am. Chem. Soc.*, 131 (2009) 3875-3877.
- [184] J. An, R.P. Fiorella, S.J. Geib, N.L. Rosi, *J. Am. Chem. Soc.*, 131 (2009) 8401-8403.
- [185] J. An, N.L. Rosi, *J. Am. Chem. Soc.*, 132 (2010) 5578-5579.
- [186] A. Torrisi, C. Mellot-Draznieks, R.G. Bell, *J. Chem. Phys.*, 132 (2010) 044705.
- [187] K.C. Stylianou, J.E. Warren, S.Y. Chong, J. Rabone, J. Bacsá, D. Bradshaw, M.J. Rosseinsky, *Chem. Commun.*, 47 (2011) 3389-3391.
- [188] P.S. Nugent, V.L. Rhodus, T. Pham, K. Forrest, L. Wojtas, B. Space, M.J. Zaworotko, *J. Am. Chem. Soc.*, 135 (2013) 10950-10953.
- [189] K. Sumida, D.L. Rogow, J.A. Mason, T.M. McDonald, E.D. Bloch, Z.R. Herm, T.-H. Bae, J.R. Long, *Chem. Rev.*, 112 (2012) 724-781.
- [190] T. Li, J.E. Sullivan, N.L. Rosi, *J. Am. Chem. Soc.*, 135 (2013) 9984-9987.
- [191] T. Li, N.L. Rosi, *Chem. Commun.*, 49 (2013) 11385-11387.
- [192] D.J. Heldebrant, P.K. Koech, M.T.C. Ang, C. Liang, J.E. Rainbolt, C.R. Yonker, P.G. Jessop, *Green Chem.*, 12 (2010) 713-721.
- [193] A. Barbarini, R. Maggi, A. Mazzacani, G. Mori, G. Sartori, R. Sartorio, *Tetrahedron Lett.*, 44 (2003) 2931-2934.
- [194] E.R. Parnham, R.E. Morris, *Acc. Chem. Res.*, 40 (2007) 1005-1013.
- [195] Y. Liu, V.C. Kravtsov, R. Larsen, M. Eddaoudi, *Chem. Commun.*, (2006) 1488-1490.
- [196] T. Wu, J. Zhang, C. Zhou, L. Wang, X. Bu, P. Feng, *J. Am. Chem. Soc.*, 131 (2009) 6111-6113.
- [197] S.-T. Zheng, Y. Li, T. Wu, R.A. Nieto, P. Feng, X. Bu, *Chem. Eur. J.*, 16 (2010) 13035-13040.
- [198] K. Li, D.H. Olson, J. Seidel, T.J. Emge, H. Gong, H. Zeng, J. Li, *J. Am. Chem. Soc.*, 131 (2009) 10368-10369.
- [199] T. Wu, X. Bu, R. Liu, Z. Lin, J. Zhang, P. Feng, *Chem. Eur. J.*, 14 (2008) 7771-7773.
- [200] B. Wang, A.P. Cote, H. Furukawa, M. O’Keeffe, O.M. Yaghi, *Nature*, 453 (2008) 207-211.
- [201] R. Banerjee, A. Phan, B. Wang, C. Knobler, H. Furukawa, M. O’Keeffe, O.M. Yaghi, *Science*, 319 (2008) 939-943.
- [202] H. Hayashi, A.P. Cote, H. Furukawa, M. O’Keeffe, O.M. Yaghi, *Nat. Mater.*, 6 (2007) 501-506.
- [203] J.J. Gassensmith, H. Furukawa, R.A. Smaldone, R.S. Forgan, Y.Y. Botros, O.M. Yaghi, J.F. Stoddart, *J. Am. Chem. Soc.*, 133 (2011) 15312-15315.
- [204] J.J. Gassensmith, J.Y. Kim, J.M. Holcroft, O.K. Farha, J.F. Stoddart, J.T. Hupp, N.C. Jeong, *J. Am. Chem. Soc.*, 136 (2014) 8277-8282.
- [205] S. Thushari, J.A.K. Cha, H.H.Y. Sung, S.S.Y. Chui, A.L.F. Leung, Y.-F. Yen, I.D. Williams, *Chem. Commun.*, (2005) 5515-5517.
- [206] J. Weng, M. Hong, Q. Shi, R. Cao, Albert S.C. Chan, *Eur. J. Inorg. Chem.*, 2002 (2002) 2553-2556.
- [207] B.-Y. Lou, R.-H. Wang, D.-Q. Yuan, B.-L. Wu, F.-L. Jiang, M.-C. Hong, *Inorg. Chem. Commun.*, 8 (2005) 971-974.
- [208] D. Bradshaw, T.J. Prior, E.J. Cussen, J.B. Claridge, M.J. Rosseinsky, *J. Am. Chem. Soc.*, 126 (2004) 6106-6114.
- [209] N.G. Pschirer, D.M. Ciurtin, M.D. Smith, U.H.F. Bunz, H.-C. zur Loye, *Angew. Chem. Int. Ed.*, 41 (2002) 583-585.
- [210] S. Banerjee, N.N. Adarsh, P. Dastidar, *CrystEngComm.*, 11 (2009) 746-749.
- [211] D.N. Dybtsev, M.P. Yutkin, E.V. Peresypkina, A.V. Virovets, C. Serre, G. Férey, V.P. Fedin, *Inorg. Chem.*, 46 (2007) 6843-6845.
- [212] D.N. Dybtsev, A.L. Nuzhdin, H. Chun, K.P. Bryliakov, E.P. Talsi, V.P. Fedin, K. Kim, *Angew. Chem. Int. Ed.*, 45 (2006) 916-920.
- [213] M.J. Ingleson, J.P. Barrio, J. Bacsá, C. Dickinson, H. Park, M.J. Rosseinsky, *Chem. Commun.*, (2008) 1287-1289.
- [214] M. Ranocchiari, J.A.v. Bokhoven, *Phys. Chem. Chem. Phys.*, 13 (2011) 6388-6396.
- [215] J.M. Holcroft, K.J. Hartlieb, P.Z. Moghadam, J.G. Bell, G. Barin, D.P. Ferris, E.D. Bloch, M.M. Algaradah, M.S. Nassar, Y.Y. Botros, K.M. Thomas, J.R. Long, R.Q. Snurr, J.F. Stoddart, *J. Am. Chem. Soc.*, 137 (2015) 5706-5719.
- [216] R. Hulme, R.E. Rosensweig, D.M. Ruthven, *Ind. Eng. Chem. Res.*, 30 (1991) 752-760.
- [217] V. Cottier, J.-P. Bellat, M.-H. Simonot-Grange, A. Méthivier, *J. Phys. Chem. B*, 101 (1997) 4798-4802.
- [218] S.E. Jee, D.S. Sholl, *J. Am. Chem. Soc.*, 131 (2009) 7896-7904.
- [219] M. Minceva, A.E. Rodrigues, *AIChE J.*, 53 (2007) 138-149.
- [220] T. Tozawa, J.T.A. Jones, S.I. Swamy, S. Jiang, D.J. Adams, S. Shakespeare, R. Clowes, D. Bradshaw, T. Hasell, S.Y. Chong, C. Tang,

- S. Thompson, J. Parker, A. Trewin, J. Bacsa, A.M.Z. Slawin, A. Steiner, A.I. Cooper, *Nat. Mater.*, 8 (2009) 973-978.
- [221] T. Mitra, K.E. Jelfs, M. Schmidtman, A. Ahmed, S.Y. Chong, D.J. Adams, A.I. Cooper, *Nat. Chem.*, 5 (2013) 276-281.
- [222] L. Alaerts, C.E.A. Kirschhock, M. Maes, M.A. van der Veen, V. Finsy, A. Depla, J.A. Martens, G.V. Baron, P.A. Jacobs, J.F.M. Denayer, D.E. De Vos, *Angew. Chem. Int. Ed.*, 46 (2007) 4293-4297.
- [223] L. Alaerts, M. Maes, L. Giebeler, P.A. Jacobs, J.A. Martens, J.F.M. Denayer, C.E.A. Kirschhock, D.E. De Vos, *J. Am. Chem. Soc.*, 130 (2008) 14170-14178.
- [224] L. Alaerts, M. Maes, P.A. Jacobs, J.F.M. Denayer, D.E. De Vos, *Phys. Chem. Chem. Phys.*, 10 (2008) 2979-2985.
- [225] M. Maes, F. Vermoortele, M. Boulhout, T. Boudewijns, C. Kirschhock, R. Ameloot, I. Beurroies, R. Denoyel, D.E. De Vos, *Micropor. Mesopor. Mat.*, 157 (2012) 82-88.
- [226] T. Remy, L. Ma, M. Maes, D.E. De Vos, G.V. Baron, J.F.M. Denayer, *Ind. Eng. Chem. Res.*, 51 (2012) 14824-14833.
- [227] R. El Osta, A. Carlin-Sinclair, N. Guillou, R.I. Walton, F. Vermoortele, M. Maes, D. de Vos, F. Millange, *Chem. Mater.*, 24 (2012) 2781-2791.
- [228] F. Vermoortele, M. Maes, P.Z. Moghadam, M.J. Lennox, F. Ragon, M. Boulhout, S. Biswas, K.G.M. Laurier, I. Beurroies, R. Denoyel, M. Roeffaers, N. Stock, T. Düren, C. Serre, D.E. De Vos, *J. Am. Chem. Soc.*, 133 (2011) 18526-18529.
- [229] X. Kuang, Y. Ma, H. Su, J. Zhang, Y.-B. Dong, B. Tang, *Anal. Chem.*, 86 (2014) 1277-1281.
- [230] K.J. Hartlieb, J.M. Holcroft, P.Z. Moghadam, N.A. Vermeulen, M.M. Algaradah, M.S. Nassar, Y.Y. Botros, R.Q. Snurr, J.F. Stoddart, *J. Am. Chem. Soc.*, 138 (2016) 2292-2301.
- [231] H.-R. Fu, J. Zhang, *Chem. Eur. J.*, 21 (2015) 5700-5703.
- [232] J. Navarro-Sánchez, A.I. Argente-García, Y. Moliner-Martínez, D. Roca-Sanjuán, D. Antypov, P. Campíns-Falcó, M.J. Rosseinsky, C. Martí-Gastaldo, *J. Am. Chem. Soc.*, 139 (2017) 4294-4297.
- [233] L.V. Meyer, F. Schonfeld, K. Muller-Buschbaum, *Chem. Commun.*, 50 (2014) 8093-8108.
- [234] S.V. Eliseeva, J.-C.G. Bunzli, *Chem. Soc. Rev.*, 39 (2010) 189-227.
- [235] B. Yan, *RSC Adv.*, 2 (2012) 9304-9324.
- [236] J.-C.G. Bunzli, C. Pigué, *Chem. Soc. Rev.*, 34 (2005) 1048-1077.
- [237] X. Shen, B. Yan, *J. Mater. Chem. C*, 3 (2015) 7038-7044.
- [238] L.D. Carlos, R.A.S. Ferreira, V.d.Z. Bermudez, S.J.L. Ribeiro, *Adv. Mater.*, 21 (2009) 509-534.
- [239] J. Chen, F.-Y. Yi, H. Yu, S. Jiao, G. Pang, Z.-M. Sun, *Chem. Commun.*, 50 (2014) 10506-10509.
- [240] L. Basabe-Desmonts, D.N. Reinhoudt, M. Crego-Calama, *Chem. Soc. Rev.*, 36 (2007) 993-1017.
- [241] J. An, C.M. Shade, D.A. Chengelis-Czegan, S. Petoud, N.L. Rosi, *J. Am. Chem. Soc.*, 133 (2011) 1220-1223.
- [242] A.C. McKinlay, R.E. Morris, P. Horcajada, G. Férey, R. Gref, P. Couvreur, C. Serre, *Angew. Chem. Int. Ed.*, 49 (2010) 6260-6266.
- [243] J.A. Mason, J. Oktawiec, M.K. Taylor, M.R. Hudson, J. Rodriguez, J.E. Bachman, M.I. Gonzalez, A. Cervellino, A. Guagliardi, C.M. Brown, P.L. Llewellyn, N. Masciocchi, J.R. Long, *Nature*, 527 (2015) 357-361.
- [244] T. Hidalgo, L. Cooper, M. Gorman, T. Lozano-Fernandez, R. Simon-Vazquez, G. Mouchaham, J. Marrot, N. Guillou, C. Serre, P. Fertey, A. Gonzalez-Fernandez, T. Devic, P. Horcajada, *J. Mater. Chem. B*, 2017, 5, 2813



Table 1: Coordination binding modes of amino acids in MOFs.

Entry	Metal	Coordination Mode	Structural Representation of Bio-Ligand Coordination	Structural Illustration of MOF	Ref.
1	Ni	$\mu_2\text{-O}_1\text{:O}_2$	 (Gly)		[69]
2	Cu	$\mu_2\text{-N}_1\text{O}_1\text{:O}_2$	 (L-Phe)		[73]
3	Cu	$\mu_2\text{-N}_1\text{O}_1\text{:O}_2$	 (L-Gln)		[74]
4	Ni	$\mu_5\text{-N}_1\text{O}_1\text{O}_4\text{:O}_1\text{:O}_2\text{:O}_3\text{:O}_4$	 (L-Asp)		[76]
5	Ni	$\mu_2\text{-N}_1\text{O}_1\text{:O}_2$	 (L-Ala)		[77]
6	Ag/Cu	$\mu_3\text{-N}_1\text{O}_1\text{:O}_2\text{:S}_1$	 (Met)		[78]

Entry	Metal	Coordination Mode	Structural Representation of Bio-Ligand Coordination	Structural Illustration of MOF	Ref.
7	Co	$\mu_3\text{-N}_1\text{O}_1\text{:O}_2\text{:O}_3\text{O}_4$	 <p>(Glu)</p>		[84]
8	Zn	$\mu_2\text{-N}_2\text{:O}_2$	 <p>(His)</p>		[85]
9	Cu	$\mu_2\text{-N}_1\text{O}_1\text{:O}_2$	 <p>(Gly)</p>		[86]
10	Cu/Gd	-----	 <p>(Ala) + 1,3-bdc</p>		[87]
11	Co	$\mu_3\text{-N}_1\text{O}_1\text{O}_4\text{:O}_2\text{:O}_3$	 <p>(L-Asp) + bipy</p>		[89]
12	Zn	-----	 <p>dimerized Asp + bipy</p>		[90]

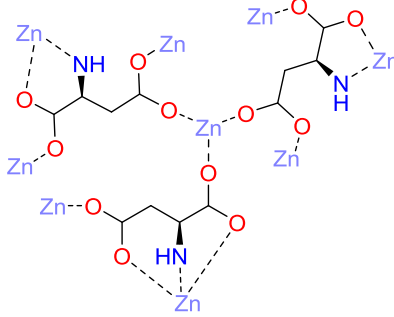
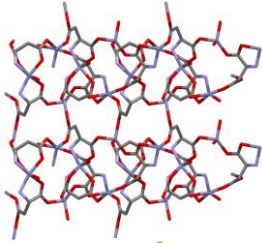
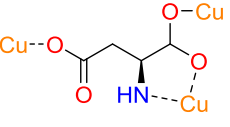
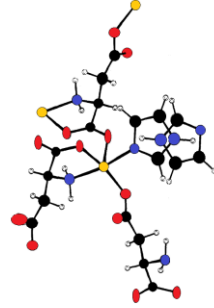
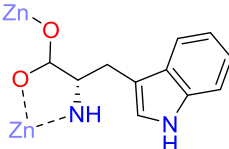
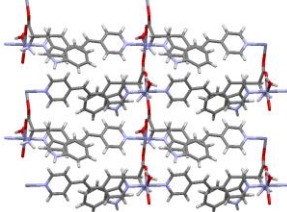
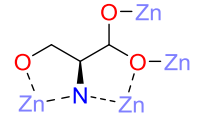
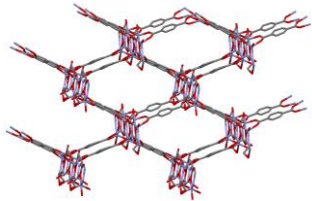
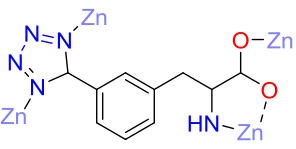
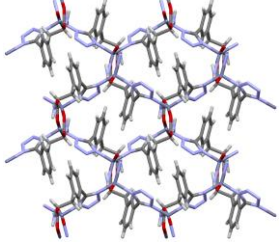
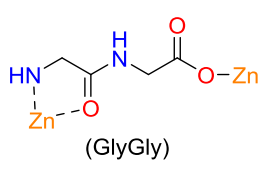
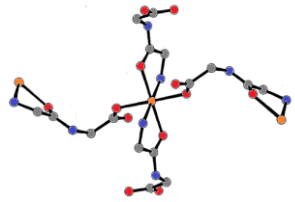
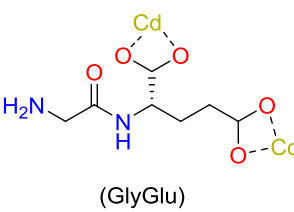
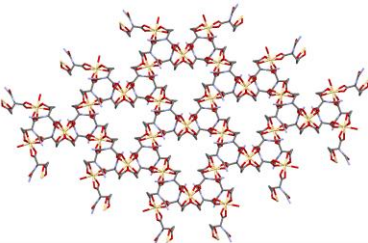
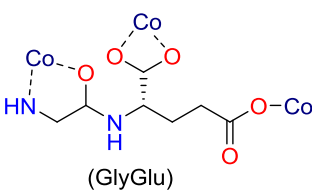
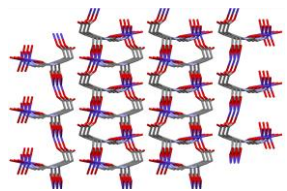
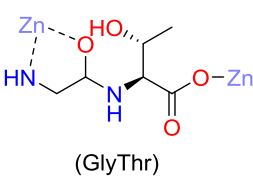
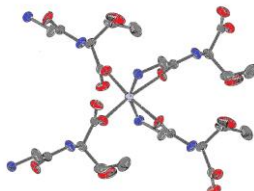
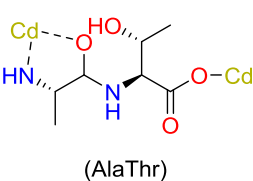
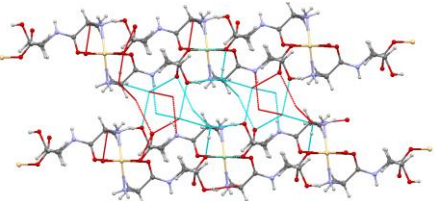
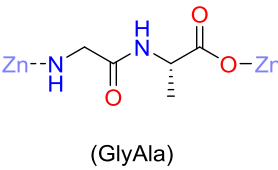
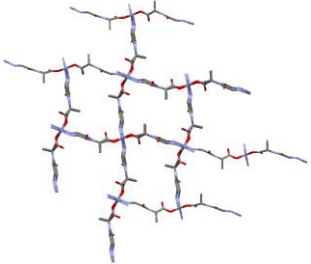
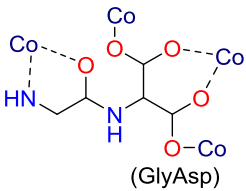
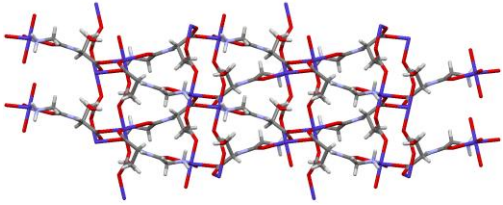
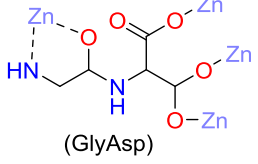
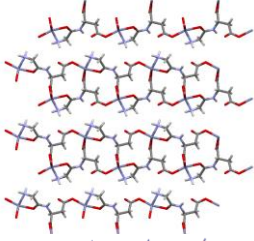
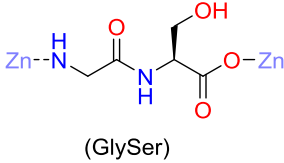
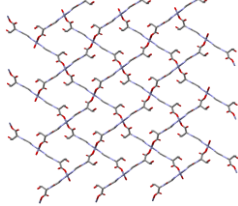
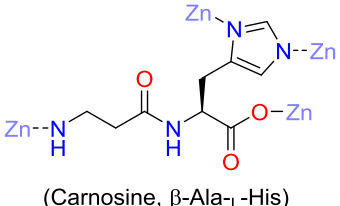
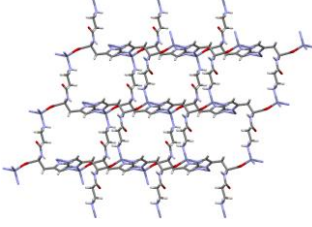
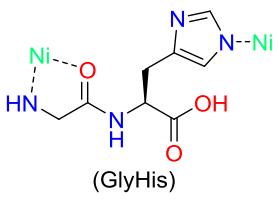
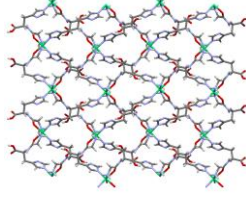
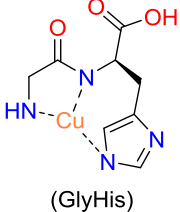
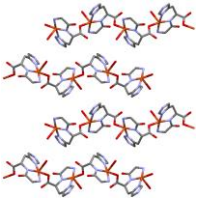
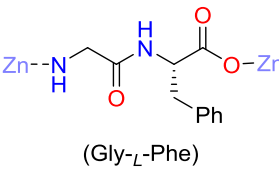
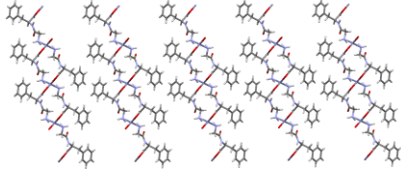
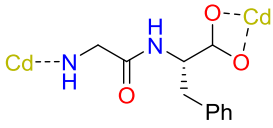
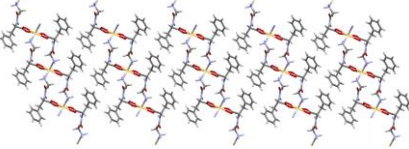
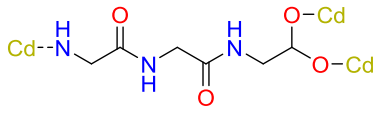
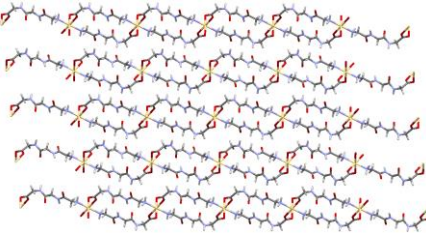
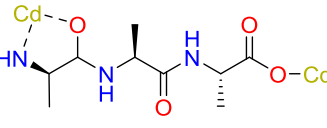
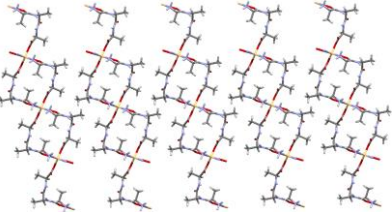
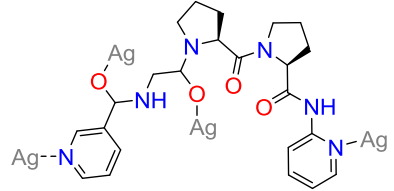
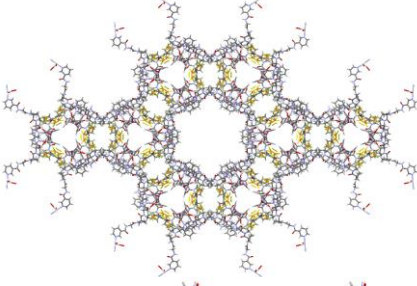
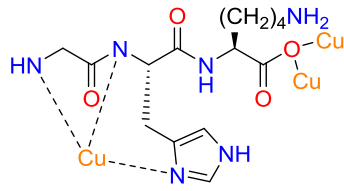
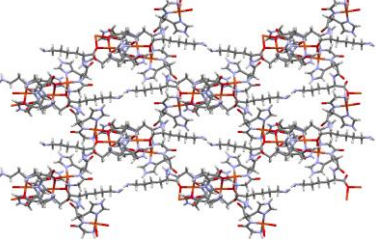
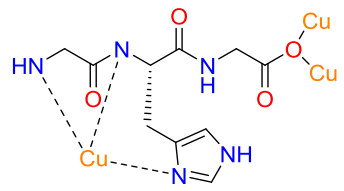
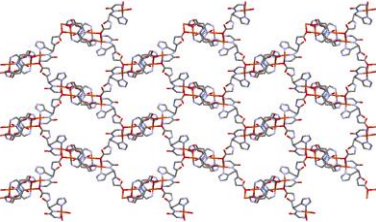
Entry	Metal	Coordination Mode	Structural Representation of Bio-Ligand Coordination	Structural Illustration of MOF	Ref.
13	Zn	----	 <p>(Asp) + bipy</p>		[91]
14	Cu	$\mu_3\text{-N}_1\text{O}_1\text{:O}_2\text{:O}_3$	 <p>(L-Asp) + Im</p>		[92]
15	Zn	$\mu_2\text{-N}_1\text{O}_1\text{:O}_2$	 <p>(Trp) + bipy</p>		[93]
16	Zn	$\mu_3\text{-N}_1\text{O}_1\text{O}_3\text{:O}_1\text{:O}_2$	 <p>(L-Ser) + bdc</p>		[94]
17	Zn	----	 <p>Modified Phe</p>		[48/95]

Table 2: Coordination binding modes of peptides in MOFs.

Entry	Metal	Coordination Mode	Structural Representation of Bio-Ligand Coordination	Structural Illustration of MOF	Ref.
1	Zn	$\mu_2\text{-N}_1\text{O}_1\text{:O}_2$	 <p>(GlyGly)</p>		[101]
2	Cd	$\mu_2\text{-O}_{10}\text{O}_{11}\text{:O}_{13}\text{O}_{14}$	 <p>(GlyGlu)</p>		[102]
3	Co	$\mu_2\text{-N}_2\text{O}_5\text{:O}_3\text{O}_4\text{:O}_2$	 <p>(GlyGlu)</p>		[65]
4	Zn	$\mu_2\text{-N}_1\text{O}_1\text{:O}_3$	 <p>(GlyThr)</p>		[103]
5	Cd	$\mu_2\text{-N}_1\text{O}_1\text{:O}_3$	 <p>(AlaThr)</p>		[104]
6	Zn	$\mu_1\text{-O}_1\text{O}_4\text{N}_2\text{N}_4$	 <p>(GlyAla)</p>		[105]

Entry	Metal	Coordination Mode	Structural Representation of Bio-Ligand Coordination	Structural Illustration of MOF	Ref.
7	Co	$\mu_3\text{-O}_2\text{O}_4\text{:O}_3\text{:O}_5$	 <p>(GlyAsp)</p>		[106]
8	Zn	$\mu_4\text{-N}_1\text{O}_1\text{:O}_2\text{:O}_3\text{:O}_4$	 <p>(GlyAsp)</p>		[106]
9	Zn	$\mu_2\text{-N}_5\text{:O}_{13}$	 <p>(GlySer)</p>		[107]
10	Zn	----	 <p>(Carnosine, <math>\beta</math>-Ala-L-His)</p>		[108]
11	Ni	$\mu_1\text{-N}_4\text{N}_{11}\text{O}_3$	 <p>(GlyHis)</p>		[109]
12	Cu	$\mu_1\text{-N}_2\text{N}_3\text{N}_4$	 <p>(GlyHis)</p>		[109]
13	Zn	$\mu_2\text{-N}_1\text{:O}_2$	 <p>(Gly-L-Phe)</p>		[110]

Entry	Metal	Coordination Mode	Structural Representation of Bio-Ligand Coordination	Structural Illustration of MOF	Ref.
14	Cd	$\mu_2\text{-N}_1\text{:O}_2\text{O}_3$	 <p>(Gly-<i>L</i>-Phe)</p>		[110]
15	Cd	$\mu_3\text{-N}_1\text{:O}_3\text{O}_4$	 <p>(GlyGlyGly)</p>		[104]
16	Cd	$\mu_3\text{-N}_1\text{O}_2\text{:O}_3$	 <p>(AlaAlaAla)</p>		[104]
17	Ag	$\mu_4\text{-N}_{1A}\text{:O}_{1A}\text{:O}_{2A}\text{:N}_{6A}$	 <p>(GlyProPro)</p>		[112]
18	Cu	$\mu_4\text{-N}_3\text{:N}_7\text{:N}_{10}\text{:O}_{20}$	 <p>(Gly-<i>L</i>-His-<i>L</i>-Lys)</p>		[113]
19	Cu	$\mu_4\text{-N}_3\text{:N}_7\text{:N}_{10}\text{:O}_{20}$	 <p>(Gly-<i>L</i>-His-Gly)</p>		[113]

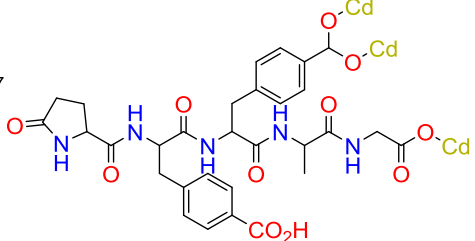
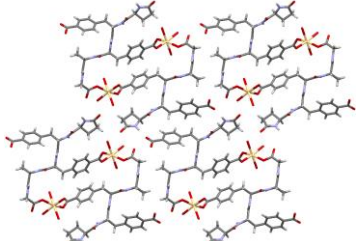
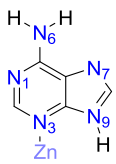
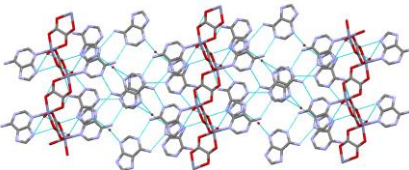

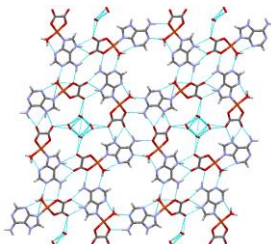
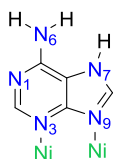
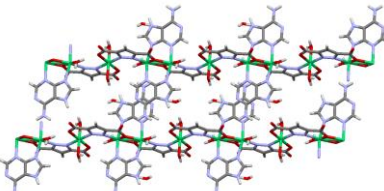
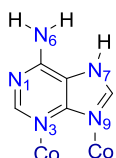
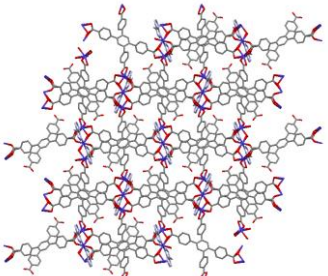
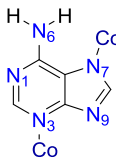
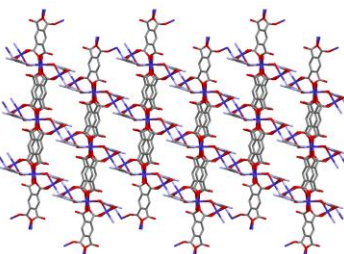
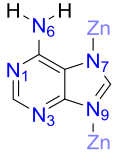
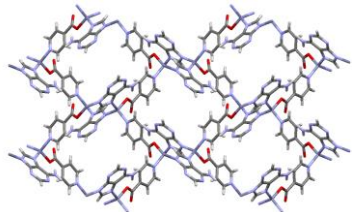
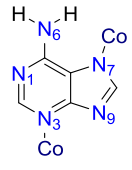
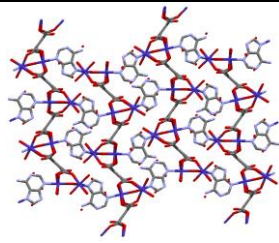
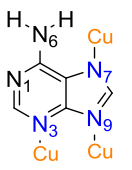
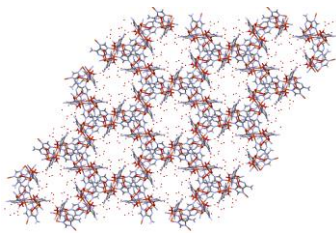
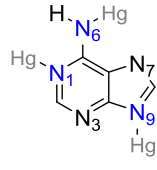
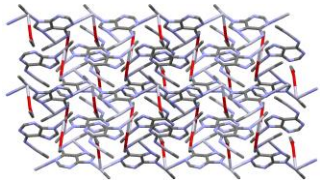
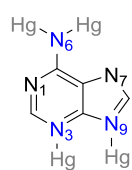
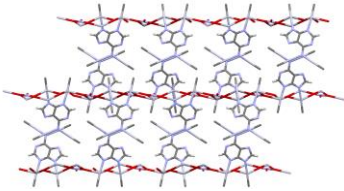
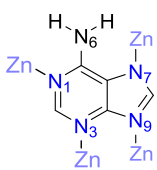
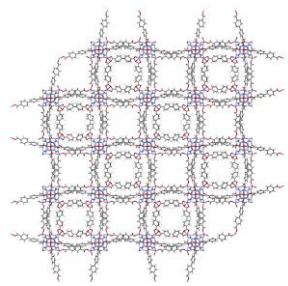
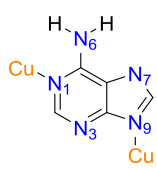
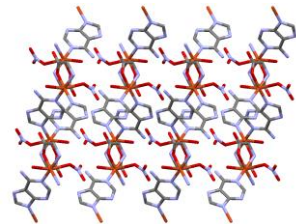
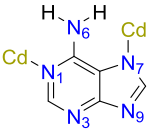
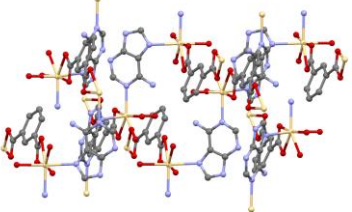
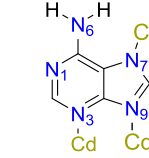
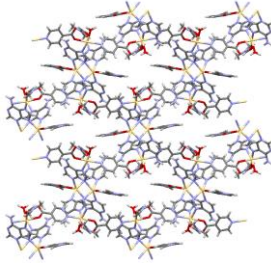
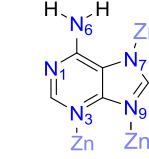
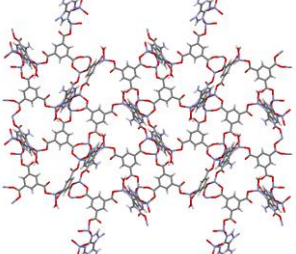
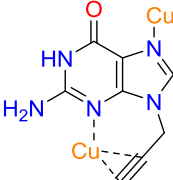
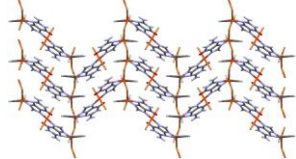
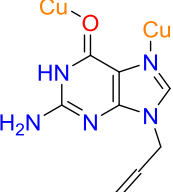
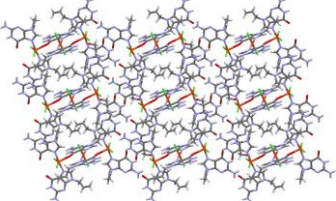
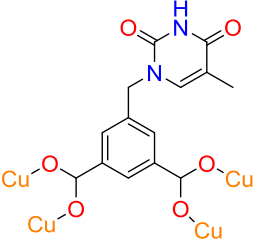
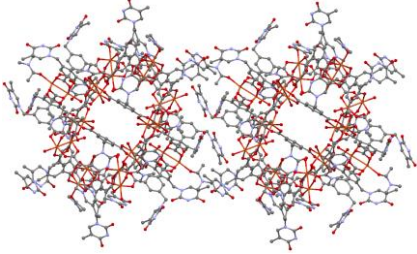
Entry	Metal	Coordination Mode	Structural Representation of Bio-Ligand Coordination	Structural Illustration of MOF	Ref.
20	Cd	$\mu_3\text{-O}_5\text{:O}_6\text{:O}_7$	 <p data-bbox="553 527 938 579">(Glu-<i>p</i>-CO<sub>2</sub>Phe-<i>p</i>-CO<sub>2</sub>Phe-Ala-Gly-OH) After intramolecular cyclization</p>		[114]



Table 3: Coordination binding modes of nucleobases in MOFs.

Entry	Metal	Coordination Mode	Structural Representation of Bio-Ligand	Structural Illustration of MOF	Ref.
1	Zn	[N <sub>3</sub> ]			[118]
2	Cu	[N <sub>9</sub> ]			[123]
3	Ni	[N <sub>3</sub> , N <sub>9</sub> ]			[124]
4	Co	[N <sub>3</sub> , N <sub>9</sub> ]	 <p>[Ade + BTEC]</p>		[121]
5	Co	[N <sub>3</sub> , N <sub>7</sub> ]	 <p>[Ade + TCPB]</p>		[121]
6	Zn	[N <sub>7</sub> , N <sub>9</sub> ]	 <p>(Ade + Imidazole)</p>		[124]

Entry	Metal	Coordination Mode	Structural Representation of Bio-Ligand Coordination	Structural Illustration of MOF	Ref.
7	Co	[N <sub>3</sub> , N <sub>7</sub> ]			[121]
8	Cu	[N <sub>3</sub> , N <sub>7</sub> , N <sub>9</sub> ]			[118]
9	Hg	[N <sub>1</sub> , N <sub>6</sub> , N <sub>9</sub> ]			[128]
10	Hg	[N <sub>3</sub> , N <sub>6</sub> , N <sub>9</sub> ]			[129]
11	Zn	[N <sub>1</sub> , N <sub>3</sub> , N <sub>7</sub> , N <sub>9</sub> ]			[52]
12	Cu	[N <sub>1</sub> , N <sub>9</sub> ]			[125]

Entry	Metal	Coordination Mode	Structural Representation of Bio-Ligand Coordination	Structural Illustration of MOF	Ref.
13	Cd	[N <sub>1</sub> , N <sub>7</sub> ]	 <p>(Ade + isonicitaiic)</p>		[126]
14	Cd	[N <sub>3</sub> , N <sub>7</sub> , N <sub>9</sub> ]	 <p>(Ade + isonicitaiic)</p>		[132]
15	Zn	[N <sub>3</sub> , N <sub>7</sub> , N <sub>9</sub> ]	 <p>(Ade + BTC)</p>		[162]
16	Cu	---	 <p>Modified Guanine</p>		[146]
16	Cu	---	 <p>Modified Guanine</p>		[146]
17	Cu	$\mu_4$ -O <sub>1</sub> :O <sub>2</sub> :O <sub>3</sub> :O <sub>4</sub>	 <p>Isophthalate moiety with thymine-incorporation</p>		[133]

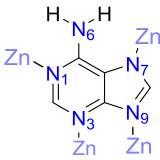
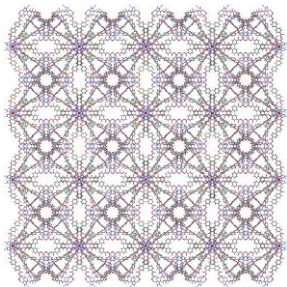
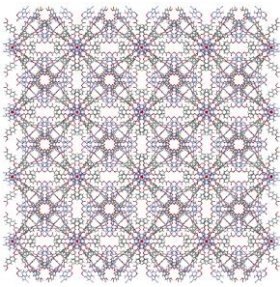
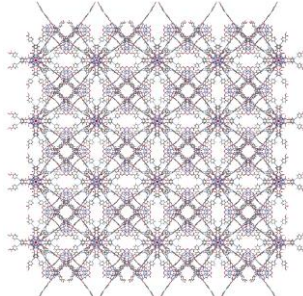
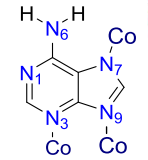
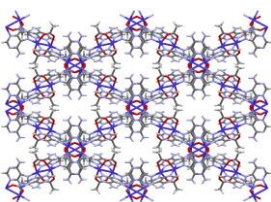
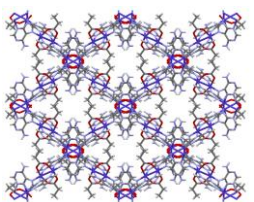
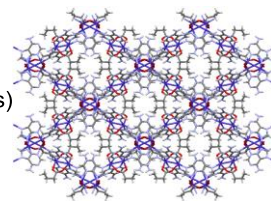
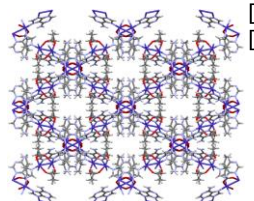
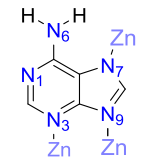
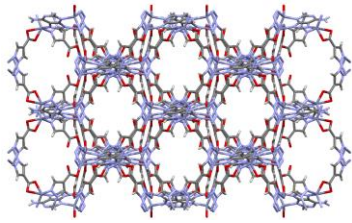
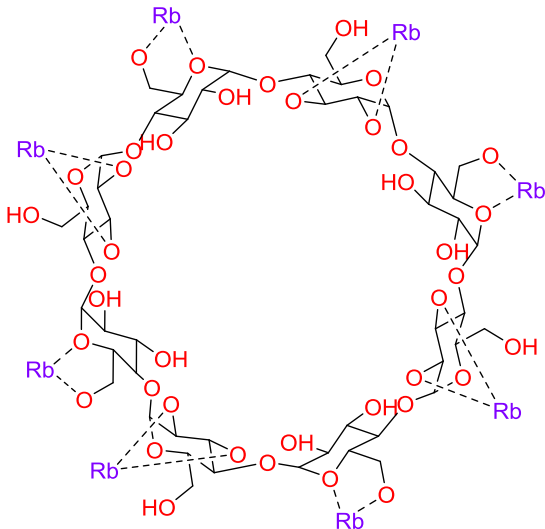
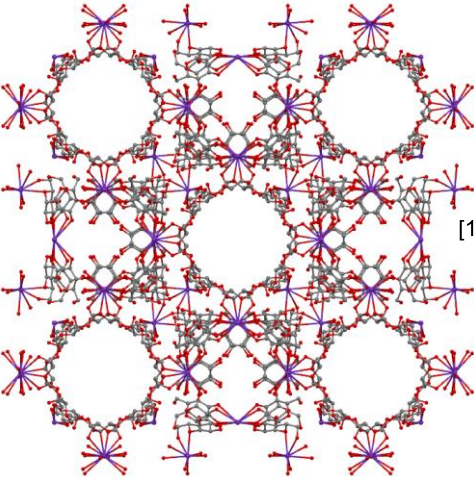
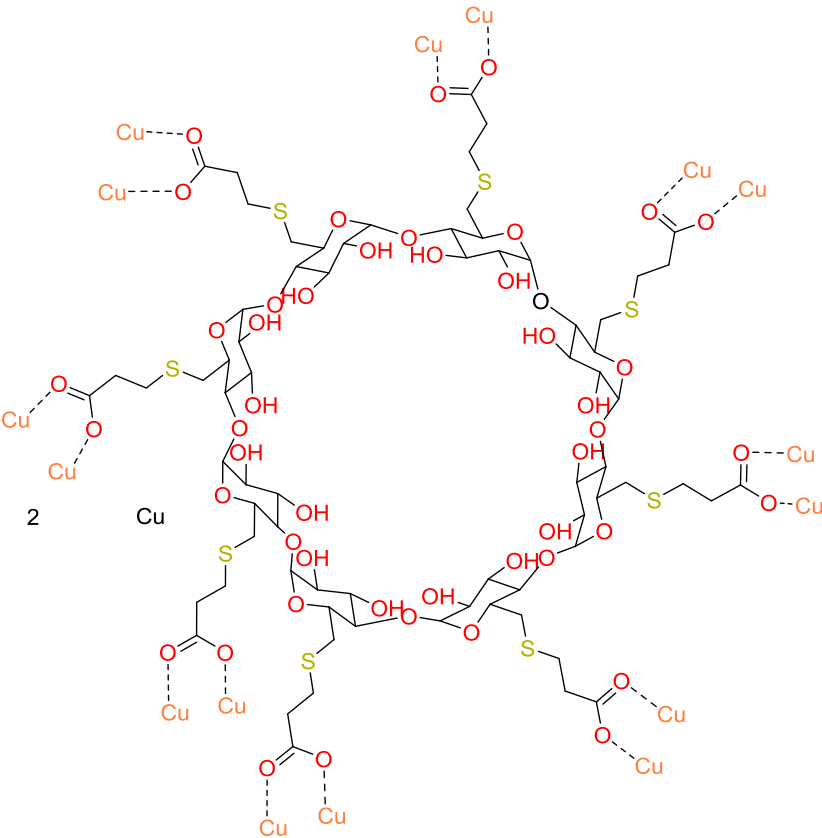
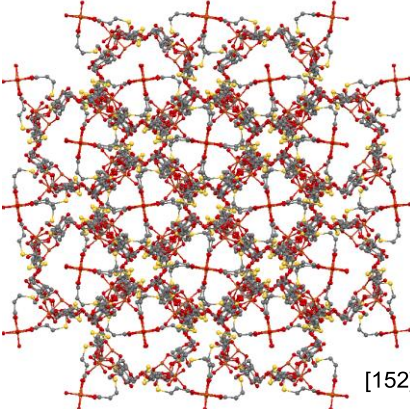
Entry	Metal	Coordination Mode	Structural Representation of Bio-Ligand Coordination	Structural Illustration of MOF	Ref.
18	Zn	[N <sub>1</sub> , N <sub>3</sub> , N <sub>7</sub> , N <sub>9</sub> ]		 bio-MOF-100 [115]  bio-MOF-101 [161]   bio-MOF-102 [161]	
19	Co	[N <sub>3</sub> , N <sub>7</sub> , N <sub>9</sub> ]	 (Ade + ligands)	 bio-MOF-11  bio-MOF-12   bio-MOF-13  bio-MOF-14	[130] [164]
20	Zn	[N <sub>3</sub> , N <sub>7</sub> , N <sub>9</sub> ]	 (Ade + pyrazole)		[231]

Table 4: Coordination binding modes of saccharides in MOFs.

Entry	Metal	Structural Representation of Bio-Ligand Coordination	Structural Illustration of MOF	Ref.
1	Rb			[113]
2	Cu			[152]